CNIC-01755
CNDC-0036
INDC(CPR)-060/L

COMMUNICATION OF NUCLEAR DATA PROGRESS

No. 29 (2003. 12)

China Nuclear Data Center
China Nuclear Information Centre
China Nuclear Industry Audio & Visual Publishing House

COMMUNICATION OF NUCLEAR DATA PROGRESS

Abstract: This is the 29th issue of *Communication of Nuclear Data Progress* (CNDP), in which the progress and achievements in nuclear data field in 2002 in China are carried. It includes the evaluations of complete neutron data for n+^{55,58}Mn, ^{99,100}Mo and covariance data evaluation for ^{63,65,Nat}Cu; the evaluations of mass distribution data from ^{252}Cf spontaneous fission, prompt and delayed neutron yields for ^{233}U; the studies for level width broaden effect; benchmark testing calculation for ^{232}Th; establishment of file-6 of n+^{12}C for CENDL-3 et al.

EDITORIAL NOTE

From this issue, the editorial board has been changed. With this opportunity, the new editorial board wishes to express our deepest thanks to Profs. Liu Tingjing and Zhuang Youxiang who are the key contributors for the CNDP as editor-in-chiefs since the first issue of this publication. Profs. Zhang Jingshang, Zhou Zuying and Zhuang Youxiang are responsible mainly for the nuclear data calculations, experiments and evaluations respectively in the new editorial board. I sincerely hope that our readers and colleagues will not spare their comments in order to improve the CNDP.

Zhao Zhixiang
Editor-in-Chief

Contact address:
Ge Zhigang
China Nuclear Data Center
China Institute of Atomic Energy
P. O. Box 275-41, Beijing 102413
People's Republic of China
Telephone: 86-10-69357275
Facsimile: 86-10-69357008
E-mail: gezg@iris.ciae.ac.cn

Communication of Nuclear Data Progress

No.29 (2003) Beijing

CONTENTS

Covariance Data Evaluation of Some Experimental Data for n+$^{65, 63, Nat}$Cu

JIA Min[1] LIU Jianfeng[1] LIU Tingjin[2]

1 Physics Department, Zhengzhou University, Zhengzhou 450052

2 China Nuclear Data Center, CIAE, P.O.Box275(41), Beijing 102413

【**abstract**】 *The evaluation of covariance data for $^{65, 63, Nat}$Cu in the energy range from 99.5 keV to 20 MeV was carried out using EXPCOV and SPC code based on the experimental data available. The data can be as a part of the covariance file 33 in the evaluated library in ENDF/B6 format for the corresponding nuclides, and also can be used as the basis of theoretical calculation concerned.*

Introduction

Copper is a very important structure material in nuclear engineering. With the development of the reactor physics and computer technology, the covariance matrix of nuclear data becomes more and more important**.** The error, as traditionally given, is only the diagonal elements of the covariance matrix, which just describes the accuracy of the data. The complete error information is given out by the covariance matrix, which describes not only the accuracy of the data but also the correlation of them.

The experimental data of $^{65, 63, Nat}$Cu were selected from EXFOR (experimental neutron data) library and evaluated in the smooth energy range[1] below 20 MeV, namely from 99.5 keV or threshold energy to 20MeV. The covariance matrixes were constructed according to the error analysis of experimental data. The program SPC[2] was used to fit the data and merge the covariance matrixes.

1 Selection and Analysis of Experimental Data

The experimental data were taken from EXFOR library through the on-line experimental data retrieval code. For one reaction channel of ^{65,63,Nat}Cu, there are lots of sets of data sometimes, but they are not all valuable and useful for the covariance data evaluation. Therefore, the data need to be selected and evaluated. Usually the data are selected according to the following principles: 1). Times. The data measured later are taken with more credibility. 2). Lab. The famous labs are thought to possess advanced technology and equipments to get better data. 3). Advanced measurement method. There are many methods such as TOF (the time of flight), ACTIV (activation). 4). The number of measurement data point. The more the data points are, the better it is to make curve fitting and construct covariance matrix. In general, it is suitable to be within 50 data points.

According to the principles mentioned above, the reaction types, for which the experimental data are available, are as follows: the cross sections of (n,tot), (n,2n), (n,el), (n,γ), (n,inl), (n,non) for ^{Nat}Cu; the cross sections of (n,tot), (n,2n), (n,el), (n,γ), (n,α) for ^{63}Cu; the cross sections of (n,tot), (n,2n), (n,el), (n,γ), (n,α), (n,p), (n,nα) for ^{65}Cu. There are no measured data or only a few experimental data for other reaction channels.

The evaluations for some typical reactions are given as following.

1.1 ^{Nat}Cu (n,tot)

There are many sets of measured data for this reaction (more than 45 sets). They were plotted and compared directly using the retrieval and plot code TT[3], developed by China Nuclear Data Center. We excluded the data discrepant from others greatly and with the data points number less than 4. The remained 11 sets of data are in agreement ultimately in trend. The data of N.Nereson, A.Bratenshl and M.Mazari [5,6,7] were abandoned because they were measured before 60's. The data of W.F.E.Pineo and J.C.Albergotti[8,9] are correct in trend, but their energy range is small and covered by others. So they were also abandoned. The J.F.Whalen's data[10] in the lowest energy range are in good accordance with

others but the data points are so many even accounting to 621 points. While the W.P.Poenitz's data[12] with 23 data points are more perfect. The trend of D.C.Larson's data[11] is discrepant with others in lower energy range and no error information is given in the EXFOR entry, so it was also excluded. As a result, the data of 4 sets[12~15] were adopted. Among them, the data points of D.G.Foster and R.W.Finlay[14,15] were merged because their data points are too many and the data of the later in energy range from 20 MeV to 600 MeV were rejected. The results and their fit values (see section 2) are shown in Fig.1(a).

1.2 ^{63}Cu (n,γ)

Excluding the data deviating from others large and the data with only a single datum point, there are only 5 sets of data remained. The data of A.G.Dovbenko[16] are only a part of V.A.Tolstikov's [19], so they were abandoned. The J.M.Blair's data [17] were also abandoned because their trend is not correct. At last, the data of Voignier[18], Tolstikov[19] and Zaikin[20] were adopted and shown in Fig.2(a).

1.3 ^{65}Cu (n,2n)

After preliminary selection, there are 7 sets of data remained. From comparing, it can be seen that the M.Bormann's data[21] deviate from others badly and they were abandoned. The R.J.Prestwood's data[22] with ^{238}U(n,f) as monitor were found systematically lower than A.Paulsen's data [26] measured in Gel laboratory. It is well known that the threshold energy of ^{238}U(n,f) is about 1 MeV far from the threshold energy of ^{65}Cu(n,2n) and there is larger influence of the low energy neutrons, so the data were diminished. While the later with telescope counter as monitor has no that effect. The data of Y.Ikeda and P.N.Ngoc[23,24] are in small energy range just from 13 MeV to 15 MeV, also being abandoned. The data of D.C.Santry [25], A.Paulsen[26] and M.Bormann[27] are in good agreement within the error bar, so all of them were adopted. Fig.3(a) shows the result.

1.4 ^{65}Cu (n,p)

The trend of the data measured by Y.Ikeda[28] and N.I.Molla [29] is not correct and the data of T.B.Ryves [30] fluctuate too much. So all of them were eliminated. D.C.Santry[31] measured 3 sets of data covering the energy range from 3.5 MeV to 20 MeV, and the trend is correct. But they are systematically deviated from 13.5 MeV to 15 MeV comparing with the M.Bormann's data[32]. It was found that the former used the ^{32}S(n,p) cross section as monitor normalized at 14.5 MeV with the standard 226 mb, while the later with ^{56}Fe(n,p) as monitor at 14.1 MeV with 112.5 mb. Also the two standards are almost the same as the new ones. In addition, they are in agreement with the P.N.Ogoc's data[33] within the error bar. So all of them were selected. The results are shown in Fig.4(a).

The key point to error analysis for the adopted data is to distinguish the statistical and systematical error, or the short, middle and long range error, the later contribution to correlation. Generally, the errors of the sample quantification, standard cross section etc. are long range error, the errors of detector efficiency calibration, correction of multiple scattering etc. are middle range error and the count statistical error is short one. But it should be pointed out that the statistical error could act as systematical one in some cases of the covariance analysis and evaluation. For instance, the statistical error including in the cross section measurement becomes systematical one when the cross section is used as standard for the relative measurement of another cross section. Another thing is that nothing about the information of error is given in some EXFOR subentry or only the total error of the data is given. In this case, the evaluator should read the reference paper concerned and give an estimation of the systematical error according to the experimental set up such as the measurement methods, the detector efficiency calibration, the monitor used etc. An example of error analysis is given in Table 1, which is just a part of the error analysis of the data.

Table 1 Error analysis for ^{63}Cu (n,γ) reaction of experimental data measured by J.Voignier

Data	Error type		Percent	
Voignier[18] (1986) (22006003)	Short range	Statistical error	1.5	1.5
	Middle range	Efficiency of gamma ray spectrometer	6	6.42
		Correction for γ ray attenuation in the sample	1	
		Correction for n transmission through sample	0.5	
		Correction for neutron multiple scattering	2	
	Long range	Neutron long counter efficiency	2	2.92
		Target to sample distance	1.5	
		Extrapolation of gamma strength function	1.5	

2 Covariance Matrix Construction and Mergence

The idea[4] of the covariance matrix construction is as follows.

The measured data f, say cross section, are usually some kind of functions of basic parameters x_k, which can be measured directly in experiment. In general case, x_k vary with energy E. So at energy points i and j, we can get

$$f_i = f(x_{1i}, x_{2i}, \cdots, x_{Ni}) \tag{2.1a}$$

$$f_j = f(x_{1j}, x_{2j}, \cdots, x_{Nj}) \tag{2.1b}$$

Making Taylor expansion of f_i and f_j respectively, and neglecting the higher order terms, it can be written as:

$$\begin{aligned} f_i &= f\left(\langle x_i \rangle\right) + \sum_{k=1}^{N} \frac{\partial f}{\partial x_k}\Big|_i \left(x_{ki} - \langle x_{ki} \rangle\right) \\ &= f_i^0 + \sum_{k=1}^{N} \frac{\partial f}{\partial x_k}\Big|_i \Delta x_{ki} \end{aligned} \tag{2.2a}$$

$$\begin{aligned} f_j &= f\left(\langle x_j \rangle\right) + \sum_{k=1}^{N} \frac{\partial f}{\partial x_k}\Big|_j \left(x_{kj} - \langle x_{kj} \rangle\right) \\ &= f_j^0 + \sum_{k=1}^{N} \frac{\partial f}{\partial x_k}\Big|_j \Delta x_{kj} \end{aligned} \tag{2.2b}$$

From (2.2a, 2.2b), it can be obtained

$$\begin{aligned} \mathrm{Cov}(f_i, f_j) &= \left\langle \left(\sum_{k=1}^{N} \frac{\partial f}{\partial x_k}\Big|_i \Delta x_{ki} \right) \left(\sum_{k'=1}^{N} \frac{\partial f}{\partial x_{k'}}\Big|_j \Delta x_{k'j} \right) \right\rangle \\ &= \sum_{k,k'=1}^{N} \rho_{ij}^{kk'} \Delta f_{ki} \cdot \Delta f_{k'j} = \sum_{k=1}^{N} \rho_{ij}^{k} \cdot \Delta f_{ki} \cdot \Delta f_{kj} \end{aligned}$$

$$(\text{Assume } \rho_{ij}^{kk'} = 0, \text{ when } k \neq k') \tag{2.3}$$

Where $\rho_{ij}^{kk'}$ is the correlation coefficient between parameter x_k and x_j at energy points i and j. ρ_{ij}^{k} is the correlation coefficient of parameter x_k at energy point i and j. Δf_{ki} (Δf_{kj}) is the error of the data f_i (f_j) contributed from the kth parameter at energy point i (j). So if the partial error from each parameter and their correlation coefficients at different energy point are known, the covariance matrix of indirectly measured data can be calculated.

Based on the formulas (2.3), a code EXPCOV[34] was developed for constructing the covariance matrix of the experimental data. By using the code and based on the error analysis of adopted experimental data mentioned above, the covariance matrixes of experimental data for $^{65,\ 63,\ Nat}$Cu were calculated for total cross section, capture cross section, (n, 2n) cross section etc.

In most cases, the data of every reaction channel for ^{65,63,Nat}Cu include several sets of data, which cover different energy range respectively. So the covariance matrixes calculated show the correlation of data in their own energy range only. But what needed is a matrix covered all these different energy ranges and gives out the correlation of all data. For this purpose, the spline program SPC[2] was used to merge the covariance matrixes. Moreover it could make curve fitting and give the smooth optimum values in mathematics as the recommended data.

Among all parameters for fitting the data, the knot selection is a very important step. Generally the knot is selected at the peaks and valleys or the certain structures. And between two knots must have data point. The parameters used in the above 4 reactions are given in Table. 2. The fit values of cross section and the covariance matrixes for ^{65,63,Nat}Cu were obtained by adjusting the parameters concerned. The comparison of the fit values with the experimental data and the correlation coefficient matrix are shown in Figs.1~4 as examples.

Table 2 The parameter values used in the fitting

	Data sets	Knot num.	Spline order	Energy points of output covariance
^{Nat}Cu (n, tot)	4	7	3	21
^{63}Cu (n,γ)	3	5	3	7
^{65}Cu (n, 2n)	3	5	3	10
^{65}Cu (n, p)	5	8	2	18

3 Conclusion Remarks

The covariance data for ^{65,63,Nat}Cu were evaluated and recommended in the energy range from 99.5 keV to 20 MeV based on the available experimental data using the codes EXPCOV and SPC. The data can be as a part of the covariance file 33 in the evaluated library in ENDF/B-6 format for the corresponding nuclides, and also can be used as the basis of theoretical calculation concerned.

The evaluation of the covariance data of the experimental data follows the following steps: 1) experimental data analysis and selection, which is the physical basis for the evaluation; 2) construction of the covariance matrix for each set of data with code EXPCOV; 3) merge of all covariance matrices for each reaction channel with code SPC. The later two are the mathematics processing of the data. The practical evaluation for these nuclides shows that the method is workable and the results are reasonable.

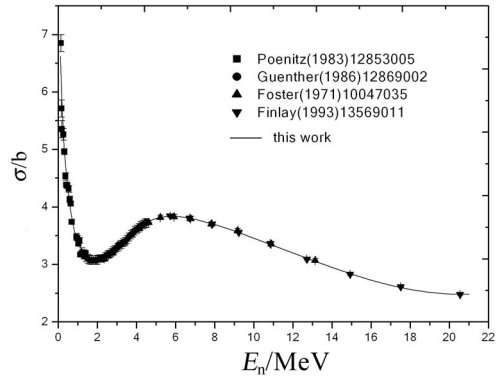

Fig.1 (a) ^{Nat}Cu total cross section

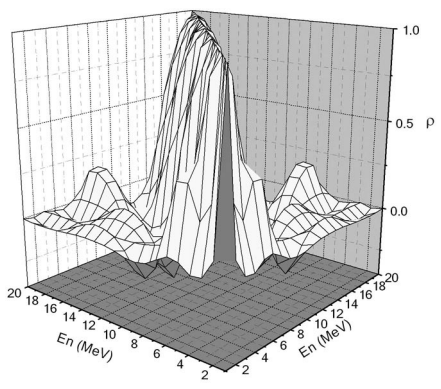

Fig.1 (b) Correlation coefficient matrix for ^{Nat}Cu (n, tot)

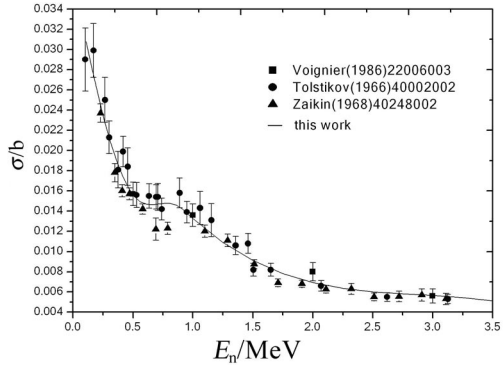

Fig.2 (a) ^{63}Cu (n,γ) cross section

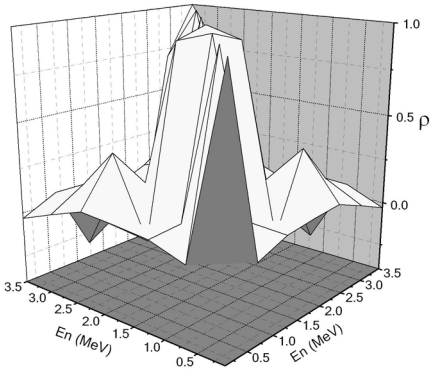

Fig.2 (b) Correlation coefficient matrix for ^{63}Cu (n,γ) cross section

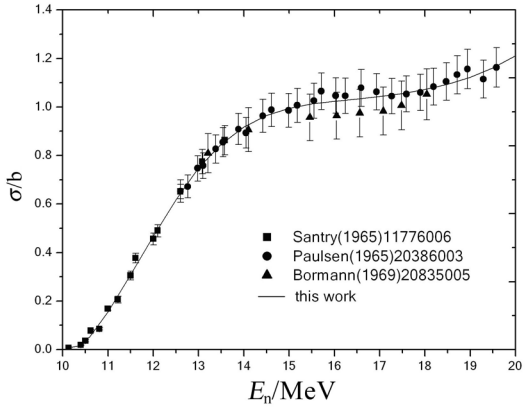

Fig.3 (a) ^{65}Cu (n,2n) cross section

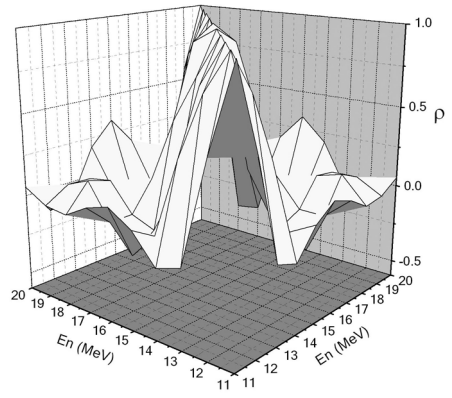

Fig.3 (b) Correlation coefficient matrix for ^{65}Cu (n,2n) cross section

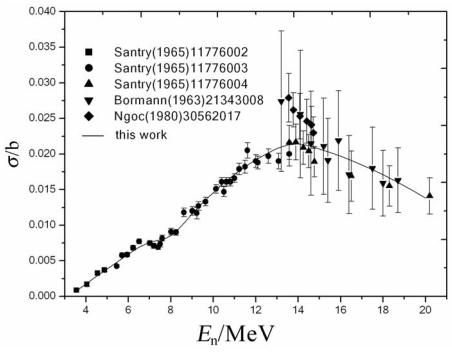

Fig. 4(a) ^{63}Cu (n,p) cross section

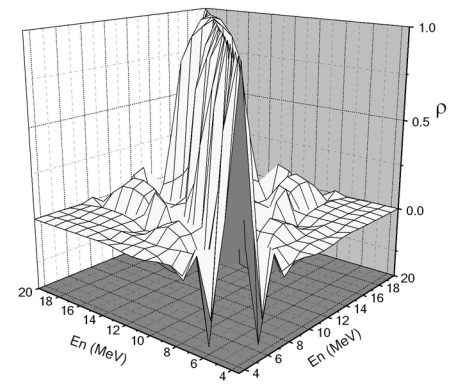

Fig. 4(b) Correlation coefficient matrix for ^{65}Cu (n, p) cross section

Acknowledgement

The authors are grateful to the Chinese Nuclear Data Center for its support and also wish to thank JIN Yongli, WANG Shunuan, RONG Jian et al. for their valuable help.

References

[1] MA Gonggui. CNDP, 21, 59(1999), 22, 64(1999), 23, 91(2000)

[2] LIU Tingjin, et al. CNDP, 11, 116(1994)

[3] JIN Yongli. to be published.

[4] LIU Tingjin, et al. Chinese J. Nucl. Physics, 14(2), 173(1992)

[5] N.Nereson, et al. PR, 89, 775, 5302(EXFOR11060)

[6] A.Bratenshl, et al. PR, 110, 927, 5805 (EXFOR 11155)

[7] M.Mazari, et al. AIF, 1, 69, 5506 (EXFOR 30037)

[8] W.F.E.Pineo, et al. AP, 84, 165, 7405(EXFOR 10542)

[9] J.C.Albergotti, et al. NP, 82, 652, 6607(EXFOR 11467)

[10] J.F.Whalen,et al. ANL-7710, 12, 197101(EXFOR 10071)

[11] D.C.Larson, et al. C,80BNL,, 277, 8007(EXFOR 12882)

[12] W.P.Poenitz, et al. R,ANL-NDM-80, 8305(EXFOR 12853)

[13] P.Guenther, et al. NP/A, 448, 280, 8601(EXFOR 12869)

[14] D.G.Foster, et al. PR/C, 3, 576, 197102(EXFOR 10047)

[15] R.W.Finlay, et al. PR/C, 47, 237, 9301(EXFOR 13569)

[16] A.G.Dovbenko, et al. AE, 27, (5), 406, 6911(EXFOR 40331)

[17] J.M.Blair, et al. R, LAMS-95, 44(EXFOR 11796)

[18] J.Voignier, et al. NSE, 93, 43, 86(EXFOR 22006)

[19] V.A.Tolstikov, et al. AE, 21, (1), 45, 6606(EXFOR 40002)

[20] G.G.Zaikin, et al. AE, 25, (6), 526, 6812(EXFOR 40248)

[21] M.Bormann, et al. ZP, 174, 1, 6302(EXFOR 21343)

[22] R.J.Prestwood, et al. PR, 121, 1438, 6103(EXFOR 11645)

[23] Y.Ikeda, et al. R,JAERI-1312, 88(EXFOR 22089)

[24] P.N.Ngoc, et al. T,NGOC,, 80(EXFOR 30562)

[25] D.C.Santry, et al. CJP, 44, 1183,65(EXFOR 11776)

[26] A.Paulsen, et al. NUK, 7, 117, 6503(EXFOR 20386)

[27] M.Bormann, et al. NP/A, 130, 195, 6906(EXFOR 20835)

[28] Y.Ikeda, et al. JAERI-1312, 88(EXFOR 22089)

[29] N.I.Molla, et al. 94GATLIN, 2, 938, 9405(EXFOR 31449)

[30] T.B.Ryves, et al. MET, 14, (3), 127, 7806(EXFOR 20772)

[31] D.C.Santry, et al. CJP, 44, 1183, 65(EXFOR 11776)

[32] M.Bormann, et al. ZP, 174, 1, 6302(EXFOR 21343)

[33] P.N.Ogoc, et al. T, NGOC, , 80(EXFOR 30562)

[34] WANG Fengge, et al. Master thesis (2002)

Evaluation of Mass Distribution Data from ^{252}Cf Spontaneous Fission

LIU Tingjin

China Nuclear Data Center, CIAE, P.O.Box275(41), Beijing 102413

【**abstract**】 *The mass distribution data of ^{252}Cf spontaneous fission were evaluated based on 7 sets of available experimental data. The measured data were corrected for the standards and γ intensity used by using the new evaluated ones. The errors were made necessary adjusting. The evaluated experimental data were fitted with spline function without any restriction and with symmetric restriction. These two sets of fit data were recommended as reference data of the mass distribution of ^{252}Cf spontaneous fission. The errors of the recommended data were considerably reduced comparing with the measured ones. The light and heavy peaks are not completely symmetric. Also there are fine structures on the right side of the light peak at A=109~111 and left side of the heavy peak at A=137~139. These should be paid attention and studied further.*

Introduction

As well known, the average neutron number and spectrum of ^{252}Cf spontaneous fission are used as the standards in the neutron data measurement and evaluation, the data were recommended internationally[1]. The mass distribution data of ^{252}Cf spontaneous fission play the same role as mentioned above in the fission yield data measurement and evaluation, they are also used as reference. So the data were evaluated. This is the continuation of our reference fission yield data evaluation of ^{235}U and ^{238}U[2] in 2001.

The data were evaluated based on the experimental data available up to now and summarized in this paper. The collection, evaluation and processing of the experimental data are described in sections 1 and 2, the results are given and some problems concerned are discussed in section 3, and finally, conclusion remarks are given in section 4.

1 Collection and Evaluation of Experimental Data

The data, concerning the mass distribution, including "chain yield", "cumulative yield" and "fragment mass yield" were retrieved from EXFOR master library and collected from CINDA and publications concerned. As the data were evaluated for mass distribution, the "chain yield" and "fragment mass yield" measured for more product nuclides were collected first, but "chain yield" measured for less product nuclides and "cumulative yield" were also collected. The later were reviewed in the evaluation to see if need and can get some supplement information and data from them. As a result of collection and primary selection, following 8 sets of data were taken and evaluated.

1.1 H. W. Schmitt[3]

The kinetic energy and time-of-flight of fission fragments were measured by means of surface barrier semiconductor detector. The linear signal of the detector was used to determine the energy E, and the fast timing signal, taken from the transformer secondary, was used as the stop signal of the time-of-flight. The energy and mass distribution were deduced from these energy and time-of-flight spectra. The energy was calibrated with Tandem for ^{79,81}Br and ^{127}I. The mass resolution of the measurement was 1.8 amu for ^{79}Br(2.25%) and 3.2 amu for ^{127}I(2.5%). The post neutron emission mass distribution of the fission fragments was given. The data were corrected for mass resolution with the following formula:

$$N_C(A) = N_U(A) - \frac{\sigma^2}{2}\frac{d^2N_C(A)}{dA^2} \quad (1)$$

where N_C, N_U are the corrected and uncorrected yields respectively, and σ is the mass resolution (full width at half maximum).

The measurement was completed with so called kinetic energy method. The yields of all fragments were measured simultaneously, so the systematic error introduced due to the measurement for individual product nuclides in the radionuclide method can be avoided. Comparing radionuclide method with mass spectrometry method, more nuclides can be measured and the mass range is wider. Due to this is a two-dimensional measurement and furthermore the intensity of the source used is lower (3×10^5 fission per minute), so the count statistic is poorer (maximum at peak only ~350) and the statistic

error is larger. No error was given by the authors either in the paper or in the EXFOR entry. The main error is from statistic and assigned as 5% at peak Y_0, and others were given as $5(Y_0/Y)^{1/2}$ %.

1.2 Thierens[4]

The chain yields of 43 product nuclides were determined with the catcher foil technique and γ Ge(Li) spectrometry method. The intensity of the source used is 1.2×10^6 fis/min. The efficiency of the detector was calibrated and the error was about 5%. The error from γ peak area statistic was neglected. To give the chain yield from measured cumulative yield, the measured data were corrected by using the charge distribution formula with c=0.8

$$p(z)=\frac{1}{\sqrt{\pi c}}\exp[-\frac{(z-z_p)^2}{c}] \qquad (2)$$

Due to the data were measured in earlier date, the γ decay data used were taken from Nuclear Data Sheets, Nuclear Physics and other literatures in 1972-1975. Most of them have been updated now. So the data were corrected for γ decay intensity by using the newly recommended data, first taken from CNDC evaluation and then "Table of Radio Isotopes"(eighth version). Due to the yields were determined from γ ray measurements in different ways, the correction factor β were calculated correspondingly:

(1) The yield was determined by one γ ray, $\beta=\frac{I_0}{I_s}$, where I_0 is for the γ intensity used by the author, and I_s is for the new γ intensity;

(2) The yield was determined by multi γ rays, $\beta=\frac{1}{W}\sum w_i\frac{I_{0i}}{I_{si}}$, where $W=\sum_i w_i$ and $W_i=\Delta I_{0i}^{-2}$;

(3) The yield was determined by M product nuclides and N_j γ rays for j-th nuclide, $\beta=\frac{1}{M}\sum_j\frac{1}{N_j}\sum_i\frac{I_{0ji}}{I_{Sij}}$, where subscript i is for γ ray and j is for nuclide.

1.3 J. Blachot[5]

The chain yields of 27 mass chains were measured by using Al foil as product nuclide catcher. The intensity of the source used is 5×10^6 fis/s, and the time of irradiation is 1~17 days. The fission products were first separated chemically into fractions containing rare earths, alkalis, alkali-earth, ruthenium and zirconium and niobium, and then the γ rays for the individual nuclide of them were measured with Ge(Li) detector, whose energy resolution is 2.5 keV at 1.3 MeV. The yields of heavy peak were normalized into 100%, giving a yield 6.05 pc/fis for ^{140}Ba monitor, and the yields of others were normalized to ^{140}Ba. The data were corrected for the contribution from the nuclides after the nuclide measured in the mass chain with charge distribution formula like equation (2).

As monitor, the yield for ^{140}Ba (A=140 mass chain) were evaluated specially in this work (see below), as a result, 5.674±0.098 was obtained. So the data were corrected to this new monitor data. The data at A=99, 111, 117, 135,137, 149 were deleted due to they are too large (A=149) or too small (others).

1.4 W. E. Nervik[6]

The R-values of 36 product nuclides (A=77~166) were measured with radiochemistry method. The product nuclides were collected with Al foil and separated chemically, and the γ or β radioactive were measured with NaI detector or β counter. The intensity of the ^{252}Cf source used was 1×10^6/m, 2×10^7/m or 7×10^7/m. The R-values were relative to the yields of ^{99}Mo and the same nuclide as measured from ^{235}U fission at thermal energy and ^{99}Mo from ^{252}Cf spontaneous fission. The chain yields were calculated by using the yields concerned, they are 6.14 pc/fis for ^{99}Mo from ^{235}U fission at thermal energy and 2.57 ± 0.03 for ^{99}Mo from ^{252}Cf spontaneous fission. The former was taken from the evaluated data, which is almost the same as recently recommended by us(6.15 pc/fis). The later was measured by the author(the average of three direct measurements).

The data were read from Table 1 of the paper (there is no entry in EXFOR Library). As monitor, the yield for ^{99}Mo from ^{252}Cf spontaneous fission was evaluated specially in this work(see below), the recommended value is 2.583±0.062. The data were corrected with this data. The errors given in the paper are the deviation of the multi measurements, furthermore, the time of measurements was not so much, only reflecting the repetition character of the measurements, not real one, so they were not used and were assigned as 8% for yield $Y\geqslant1$%, 15% for 0.05% $\leqslant Y<1$% and 25% for $Y<0.05$%. The errors assigned are quite large, because the measurement was at quite early date, using NaI as detector. The data at A=112, 125, 137 were deleted due to they are too small.

1.5 K.F.Flynn[7]

The cumulative yields of 39 product nuclides were measured with radiochemistry separation, followed by β counting or direct γ spectrum measurement. The absolute measurements were made by determining the fission rates for nuclides ^{99}Mo, ^{111}Ag, ^{132}Te, ^{140}Ba. The data were normalized to yield 2.60 pc/fis of ^{140}Ba monitor, which is the average of three sets of data, one of them 2.48±0.13 was

absolutely measured by the author, other two were taken from the literatures. The recommended data were cumulative ones, not corrected with the charge distribution to give out the chain yields, but the author declared that from the calculations the corrections for all were smaller than 1%. The errors given were estimated, they were about 10% in general, and about 5% for multi measurements.

First, the data were checked to see if they could be used as chain yields. It was found that the data of ^{123,125}Sn and ^{127,129}Te are only for ground (the former) or isometric (the later) states, there are large differences from the corresponding chain yields. The data of the ground and isometric states of nuclide ^{115}Cd were summed to get the chain yield. Second, the data were corrected for the ^{140}Ba monitor data by using the new evaluated data in this work (see below) 2.583±0.062 pc/fis. Third, the data were compared with others, it was found that the data of light peak (A=121~129) are systematically small. They were deleted.

1.6 LI Ze[8]

44 chain yields from mass number 85 to 157 were absolutely measured with Ge(Li) γ ray spectrum method. The efficiency of the detector was calibrated carefully and the energy resolution was 1.85 keV at 1.332 MeV. Al catcher foil technique was used, and the collection efficiency of the catcher foil for fission fragments was studied precisely to get the fission rate. The ^{252}Cf source used was 0.3μg, (1.226±0.018) ×104 fis/s in the 0.374π sterad. The areas under the light and heavy peaks are 99.76% and 102.08% respectively. The data were corrected for the decay of the products during the collection, cooling, measurement, γ pile and cascade effect. To get the chain yields, the data were corrected by using the charge distribution formula (2) with constant c=0.8. The errors given in the data table include statistic, fission rate(1.5%), detector efficiency(2.4% or 4.2%), correction for pulse pile(0.5%) and γ cascade (0.2%~2.4%).

As regards as the data measured by radio-chemistry and γ spectrum method (not kinetic energy method), more nuclides were measured in this work. Furthermore, this is an absolute measurement, and the integral areas of the light and heavy peaks are in agreement with 100% within the error of the fission rate. Using new γ decay data, taken from CNDC evaluation or "Tables of Radio Isotopes" (8th version), the data were corrected. But for ^{117}Cd, there may be something wrong for the γ intensity given by the author, the yield was not corrected.

1.7 CHEN[9]

The chain yields of 35 mass chains were measured absolutely with radiochemistry method by using the source, whose intensity was already known. The recovery efficiency of chemistry separation was measured. The radioactivieies were recorded with proportional counter and scintillator for β and NaI for γ rays. The efficiency of the γ detector was calibrated experimentally. In the measurements of each nuclide, either the calibrated efficiency γ curve was used, or the efficiency of the γ and β detectors was measured directly. The errors of the data are about 3%~15%, including the errors of the detector, chemical recovery efficiency, fission rate and peak area count.

The data were read from Table 1 of the paper (no entry in EXFOR Library). Comparing with LI's data, agreement between them is quite well, but there are fewer data in the valley range. The chain yields for A=113, 134, 135, which were deduced from ^{113g}Ag, ^{134}Te, ^{135}I respectively, are too large. These nuclides are far from the corresponding stable nuclides of the chain by 2-3 charges. The correction factors, taken from the literatures, are quite large (calculated by using ENDF/B-6 data are more large), the yields deduced are not reliable, and their errors are enlarged 10% for mass chains 113,135 and 13% for mass chain 134. Also the error for ^{99}Mo was enlarged from 3.5% to 5%.

1.8 J.S.Fraser[10]

The fragment mass distributions of pre and post neutron emission were measured by using double time of flight method with a source of intensity 6×10^4~3×10^5 fis/m. The flight paths were 144.3 cm and 146.2 cm, and the time resolution was 1.35 ns. The data were corrected for the mass resolution.

The mass yields were given for each mass number in the mass range from 80 to 172, which are quite complete. But the statistic of the data is poorer due to the weak source and long flight distance. Furthermore, there may be some problems for the energy and mass calibration. Comparing with others, for example LI and Schmitt, the light peak is "thin", and the heavy peak is systematically somewhat move to right (Fig.1). The data were abandoned in the evaluation at last.

The all adopted, corrected, adjusted experimental data are shown in Fig.2. There are 7 sets of data altogether. It can be seen that they are in agreement within error bar, except for a few special data points.

2 Processing of the Evaluated Experimental Data

The evaluated experimental data were processed as following.

2.1 The Data at Mass Number 99 and 140

The data at mass number 99 and 140 were used as monitor in the measurements of Blachot, Flynn and Nervik, and these data need to be renormalized to

them. So, they were processed specially first. The data accepted at these mass numbers are listed in Table 1. They were averaged with weight by using code AVERAG[11]. The mean and their external, as given in Table 1, were recommended. It should be point out that the reduced χ^2 (1.4) is larger than 1 for A=99, this is due to the deviation of Schmitt's data from others.

Table 1 Data at A=99,140

Author	A=99		A=140	
Chen	2.52	0.13	5.77	0.20
Lize	2.55	0.11	5.76	0.18
Flynn	2.48	0.13	5.50	0.28
Nervik	2.57	0.21	6.32	0.51
Schmitt	3.10	0.22	5.81	0.31
Thierens	2.67	0.12	5.35	0.22
Mean	2.583	0.062	5.674	0.098

2.2 Spline Fitting for Experimental Data

The adopted evaluated experimental data were fitted with code SPF[12], a spline fit code for multi sets of data with knot optimization. The primary knots were selected carefully based on the shape of the curve and optimized by the code automatically. The best result was got with 26 knots, and the reduced χ^2 is 1.551. To distinguish the symmetric spline fitting (see below), this is called normal spline fitting hereafter.

2.3 Symmetric Spline Fitting

Suppose that the all fission is binary one, on which is based all Gaussian model[13,14] of the fission mass distribution, the fragment mass distribution should be symmetric to the mass number $\overline{A}=(A_f-\overline{\nu})/2=124.1$, where A_f is the mass of fission system, and $\overline{\nu}$ is 3.7661, the average neutron number of the fission, recommended internationally[1]. To get the symmetric fitting, the experimental data under the light peak were reflected around $\overline{A}$, that is $A'=252-\overline{\nu}-A$, and put them together with the data under heavy peak, then fit them by spline function, also of course, with carefully selecting and adjusting the knots to get the best fitting (the reduced χ^2=1.795) as above. Finally, the fit data were reflected to the light peak, and get a symmetric fit data for the mass distribution.

3 Results and Discussion

The spline fit data are shown in Fig.2 with comparing to evaluated experimental data.

To check the correctness of the spline fit curve, the total yields under the light and heavy peaks as well as $\overline{\nu}$, nu bar, were calculated. The borderline of light and heavy peak is taken 124, which was calculated from the mass number of the ^{252}Cf and the nu bar 3.7661. The results are listed in Table 2. It can be seen that for the fitting with no restriction, the integral yield under heavy peak is very well in agreement with 100 %, and the total yield under light peak is in agreement with 100% within error 1.3 %, the nu bar is in agreement with the internationally recommended value 3.7661 within error 2.93 %. For fitting with symmetric restriction, the integral yield under light and heavy peaks is in agreement with 100% within error 1.0 %, the nu bar is in agreement with the internationally recommended value 3.7661 within error 1.86 %.

The comparison between the results of normal and symmetric spline fitting is shown in Fig.3. It can be seen that, in general, they are in agreement very well, but there are some difference at the peaks. For light peak, the peak of normal fitting is narrower than symmetric one, and for the heavy peak, the situation is opposite. Also the right side of the light peak is thinner for the data of normal fitting than symmetric one and the left side of the heavy peak is opposite (see Fig.3). The fact that the χ^2 of the fitting is 1.551 for normal fitting and is 1.795 for symmetric fitting shows that there is asymmetric mass distribution to some content.

Is there a systematic trend that the peak of light fragment is higher and thinner, and the area under the peak is somewhat smaller? The fit results show this. Also the individual experimental data by different authors show the same thing. In Table 3 is shown some results by different authors, who measured more product nuclides and the integral yields under peaks can be calculated more reliably. The data were given in the paper for LI and CHEN, and calculated in this work for Schmitt and Fraser by using the data given by the authors without any correction or adjusting. It can be seen that the yields under light peak of all four authors are smaller than ones under heavy peak. Comparing the light and heavy peaks of LI's and Schmitt's data (Figs.4, 5), it can be seen that the light peak is thinner than heavy one. All of these could not be explained by experimental measurement error, and should say it is a systematic trend. Possibly, there is physical background. In the fission process, in addition to binary fission emitting neutrons, there may be some other fission processes like emitting α or other light particles or trinary fission. G. K. Mehta's[15] investigation showed that the α-particle accompanied fission is 1% of the binary fission, and the mass distribution of α-particle accompanied fission shifts to the left of ordinary binary fission, but the shift is different, larger for light peak, and smaller for heavy peak. Also the light peak becomes thinner, the half width at the half

maximum changes from about 7.5 to 6.8 amu (see Fig.4 of the paper). α-particle or other light particle accompanied fission also makes nu bar increase, this corresponds to the nu bar (Table 2, no restriction) larger than the internationally recommended based on the measuring neutron.

The experimental and fit data show that there is a "shoulder" on the right side of light peak, at mass number 109~111, and correspondingly on the left side of heavy peak, at mass number 137~139. It was discussed in many papers[3,6,10] that there is fine structures on the mass distribution of ^{252}Cf spontaneous fission, although the structures given by them were not completely same, and could not say certainly for each individual measurement due to these structures are only for one, two or three mass number and the errors of the data are quite larger, maybe statistical fluctuation. Now, the data are fitting of 7 sets of experimental data, and show a "shoulder", a systematical behavior, there should be structures at mass number A=109~111, 137~139, although the shape of the structures could not say certainly due to so many sets data put together and the fine structures may be wiped to flat. The fine structures should be determined further by the measurements with high accuracy.

Comparing the errors of spline fit data without and with symmetric restriction with the errors of the evaluated experimental data (see Table 4), it can be seen that the errors of fit data are considerably reduced, especial for the data at peaks (from 3%~10% to about 1.5% and 1.1%). This is due to the statistical reason. As well known that in the case of the statistical consistency of the data, multi measurements make the error reduced. In present case, there are 7 sets of data used for fitting, which makes the error reduced, roughly, $7^{1/2}$=2.6 times. Furthermore, the cure fitting also makes the error reduce due to more data points are considered in the fitting. There are exceptional points, whose errors are larger than fitted experimental data. This is due to statistical inconsistency, there are large differences between the each set of data for them.

Table 2 The reduced x^2, total yield and nu bar from fit data

Fit mode	Reduced χ^2	Total yield			Nu bar
		Light peak	Heavy peak	Total	
No restriction	1.551	98.76	99.77	198.52	3.8764
Symmetric	1.795	98.98	98.96	197.95	3.6962

Table 3 The integral yields under light and heavy peak by different authors

Author	LI Ze	CHEN	Schmitt	Fraser
Light	99.76	98.43	99.88	97.34
Heavy	102.08	100.97	99.99	97.98

Table 4 Error comparison of the fit data with evaluated experimental data(%)

Author	Peaks	Valley	Wings	Comments
J.Blachot	5–7	40–100	10–21	
CHEN	3–5	20–50	10–16	
K.F.Flynn	5–10		~10	No data at valley
LI	3–5	~20	10–15	
W.E.Nervik	~8	~15	15–25	
H.W.Schmitt	~5	10–68	10–50	More nuclides at valley and wings
H.Thierens	5–8	~10	10–18	
Normal fitting	~1.5	10–28	10–25	Except for special points 123,124,167,168
Symmetric fitting	~1.1	10–28	10–25	Except for special point 124

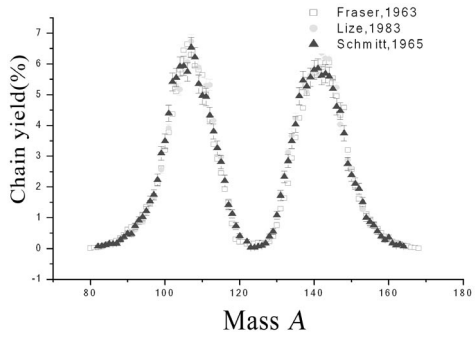

Fig.1 Comparison of Fraser's data with Lize's and Scmitt's data

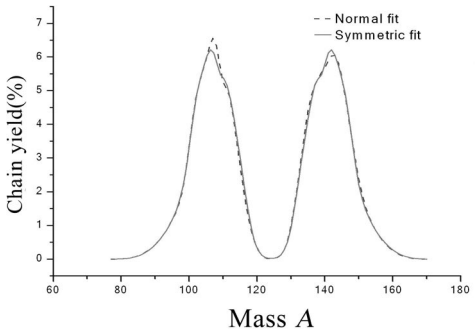

Fig.3 Comparison of normal and symmetric fit data

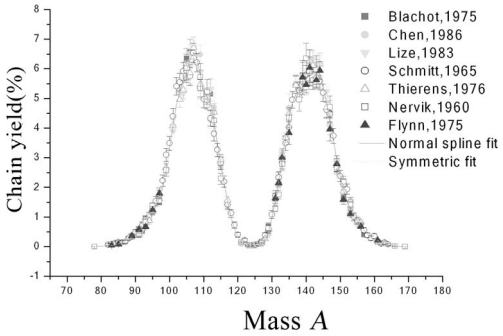

Fig.2 Mass distribution of ^{252}Cf spontaneous fission

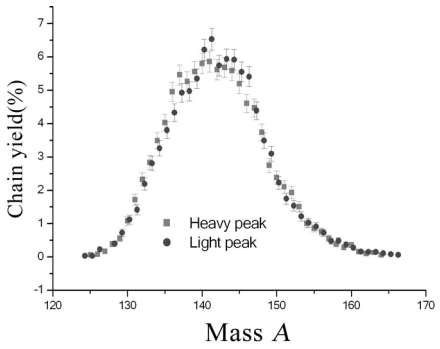

Fig.4 Symmetry comparison of Scmitt's data

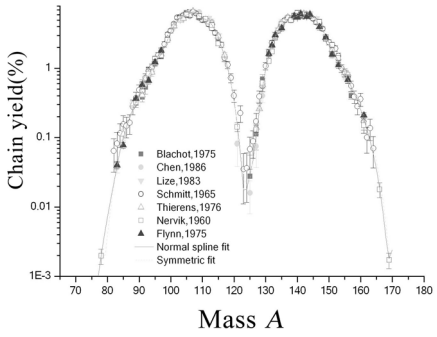

Fig.2-1 Mass distribution of ^{252}Cf spontaneous fission

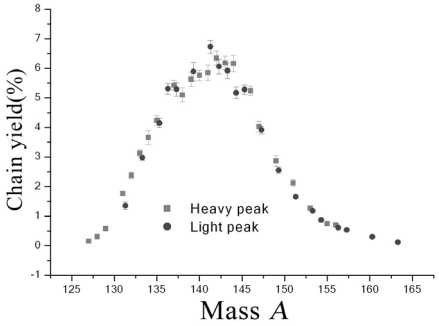

Fig.4-1 Symmetry comparison of Li's data

4 Conclusion Remarks

The mass distribution data of ^{252}Cf spontaneous fission were evaluated based on 7 sets of available experimental data. The measured data were corrected for the standards and γ intensity used by using the new evaluated ones. The errors were made necessary adjusting. The evaluated experimental data were fitted with spline function without any restriction and with symmetric restriction. These two sets of fit data were recommended as reference data of the mass distribution of ^{252}Cf spontaneous fission. The errors of the recommended data were considerably reduced comparing with the measured ones.

The light and heavy peaks are not completely symmetric to the mass number $A_{f-\overline{\nu}}$. The light peak is somewhat thinner, and the area under it is about 1% smaller than one under heavy peak. Also there are fine structures on the right side of the light peak in A=109~112 and left side of the heavy peak 136~139. There should be physical background for these phenomena, and should be paid attention to determine it accurately and to study the physical reason further.

References

[1] H. Conde. NEANDC-311"U", INDC(SEC)-101, P.99 and 108(1992)

[2] LIU Tingjin, et al. CNIC-01679, CNDC-0033(2002)

[3] H. W. Schmitt, et al. Phys. Rev., 137(4), 837 (1965)

[4] H. Thierens, et al. Nucl. Instr. & Meth., 134, 299(1976)

[5] J. Blachot, et al. Radiochi. Acta, 134, 299(1976)

[6] W. E. Nervik. Phys. Rev., 119(5), 1685(1960)

[7] K. F. Flynn, et al. Jour. Inorg. Nucl. Chem., 37, 881(1975)

[8] LI Ze, et al. Chin. Jour. of Nucl. Phys., 5(3), 221(1983)

[9] CHEN Qingjiang, et al. Atom. Ener. Scie. & Tech.(in Chinese), 20(2), 161(1986)

[10] J. S. Fraser, et al. Can. Jour. of Phys., 41, 2080(1963)

[11] LIU Tingjin. CNDP,19,103(1998)

[12] LIU Tingjin, et al. CNDP, 2, 58(1989)

[13] A. C. Whal. Systematics of Fission-Product Yields, Private Comm. (2001)

[14] Katakura. A New Parameter Set of Fission Product Mass Yields Systematic, Private Comm.,(2002)

[15] G. K. Mehta, et al. Phys. Rev.,C7(1), 373(1973)

Evaluation of Prompt and Delayed Neutron Yields for ^{233}U from 10^{-5} eV to 20 MeV

YU Baosheng CHEN Guochang

China Nuclear Data Center, CIAE, P.O.Box275(41), Beijing 102413

【**abstract**】 *The neutron number of prompt (ν_p) and delayed (ν_d) emission per fission event was evaluated for ^{233}U based on absolute measurements and measurements relative to the spontaneous fission ν of ^{252}Cf. In addition to experimental data, some systematics was used. The dependence of prompt neutron number on incident neutron energy was given by approximated linear function from 10^{-5} eV to 20 MeV.*

Introduction

For safety and economic reasons, the reactor physicist and designer need to make neutron calculation of multiplying media with a very good accuracy. The accurate number of prompt and delayed neutron in neutron-induced fission of ^{233}U is required very much along with the quick development for U-Th fuel cycle reactors and nuclear system concerned. For nuclear technique application, the number of neutron emitted per fission event is required with the accuracy from 0.25% to 0.5% in general. The data were evaluated based on the experimental data available and compared with ENDF/B-VI, JENDL-3.2 and JENDL-3.3.

1 Evaluation of Prompt Neutron Yield

The experimental data of prompt and delayed neutron yields were measured by using absolute and ratio measurement techniques. The main measured data [1~17] from 1956 up to now were collected, analyzed and evaluated and they are all summarized in Table 1.

The early data were measured by B.C.Dievn[1] at 0.08 MeV, J.C.Hopkins[6] from 0.28 MeV to 3.93 MeV and D.S.Mather[7] from 0.96 MeV to 4.0 MeV, respectively. The data provided by D.S.Mather[7] are only in several energy bind between 0.96 MeV and 4.0 MeV. The data of B.C.Diven[1], J.C.Hopkins[6] and D.S.Mather[7] were measured by using moderating large liquid scintillator detector. Because this kind of detector is also sensitive to γ-ray, so the data with it are usually with large γ-ray background. The data measured by B.C.Diven[1] and by J.C.Hopkins[6] were of large statistical errors and fluctuation. So the data[1,6,7] were abandoned.

Much important improvement was performed along with the development of the nuclear technique. The ν_p was measured relatively to spontaneous fission ν_p of ^{252}Cf. The difference of detector efficiencies for fragment and neutron from ^{252}Cf and ^{233}U fission was taken into account. The accurate data have been carried out mainly since 1970.

The data of J.W.Boldeman[8] were measured with a 240 L gadolinium-loaded liquid scintillator and a high-speed methane-filled double ionization chamber in energy region from 0.3 MeV to 1.87 MeV in 1971. The coincidence technique between fission fragment and prompt neutron were used to avoid alpha piling up. The time-of –flight method was used to improve the ratio of induced fission to spontaneous fission. The corrections were carried out for background effects, dead-time loses, delayed γ-ray effects and so-called "France effect" (the detecting efficiency for the prompt fission γ-ray has a bearing on the fission neutron number in liquid scintillator stank). The data are quite accurate.

The data of B.Nurpeisov[10] were measured by using Li(p,n) and T(p,n) monoenergetic neutron sources from 0.08 MeV to 1.4 MeV in 1973. In order to reduce γ-ray background, the proportional counter system was used, which consists of 24 ^3He counters in cylindrical paraffin block (or using Born counters with organic moderator). The detector was calibrated with serial of neutron sources. The γ-ray background was reduced. The multiplayer ionization chamber with 85% counting efficiency was used for detecting fission fragment. The difference of detector efficiencies for fragments and neutrons of ^{252}Cf and ^{233}U fission was taken into account.

Table 1 Information concerning prompt neutron yields for ^{233}U(n,f) reaction

Year	Author	En(MeV)	Detector	Monitor Reaction	Standard Used	Comment
1956	B.C.Diven	0.08	MTAK	^{235}U(n,f)	2.47±0.03	to 0.0253 eV
1956	I.Johnstone	14.1	PROPC	^{235}U(n,f)		
1958	A.N.Protopopov	14.8	PROPC FISCH	^{233}U(n,f)	2.52±0.03	to 0.0253eV
1958	G.N.Smirenkin	4.0,15.0	PROPC FISCH	^{233}U(n,f)	2.55	to 0.0253eV
1961	N.N.Flerov	14.0	BF3-PROPC	^{233}U(n,non)	2.85±0.1	
1963	J.C.Hopkins	0.28~3.93	MTAK	^{252}Cf(0,f)	3.771	same group of Ref.1
1965	D.S.Mather	0.96~4.0	SCIN FISCH	^{252}Cf(0,f)	3.782±0.024	to 0.0253 eV
1971	J.W.Boldeman	0.3~1.87	STANK	3.782	3.782	
1972	A.I.Sergachev	0.07~2.1	SOLST	absolute		
1973	B.Nurpeisov	0.08~1.4	BF3-PROPC	^{252}Cf(0,f)	3.756	same group of Ref.4
1973	B.Nurpeisov	0.08~0.7	BF3-PROPC	^{252}Cf(0,f)	3.756	Revised early data
1975	B.Nurpeisov	0.0~4.89	BF3-PROPC	^{252}Cf(0,f)	3.756	

MTANK: Moderating Tank Detector
SCIN : Large Liquid Scintillation Counter(Loaded with Gadolinium)
FISCH : Fission Chamber
PROPC: BF-3 Proportional Counter
SILST: Silicon detector

In the meantime, a set early experimental data were renormalized by recommended standards from 0.08 MeV to 0.7 MeV. As a result the data measured by B.Nurpeisov[10,11] and J.W.Boldeman[8] are consistent with each other within errors.

In order to measure the prompt fission neutron yields, the fission number induced by neutron and the prompt neutron were absolutely measured simultaneously by A.I.Sergachev[9]. The fission fragments were detected by using a high-speed methane-filled ionization chamber. A silicon semiconductor detector was used to detect prompt neutron and to coincidence with the fission fragments. The data in the energy range from 0.07 MeV to 2.1 MeV are in agreement with ones of B.Nurpeisov[10,11] and J.W.Boldeman[8] within errors.

The data were measured by B.Nurpeisov[12] below 4.89 MeV in 1975 again, by using proportional ^{3}He counters as neutron detector. The neutron detector system was calibrated by serial of neutron sources. A scintillator was used for fission neutron spectrum measurement, so the γ-ray background was further reduced. The difference of detector efficiencies for fragments and neutrons of ^{252}Cf and ^{233}U fission was taken into account. The data are in agreement with ones of J.W.Boldeman[8], A.I.sergachev[9], within errors.

Around 14 MeV, there are data measured by I.Johnstone[2], G.N.Smirenkin[4] and N.N.Flerov[5]. The data of I.Johnstone[2] were systematic divergence with other ones and there is no monitor information. So the data could not be corrected and were abandoned. Meanwhile, the data were measured by G.N.Smirenkin[4] at 4.0 MeV and 15.0 MeV in 1958. The data of G.N.Smirenkin and B.Nurpeisov were from same group, and the data at 4.0 MeV are consistent each other. So only G.N.Smirenkin's data were used. The data measured by A.N.Protopopov[3] at 14.8 MeV are consistent with G.N.Smirenkin's data[4]. The data of A.N.Protopopov[3], G.N.Smirenkin[4] and N.N.Flerov[5] were all corrected by renormalized to recommended standards. The renormalized data are consistent with each other and were all adopted.

Below 0.08 MeV, there are five sets of data measured by B.C.Diven[1], A.I.Sergackev[9] and B.Nurpeisov[10~12]. The thermal energy point value was evaluated by N.E.Holden[13] in 1988, and the evaluated value was in very good agreement with there works within errors.

2 Recommendation of Prompt Neutron Data

2.1 Reference Standard

For the prompt neutron number of ^{233}U, the early experimental data were measured relatively to the prompt neutron yields of ^{233}U(or ^{235}U) at thermal energy point. With the improvement of measured method, prompt neutron emission at thermal energy of ^{235}U (or ^{233}U) and spontaneous fission of ^{252}Cf were studied in more detail to understand the characteristics. The ν_p value of ^{252}Cf spontaneous fission was gradually used as the reference standard.

The distinct advantages of ^{252}Cf are its relatively high spontaneous fission rate with respect to its alpha decay rate and easy to get high intensity spontaneous fission neutron source.

Before 1972, the prompt neutron number measured by large liquid scintillator is systematically higher 7% than that by using proportional counter system, and the errors of themselves were larger than 1%. In order to found the reason of the discrepancy, further experiments were made with the improved measurement method. In 1972, at IAEA Panel on Neutron Standard Reference Data[18], a preliminary value 3.724±0.008 was recommended based on experimental data available and taken in the systematically high value of liquid scintillator measurement.

Through the improvement of measured method, it was found that the discrepancy comes from the effects of delayed γ-ray and "France effect". In addition, the corrections are needed in ν_p measurements for differences of the efficiencies of neutron detector for the fission neutron spectrum. Therefore, the improvement of neutron detection and reasonable corrections were specially paid attention in the evaluation at that time. The ν_p value of ^{252}Cf as a reference standard was discussed and reevaluated at IAEA Consultant's meeting in 1988. The recommended value ν_p was 3.7661±0.054[19]. The accuracy of this standard is adequate for all current applications of ν_p value.

2.2 Recommendation of the Data

On the basis of evaluation mentioned above, the accurately measured data[8~13] were adopted in this work. Most of the measured data were performed relatively to ^{252}Cf spontaneous fission as standard, the ^{252}Cf standard value is 3.7661±0.054. The relatively measured data were renormalized, the absolutely measured data of A.I.Sergachev[9] are quite accurate. A weighted orthogonal polyonminal least squares fitting was applied to get the dependence on incident neutron energy from 10^{-5} eV to 15 MeV.

In order to obtain the energy dependence of prompt neutron data up to 20 MeV, the fitting data above were extrapolated to 20 MeV according to their trend. The data were compared with ENDF/B-6, JENDL-3.2 and JENDL-3.3, shown in Fig.1.

3 Evaluation of Delayed Neutron Yields

Accurate delayed neutron yield data are vital to the development of static and dynamic calculations for fast reactor and to the fission physics researches. But the available delayed neutron yields data are very limited. Many scientists studied the dependence of delayed neutron yield of heavy fission nuclei on the induced fission neutron energy. Some evidence was obtained for heavy fission nuclei that the delayed neutron yield is independent of the neutron energy from 0.1 MeV to 4 MeV or 5 MeV, then drops in an energy interval of about 2 MeV, and then no measured data untill to the energy about 15 MeV.

The data were measured by C.F.masters [14] at 3.1 MeV and 14.9 MeV in 1969. Another two sets data were carried out by M.S.Krick [15] from 0.05 MeV to 1.75 MeV and from 4.0 MeV to 6.0 MeV in 1972. The data measured by C.F.masters [14] and M.S.Krick[15] were corrected for the sample composition, self-absorption in fission counters and extrapolation of fission spectra from the measurement bias to zero bias and low neutron contamination to source spectrum.

In order to recommend the accurately delayed neutron yield data, the data measured were considered and revised by A.E.Evans[16]. Some identical fission foils were used in fission chambers to monitor fission rates in the samples. And also a single ^{238}Pu-Li neutron source, which was certified by the National Bureau of Standards of USA, was used to calibrate delayed neutron detectors. The calibration result by ^{238}Pu-Li neutron source indicated that the yield measured by C.F.masters [14] and M.S.Krick [15] are 4.6% higher and should be reduced accordingly. Furthermore, the quantity of fission foils used in sample was remeasured by using a low geometry alpha-country system with well determined accuracy. The remeasured value was in agreement within 1% with the value of the foils used, so the yield values were not corrected for the sample.

The data at thermal energy point were measured by S.B.Sorzakov[17] relatively to ^{235}U prompt fission neutron yield in 1995. The data measured by S.B.Sorzakov[17] were renormalized to ^{235}U prompt fission neutron yield of ENDF/B-6. The renormalized value was adopted in this work.

On the basis of these considerations mentioned above, the delayed neutron data measured by C.F.masters [14] and M.S.Krick [15] were corrected for calibration source, and the new revised values were adopted in this works using these experimental data and considering the dependence of delayed neutron on incident neutron energy discussed above, the evaluated delayed fission neutron yields are shown in Fig.2 compared with ENDF/B-6, JENDL-3.2 and JENDL-3.3.

The total fission neutron yields are the sum of prompt and delayed fission neutron yields, shown in Fig.3 with the data from ENDF/B-6, JENDL-3.2 and calculated result.

5 Summary

The evaluation of prompt neutron number was carried out below 15 MeV based on available experimental data up to now. Present evaluated data are more reliable due to based on both of absolute and relative measurements. The dependences of total neutron emission number on incident neutron energy were given from 10^{-5} eV to 20 MeV.

In the case of delayed neutron, present evaluated data are a little lower than others at 14 MeV as shown in Fig.3. The reason is that the revised data of C.F. Wasters[14] and M.S.Krich[15] were adopted in this work. Another point is that the delayed neutron yields from ENDF/B-6 above 6 MeV is too high when the delayed neutron ν_d directly taken from ENDF/B-6. The data present used were obtained by subtracting the prompt neutron ν_p from total fission neutron number ν_{tot}.

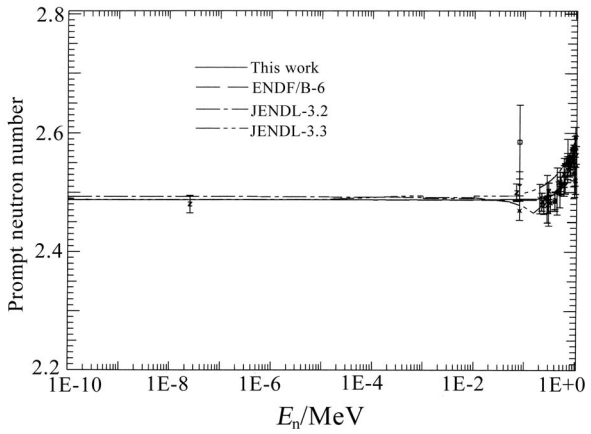

Fig.1a Comparison evaluated and measured prompt neutron yield for ^{233}U

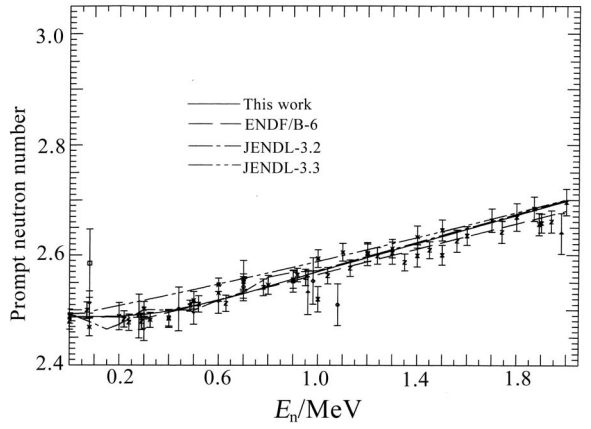

Fig.1b Comparison evaluated and measured prompt neutron yield for ^{233}U

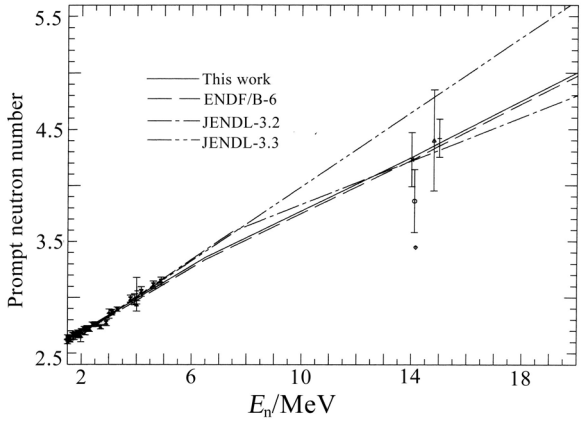

Fig.1c Comparison evaluated and measured prompt neutron yield for ^{233}U

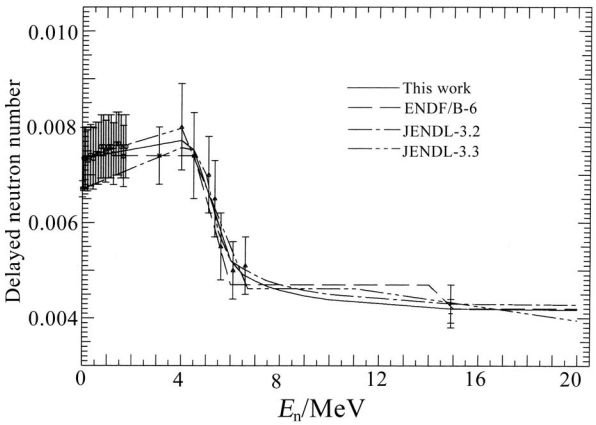

Fig.2 Comparison evaluated and measured delayed neutron yield for ^{233}U

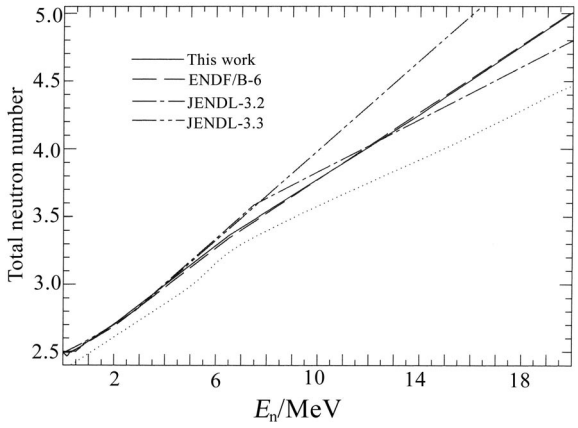

Fig.3 Comparison evaluated total fission neutron yield for ^{233}U

Acknowledgments

The authors are indebted to CNNC (China National Nuclear Corporation) and CIAE for their supports and thank Professors ZHANG Huanqiao, HAN Hongyin, TANG Guoyou and SHI Zhaomin for the interesting and helpful discussions.

References

[1] B.C.Diven, et al. Nucl. Phy., 101,1012(1956)

[2] Johnstone, et al. AWRE-NP/R-1912(1956)

[3] A.N.Protopopov, et al. AE,5,71(1958)

[4] G.N.Smirenkin, et al. AE ,4,188(1958)

[5] N.N.Flerov, et al. EXFOR Data 40639005(1961)

[6] J.C.Hopkins, et al. Nucl. Phy., 48,433(1963)

[7] D.S.Mather, et al. Nucl. Phy.,66,149(1965)

[8] J.W.Boldeman, et al. Nucl.Eng.,25,321(1971)

[9] A.I.Sergachev, et al. J.YF,16,475(1972)

[10] B.Nurpeisov, et al. EXFOR Data 40189003 (1975)

[11] B.Nurpeisov, et al. EXFOE Data 40189004 (1975)

[12] B.Nurpeisov, et al. AE,39.199(1975)

[13] N.E.Holden, et al. Nucl.Sci.Eng., 98,174(1988)

[14] C.F.Masters, et al. Nucl.Sci.Eng., 36,202(1969)

[15] M.S.Krick, et al. Nucl.Sci.Eng., 47,311(1972)

[16] A.E.Evans, et al. Nucl.Sci.Eng., 50,80(1973)

[17] S.B.Borzakov, et al. AE,79,231(1995)

[18] E.J.Axton, et al. IAEA-PL-2646-2/31(1972)

[19] J.W.Boldeman, et al. INDC(NDS)-220, 21 (1989)

Level Width Broadening Effect

ZHANG Jingshang

China Nuclear Data Center, CIAE, P.O.Box275(41), Beijing 102413

【**abstract**】 *In file-6 for double-differential cross sections, the level width broadening effect should be taken into account properly due to Heisenberg' uncertainty. Besides level width broadening effect, the energy resolution in the measurements is also needed in fitting measurement procedure. In general, the traditional normal Gaussian expansion is employed. However, to do so in this way the energy balance could not be held. For this reason, the deformed Gaussian expansion functions with exponential form for both the single energy point and continuous spectrum are introduced, with which the normalization and energy balance conditions could be held exactly in the analytical form.*

Introduction

To set up file-6 for double-differential cross sections of light nuclei with the new approach[1], the Heisenberg' uncertainty relation, as a basic principle in quantum mechanics, should be taken into account properly. However, the shape of expansion for this uncertainty is not provided. Usually the traditional Gaussian expansion form is employed for the level width broadening expansion. However, the normal Gaussian expansion does not keep the normalization and energy balance. An additional factor is added in order to keep the normalization condition[1], while in this way the energy balance is still not held. Hence a deformed Gaussian expansion is introduced accordingly, with which either the normalization or the energy balance could be held satisfactorily. In general, the Heisenberg relation uncertainty needs to be considered only at low outgoing energies and large level widths. The representation of the deformed Gaussian expansion formula is presented in this paper. The normal Gaussian expansions are introduced in section 1, while the deformed Gaussian expansions are given in section 2. The relevant calculations are performed and discussed. The remarks are given in section 3.

1 Level-broadening Expansion with Normal Gaussian Form

Because of the level widths and energy resolution in the measurements, the measured data are always in a broadening form. Therefore, the broadening effect must be taken into account properly for fitting experimental measurements. For particle emission processes, the normalized Gaussian expansion reads

$$\mathrm{G}(\varepsilon,k)=\frac{1}{\sqrt{2\pi}\Gamma}\exp\left(-\frac{(\varepsilon-E)^2}{2\Gamma^2}\right) \tag{1}$$

ε refers to the expanded outgoing energy point, E stands for the individual energy from compound nucleus to level k of its residual nucleus with the width Γ. For the first emitted particle the width is given by

$$\Gamma=\sqrt{\Gamma_1^2+\Delta E} \tag{2}$$

However, for the second particle emission, E stands for the individual energy from level k_1 to level k_2, and the width is given by

$$\Gamma=\sqrt{\Gamma_1^2+\Gamma_2^2+\Delta E} \tag{3}$$

Γ_1 and Γ_2 refer to the level widths of level k_1 and level k_2, respectively. The ΔE[2] in Eq.(3) stands for the energy deviation including the finite-energy resolution of the neutron source, due mostly to the energy reduction of the deuterium beam in the neutron producing target, and the energy spread caused by the finite timing resolution in the time-of-flight method used in the measurements. Of course, ΔE=0 is used in the file-6 in the format of ENDF/B-6 outputting, in which the energy deviation from measurements should not be involved.

To keep the normalization condition, the normalized Gaussian expansion has the following form:

$$\mathrm{G}(\varepsilon,E)=\frac{\sqrt{2}}{\sqrt{\pi}\Gamma}\frac{\exp\left(-\frac{(\varepsilon-E)^2}{2\Gamma^2}\right)}{1+\mathrm{erf}\left(\frac{E}{\sqrt{2}\Gamma}\right)} \tag{4}$$

where erf in Eq.(4) is the error function. Only in the case of $E/\sqrt{2}\Gamma \ll 1$, the Eq.(4) has obvious value from that of Eq.(1).

In the case of continuous spectrum, the spectrum of the outgoing particle is written by $S(\varepsilon')$, with the energy region $\varepsilon_{\min} \le \varepsilon' \le \varepsilon_{\max}$, which often occur in the secondary particle emission processes, the normal Gaussian expansion at energy point ε reads [1]

$$S_G(\varepsilon) = \frac{\sqrt{2}}{\sqrt{\pi}\Gamma} \int_{\varepsilon_{\min}}^{\varepsilon_{\max}} \frac{\exp\left\{-\frac{(\varepsilon-\varepsilon')^2}{2\Gamma^2}\right\}}{1+\mathrm{erf}(\frac{\varepsilon'}{\sqrt{2}\Gamma})} S(\varepsilon')\mathrm{d}\varepsilon' \qquad (5)$$

This expression keeps the value of the cross section unchangeable as shown by the following equation

$$\int_0^{\infty} S_G(\varepsilon)\mathrm{d}\varepsilon = \int_{\varepsilon_{\min}^c}^{\varepsilon_{\max}^c} S(\varepsilon')\mathrm{d}\varepsilon' \qquad (6)$$

The formulation mentioned above is employed in the model calculations of neutron induced light nuclear reactions for fitting the experimental data. It stresses that all error function appeared in Eqs. (4) and (5) is caused by the restriction of positive energy region. If energy region could be extended to negative values, then the error functions would be disappeared in these equations. Because of positive energy restriction, the energy balance is not held when using the above normal Gaussian expansion functions. As the matter of fact, the Eqs.(4) and (5) only keep the normalization condition.

2 Energy Balance

2.1 Single Energy Point Expansion

When the level broadening effect is taken into account by using the normal Gaussian expansion in the ENDF/B-6 format outputting, the energy balance is not held. For instance, for a given single value of energy *E*, the expansion formula (4) gives the energy as

$$\int_0^{\infty} \mathrm{G}(\varepsilon, E)\varepsilon\mathrm{d}\varepsilon \equiv E + \Delta E \qquad (7)$$

here

$$\Delta E = \sqrt{\frac{2}{\pi}}\Gamma \frac{e^{-E^2/2\Gamma^2}}{1+\mathrm{erf}(\frac{E}{\sqrt{2}\Gamma})} \qquad (8)$$

If let

$$x = \frac{E}{\sqrt{2}\Gamma} \qquad (9)$$

then

$$\frac{\Delta E}{E} = \frac{1}{\sqrt{\pi}x} \frac{\mathrm{e}^{-x^2}}{1+\mathrm{erf}(x)} \qquad (10)$$

Obviously, in eq.(10) the value of $\Delta E/E$ decreases rapidly with the increasing of *x*.

The calculated values of $\Delta E/E$ as the function of *x* are shown in Fig.1. From Fig.1 one can see that at low values of *x* the energy gain $\Delta E/E$ has very large percentage. Oppositely, for large values of *x* the energy gain has very small percentage. From Eq.(9) one can see that the low values of *x* correspond to the low energy or large width.

In the case of small values of *x*, the traditional normal Gaussian expansion could not work in the application.

From the point of view on the applications, when $\Delta E/E < 1\%$ the level broadening effect can be neglected. However, when $\Delta E/E > 1\%$ it is corresponding to $x \le 1.96$ or $E/\Gamma < 2.772$, the level broadening effect should be taken into account properly. In order to keep the energy balance, a correction factor $ae^{-b\varepsilon}$ is needed to be introduced as a multiplier factor in the normal Gaussian expansion function (4), the parameters *a* and *b* could be obtained by the two conditions: (1) normalization, (2) energy balance.

Therefore, the deformed Gaussian expansion function has the form as

$$\widetilde{\mathrm{G}}(\varepsilon, E) = a\mathrm{G}(\varepsilon, E)\mathrm{e}^{-b\varepsilon} \qquad (11)$$

① From the normalization condition

$$\int_0^{\infty} \widetilde{\mathrm{G}}(\varepsilon, E)\mathrm{d}\varepsilon = 1 \qquad (12)$$

carrying out the integration over ε, the value of *a* can be obtained by

$$a = \mathrm{e}^{-b^2\Gamma^2/2+bE} \frac{1+\mathrm{erf}(\frac{E}{\sqrt{2}\Gamma})}{1+\mathrm{erf}(\frac{E-b\Gamma^2}{\sqrt{2}\Gamma})} \qquad (13)$$

If *b*=0 then *a*=1 is reasonable.

② From the energy balance condition

$$\int_0^{\infty} \widetilde{\mathrm{G}}(\varepsilon, E)\varepsilon\mathrm{d}\varepsilon = E \qquad (14)$$

The expression of b is obtained by

$$b = \frac{\sqrt{2}}{\sqrt{\pi}\Gamma} \frac{\exp\left\{-\frac{(E-b\Gamma^2)^2}{2\Gamma^2}\right\}}{1+\mathrm{erf}\left(\frac{E-b\Gamma^2}{\sqrt{2}\Gamma}\right)} \qquad (15)$$

Let $x = \frac{E}{\sqrt{2}\Gamma}$ and $y = \frac{b\Gamma}{\sqrt{2}}$, Eq.(15) becomes into

the form as

$$y = \frac{1}{\sqrt{\pi}} \frac{\exp\{-(x-y)^2\}}{1+\mathrm{erf}(x-y)} \tag{16}$$

and Eq.(13) becomes into the following form

$$a = \exp(2xy - y^2) \frac{1+\mathrm{erf}(x)}{1+\mathrm{erf}(x-y)}$$

Obviously, when $x \to \infty$ then $y \to 0$, means there is no correction at large values of x.

Using the optimum searching method numerically, the calculated results of $y(x)$ are shown in Fig.2.

From Fig.2 one can see that at small values of x, y have large values, which means that the correction effect is important. However, at large values of x, the values of y become very small, and the correction effect could be omitted.

Therefore, the deformed Gaussian expansion function reads

$$\widetilde{\mathrm{G}}(\varepsilon, E, b) = \frac{\sqrt{2}}{\sqrt{\pi}\Gamma} \frac{\exp\left\{-\dfrac{(\varepsilon - E + b\Gamma^2)^2}{2\Gamma^2}\right\}}{1+\mathrm{erf}\left(\dfrac{E - b\Gamma^2}{\sqrt{2}\Gamma}\right)} \tag{17}$$

The numerical solutions of the Eq.(16) indicate that if $E/\Gamma > 2.772$, the level broadening effect could be ignored.

On the other hand the difference between the deformed Gaussian expansion function of Eq. (17) and the normal Gaussian expansion function of Eq.(4), as the examples, at E=3 MeV and $\Gamma = 1.5$ MeV, which corresponding to x=1.414, is shown in Fig.3, and at E=1 MeV and $\Gamma = 1$ MeV, which corresponding to x=0.7071, is shown in Fig.4, respectively.

In comparison with the normal Gaussian expansion as shown in Fig.3 and Fig.4, the deformed Gaussian expansion curve is moved to the low energy region, the correction effects to offset the energy gain due to the normal Gaussian expansion and to keep the energy balance. The smaller value of x is, the more composition is at the low energy region.

2.2 Continuous Spectrum Expansion

Based on the normal Gaussian expansion form of Eq. (5), the energy carried by a spectrum $S_{\mathrm{G}}(\varepsilon)$ is given by

$$\int_0^\infty S_{\mathrm{G}}(\varepsilon)\varepsilon \mathrm{d}\varepsilon = E + \Delta E \tag{18}$$

Carrying out the integration over ε at first and using the integrated relation

$$\int_0^\infty \mathrm{e}^{\frac{-(\varepsilon-\varepsilon')^2}{2\Gamma^2}} \varepsilon \mathrm{d}\varepsilon = \Gamma^2 \mathrm{e}^{\frac{-\varepsilon'^2}{2\Gamma^2}} + \varepsilon' \sqrt{\frac{\pi}{2}}\Gamma \left[1+\mathrm{erf}\left(\frac{\varepsilon'}{\sqrt{2}\Gamma}\right)\right] \tag{19}$$

The energy and energy gain are obtained, respectively.

The energy carried by the spectrum is given by

$$E = \int_{\varepsilon_{\min}}^{\varepsilon_{\max}} S(\varepsilon')\varepsilon' \mathrm{d}\varepsilon' \tag{20}$$

and the energy deviation is given by

$$\Delta E = \sqrt{\frac{2}{\pi}}\Gamma \int_{\varepsilon_{\min}}^{\varepsilon_{\max}} \frac{\mathrm{e}^{\frac{-\varepsilon'^2}{2\Gamma^2}} S(\varepsilon')}{1+\mathrm{erf}\left(\dfrac{\varepsilon'}{\sqrt{2}\Gamma}\right)} \mathrm{d}\varepsilon' > 0 \tag{21}$$

In the case of normalized constant spectrum, which is expressed by $S(\varepsilon) = 1/(\varepsilon_{\max} - \varepsilon_{\min})$, Eqs. (20) and (21) have the simple form analytically as

$$E = (\varepsilon_{\max} + \varepsilon_{\min})/2 \tag{22}$$

$$\Delta E = \frac{\Gamma^2}{\varepsilon_{\max} - \varepsilon_{\min}} \ln \frac{1+\mathrm{erf}\left(\dfrac{\varepsilon_{\max}}{\sqrt{2}\Gamma}\right)}{1+\mathrm{erf}\left(\dfrac{\varepsilon_{\min}}{\sqrt{2}\Gamma}\right)} \tag{23}$$

The calculation for n+^{9}Be reactions indicates that the energy gain from the normal Gaussian expansion in the case of continuous spectrum becomes serious, all of the normal Gaussian expansions for the ring-type continuous spectra give large energy gain, even $\Delta E/E$ >10, except from K_1=3 (the second excitation level of ^{9}Be) to K_2=1 (the ground state of ^{8}Be). Thus, the deformed Gaussian expansion ought to be added in the continuous spectrum expansion of Eq.(5). As same as that of the single energy point expansion, the exponential form correction factor $a\mathrm{e}^{-b\varepsilon}$ is added in the normal Gaussian expansion function of Eq.(5). The parameters of a and b can also be obtained by the normalization condition and the energy balance condition, respectively.

Therefore, the deformed Gaussian expansion function of continuous spectrum has the form as

$$\widetilde{S}_{\mathrm{G}}(\varepsilon) = \frac{\sqrt{2}a\mathrm{e}^{-b\varepsilon}}{\sqrt{\pi}\Gamma} \int_{\varepsilon_{\min}}^{\varepsilon_{\max}} \frac{\mathrm{e}^{\frac{-(\varepsilon-\varepsilon')^2}{2\Gamma^2}}}{1+\mathrm{erf}\left(\dfrac{\varepsilon'}{\sqrt{2}\Gamma}\right)} S(\varepsilon')\mathrm{d}\varepsilon' \tag{24}$$

In order to get the values of the parameters a and b, the two following condition give two equations.

① From the normalization condition

$$\int_0^\infty \widetilde{S}_{\mathrm{G}}(\varepsilon)\mathrm{d}\varepsilon = 1 \tag{25}$$

Carrying out the integration over ε the following relation can be given by

$$a\mathrm{e}^{b^2\Gamma^2/2}\int_{\varepsilon_{\min}}^{\varepsilon_{\max}} S(\varepsilon')\mathrm{e}^{-b\varepsilon'}\frac{1+\mathrm{erf}\left(\frac{\varepsilon'-b\Gamma^2}{\sqrt{2}\Gamma}\right)}{1+\mathrm{erf}\left(\frac{\varepsilon'}{\sqrt{2}\Gamma}\right)}\mathrm{d}\varepsilon'=1 \qquad (26)$$

This is the equation to get the parameter a. Obviously, if $b\to 0$ then $a\to 1$ this is reasonable.

② From the energy balance condition

$$\int_0^{\infty}\widetilde{S}_{\mathrm{G}}(\varepsilon)\varepsilon\mathrm{d}\varepsilon = E \qquad (27)$$

Substituting Eq.(24) into Eq.(27) and carrying out the integration over ε the following relation is obtained by

$$E=\sqrt{\frac{2}{\pi}}a\Gamma\int_{\varepsilon_{\min}}^{\varepsilon_{\max}}\frac{\mathrm{e}^{-\frac{\varepsilon'^2}{2\Gamma^2}}S(\varepsilon')}{1+\mathrm{erf}\left(\frac{\varepsilon'}{\sqrt{2}\Gamma}\right)}\mathrm{d}\varepsilon'+a\int_{\varepsilon_{\min}}^{\varepsilon_{\max}}e^{\frac{b^2\Gamma^2}{2}-b\varepsilon'}S(\varepsilon')\varepsilon'\frac{1+\mathrm{erf}\left(\frac{\varepsilon'-b\Gamma^2}{\sqrt{2}\Gamma}\right)}{1+\mathrm{erf}\left(\frac{\varepsilon'}{\sqrt{2}\Gamma}\right)}\mathrm{d}\varepsilon'-b\Gamma^2 \qquad (28)$$

Substituting Eq.(26) into Eq.(28) the equation of the parameter b is expressed by a very complex form

$$E+b\Gamma^2=\frac{\sqrt{\frac{2}{\pi}}\Gamma\mathrm{e}^{\frac{b^2\Gamma^2}{2}}\int_{\varepsilon_{\min}}^{\varepsilon_{\max}}\frac{\mathrm{e}^{-\frac{\varepsilon'^2}{2\Gamma^2}}S(\varepsilon')}{1+\mathrm{erf}\left(\frac{\varepsilon'}{\sqrt{2}\Gamma}\right)}\mathrm{d}\varepsilon'+\int_{\varepsilon_{\min}}^{\varepsilon_{\max}}\mathrm{e}^{-b\varepsilon'}S(\varepsilon')\varepsilon'\frac{1+\mathrm{erf}\left(\frac{\varepsilon'-b\Gamma^2}{\sqrt{2}\Gamma}\right)}{1+\mathrm{erf}\left(\frac{\varepsilon'}{\sqrt{2}\Gamma}\right)}\mathrm{d}\varepsilon'}{\int_{\varepsilon_{\min}}^{\varepsilon_{\max}}\mathrm{e}^{-b\varepsilon'}S(\varepsilon')\frac{1+\mathrm{erf}\left(\frac{\varepsilon'-b\Gamma^2}{\sqrt{2}\Gamma}\right)}{1+\mathrm{erf}\left(\frac{\varepsilon'}{\sqrt{2}\Gamma}\right)}\mathrm{d}\varepsilon'} \qquad (29)$$

Obviously, when the width $\Gamma\to 0$ then we have $b\to 0$ and $a\to 1$.

Since the secondly emitted particle has the energy independent ring-type spectrum by the recoil effect[1], in this case the constant spectrum, Eq.(29) can be reduced to the following form

$$E+b\Gamma^2=\frac{\sqrt{\frac{2}{\pi}}\Gamma\mathrm{e}^{\frac{b^2\Gamma^2}{2}}\int_{\varepsilon_{\min}}^{\varepsilon_{\max}}\frac{\mathrm{e}^{-\frac{\varepsilon'^2}{2\Gamma^2}}}{1+\mathrm{erf}\left(\frac{\varepsilon'}{\sqrt{2}\Gamma}\right)}\mathrm{d}\varepsilon'+\int_{\varepsilon_{\min}}^{\varepsilon_{\max}}\mathrm{e}^{-b\varepsilon'}\varepsilon'\frac{1+\mathrm{erf}\left(\frac{\varepsilon'-b\Gamma^2}{\sqrt{2}\Gamma}\right)}{1+\mathrm{erf}\left(\frac{\varepsilon'}{\sqrt{2}\Gamma}\right)}\mathrm{d}\varepsilon'}{\int_{\varepsilon_{\min}}^{\varepsilon_{\max}}\mathrm{e}^{-b\varepsilon'}\frac{1+\mathrm{erf}\left(\frac{\varepsilon'-b\Gamma^2}{\sqrt{2}\Gamma}\right)}{1+\mathrm{erf}\left(\frac{\varepsilon'}{\sqrt{2}\Gamma}\right)}\mathrm{d}\varepsilon'} \qquad (30)$$

Let $x=\frac{\varepsilon'}{\sqrt{2}\Gamma}$ and $y=\frac{b\Gamma}{\sqrt{2}}$, x and y are dimensionless, the integration limits are changed into $\varepsilon_{\min}\to x_{\min}$ and $\varepsilon_{\max}\to x_{\max}=\frac{\varepsilon_{\max}}{\sqrt{2}\Gamma}$. Therefore, Eq.(29) becomes into the form as

$$\frac{E}{\sqrt{2}\Gamma}+y=\frac{\frac{1}{\sqrt{\pi}}\mathrm{e}^{-y^2}\int_{x_{\min}}^{x_{\max}}\mathrm{e}^{-x^2}\frac{S(\sqrt{2}\Gamma x)}{1+\mathrm{erf}(x)}\mathrm{d}x+\int_{x_{\min}}^{x_{\max}}e^{-2xy}S(\sqrt{2}\Gamma x)x\frac{1+\mathrm{erf}(x-y)}{1+\mathrm{erf}(x)}\mathrm{d}x}{\int_{x_{\min}}^{x_{\max}}\mathrm{e}^{-2xy}S(\sqrt{2}\Gamma x)\frac{1+\mathrm{erf}(x-y)}{1+\mathrm{erf}(x)}\mathrm{d}x} \qquad (31)$$

In the case of normalized constant spectrum, Eq.(31) is reduced to the form as

$$\frac{E}{\sqrt{2}\Gamma}+y=\frac{\frac{\mathrm{e}^{-y^2}}{\sqrt{\pi}}\int_{x_{\min}}^{x_{\max}}\frac{\mathrm{e}^{-x^2}}{1+\mathrm{erf}(x)}\mathrm{d}x+\int_{x_{\min}}^{x_{\max}}\mathrm{e}^{-2xy}x\frac{1+\mathrm{erf}(x-y)}{1+\mathrm{erf}(x)}\mathrm{d}x}{\int_{x_{\min}}^{x_{\max}}\mathrm{e}^{-2xy}\frac{1+\mathrm{erf}(x-y)}{1+\mathrm{erf}(x)}\mathrm{d}x} \tag{32}$$

Obviously, if y =0 then Eq.(32) becomes into

$$E=\frac{\sqrt{2}\Gamma^2}{\varepsilon_{\max}-\varepsilon_{\min}}\int_{x_{\min}}^{x_{\max}}\frac{\mathrm{e}^{-x^2}}{1+\mathrm{erf}(x)}\mathrm{d}x+E \tag{33}$$

this equation could be held in any case, so that y =0 is always not the solution of Eq.(32). This condition is used for the numerical method to set the initial value of y .

If the integration limits region is tended to zero, i.e. $\varepsilon_{\min}=\varepsilon_{\max}\equiv E$, then Eq.(32) is reduced into

$$y=\frac{1}{\sqrt{\pi}}\frac{\exp\{-(x-y)^2\}}{1+\mathrm{erf}\ (x-y)} \tag{34}$$

Which is identical to Eq.(16). Thus, the correctness of Eq.(32) is proved.

For a given continuous spectrum of $S(\varepsilon)$, and its integration limits, as well as the width Γ , Eq.(29) can be solved rapidly with the optimum seeking method.

Finally the deformed Gaussian expansion function of continuous spectrum reads

$$\widetilde{S}_{\mathrm{G}}(\varepsilon)=\sqrt{\frac{2}{\pi\Gamma^2}}\mathrm{e}^{\frac{b^2\Gamma^2}{2}-b\varepsilon}\frac{\int_{\varepsilon_{\min}}^{\varepsilon_{\max}}\frac{\mathrm{e}^{-\frac{(\varepsilon'-\varepsilon)^2}{2\Gamma^2}}}{1+\mathrm{erf}\left(\frac{\varepsilon'}{\sqrt{2}\Gamma}\right)}S(\varepsilon')\mathrm{d}\varepsilon'}{\int_{\varepsilon_{\min}}^{\varepsilon_{\max}}\mathrm{e}^{-b\varepsilon'}S(\varepsilon')\frac{1+\mathrm{erf}\left(\frac{\varepsilon'-b\Gamma^2}{\sqrt{2}\Gamma}\right)}{1+\mathrm{erf}\left(\frac{\varepsilon'}{\sqrt{2}\Gamma}\right)}\mathrm{d}\varepsilon'} \tag{35}$$

Let us take two examples:

1) The energy spectrum scope is from $\varepsilon_{\min}=0.5$ MeV to $\varepsilon_{\max}=1.5$ MeV with the width $\Gamma=1$ MeV. So the energy carried by the continuous spectrum is E=1 MeV, the energy deviation is $\Delta E=0.3$ MeV, and the ratio is $\Delta E/E$ =30%. Solving Eq.(30) and using Eq.(26) we have a=1.8078, b=0.51815 MeV^{-1}. The curves of the normal Gaussian expansion function of Eq.(5) and the deformed Gaussian expansion function of Eq. (35) are shown in Fig.5.

2) The energy spectrum scope is from $\varepsilon_{\min}=0.2$ MeV to $\varepsilon_{\max}=0.4$ MeV with the width $\Gamma=1$ MeV. So the energy carried by the continuous spectrum is E=0.3 MeV, the energy deviation is $\Delta E=0.2305$ MeV, and the ratio is $\Delta E/E$ =76.6%, with the result of a=2.7430, b=2.5169 MeV^{-1}. The curves of the normal Gaussian expansion function of Eq.(5) and the deformed Gaussian expansion function of Eq. (35) are shown in Fig.6.

In comparison with the normal Gaussian expansions, as shown in Fig.5 and Fig.6, the width broadening expansion of the deformed Gaussian expansions has more composition at low energy region obviously, which offsets the energy gain caused by the normal Gaussian expansion.

The calculations indicate that the smaller of the ratio E/Γ is, the more composition is at low energy region. The deformed Gaussian expansion could raise the low energy part of the continuous spectrum.

3 Remarks

In the new method for calculating neutron induced reaction data of light nuclei to set up file-6 for double-differential cross sections, all of the emissions are carried out from discrete levels to discrete levels, and the levels have their individual life-time, then the Heisenberg' uncertainty should be taken into account properly, because the uncertainty is surely involved in the measurements of outgoing particles. Usually the traditional normal Gaussian expansion form is employed in the fitting procedure [1], but to do so in this way the energy balance could not be held. For this reason the deformed Gaussian expansion functions are introduced to keep the energy balance for both single energy points and continuous spectra in CMS. The correction factor is in exponential form to avoid the negative values occuring in the expanded spectra, which often appear in the case of linear correction factor $a+b\varepsilon$. Therefore,

the deformed Gaussian expansion functions could be employed for making the energy balance hold for the double-differential cross sections of all kinds of outgoing particles in the file-6 when the level width broadening effect is taken into account. In addition, in order to keep the energy balance in LS, from the formulation in Ref.1, it turns out that any expansions are not needed for the partial wave except l=0 wave. To do so in this way, the energy scope of the outgoing neutron angular-energy spectra could be extended by the level width broadening expansions. However, in the region of high outgoing neutron energies of the spectra, the extended part in the angular-energy spectra could become isotropic, due to no any contribution in the angular-energy spectra without the level width broadening expansions for the partial waves with l>0. This is the condition to keep the energy balance in LS.

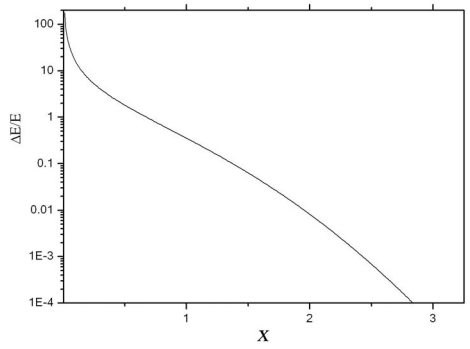

Fig.1 The energy gain $\Delta E/E$ vs x

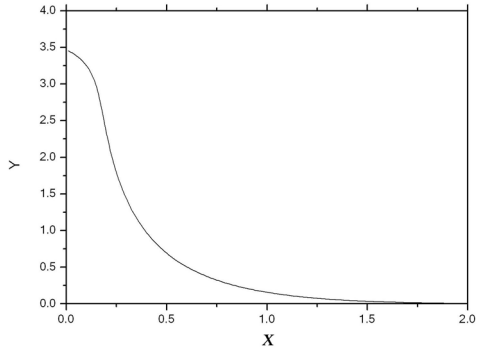

Fig.2 y vs x

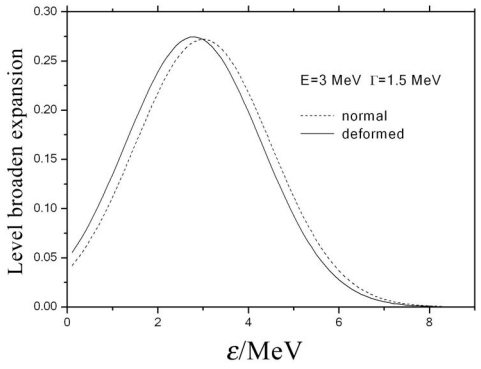

Fig.3 The level broadening expansion at E=3 MeV Γ=1.5 MeV

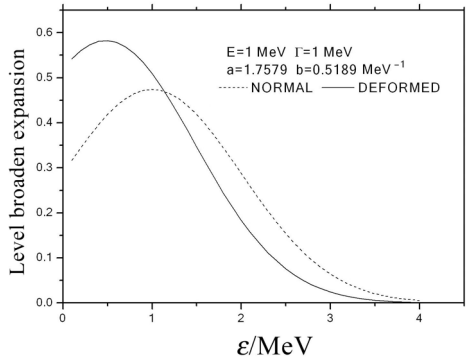

Fig.4 The level broadening expansioning at E=1 MeV Γ=1 MeV

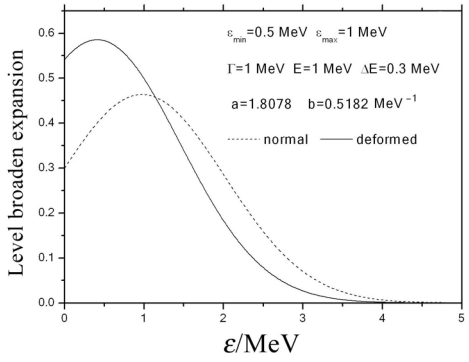

Fig.5 The width broadening of continuous spectrum

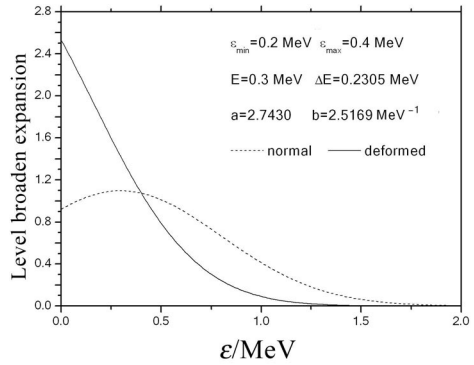

Fig.6 The width broadenning of continuous spectrum

References

[1] J.S. Zhang Jingshang, et al. Nucl.Sci. Eng.133 (1999) 218

[2] K. Chiba. Phys. Rev C 58 (1998) 220

Establishment of File-6 of n+^{12}C for CENDL-3

ZHANG Jingshang HAN Yinlu

China Nuclear Data Center, CIAE, P.O.Box275(41), Beijing 102413

【**abstract**】*A method to set up file-6 of light nuclei for evaluated neutron data library in ENDF/B-6 format below 20 MeV has been developed. By means of this method the double-differential cross sections of all kinds outgoing particles can be calculated to reproduce the experimental data with full energy balance based on the accurate kinematics. Therefore, the file-6 can be established in the form of Legendre polynomial expansion in CMS with full energy balance, so that the pseudo levels and pseudo continuum states employed in JENDL-3.2 are resigned. For n+^{12}C reactions below 20 MeV, the file 6 of (n,n3α) has been set up in CENDL-3 library with the model calculation of LUNF code. The evaluations of the relevant cross sections have been performed.*

Introduction

The evaluated neutron data library in ENDF/B-6 format of 1p shell light nuclei of below 20 MeV has been set up, which is importance in various applications, such as in the fields of biology and medicine. However, the recently established data file of ^{12}C should be updated from time to time [1]. So far there is no evaluated neutron data of n+^{12}C in CENDL neutron data library. The motivation for this work comes from the CENDL-3 project to set up file-6 of light elements. For this purpose, a new model was developed for calculating the double-differential cross sections of outgoing particles by using the LUNF code[2]. In this new method, the emissions from compound nucleus to the discrete levels of the residual nuclei, both in pre-equilibrium and equilibrium mechanism, are taken into account with angular momentum conservation. The energy balance is strictly considered to set up the file-6[2]. All the formulation could be found in Ref. [2] in detail. The calculated results of the double-differential cross sections reproduce the experimental data fairly well[2]. The reaction mechanism of light nucleus is complex. In the reaction processes of light nucleus the pre-equilibrium emissions dominate the reaction mechanism, while the equilibrium state only gives little implementation even at low neutron incident energies. The emission processes from discrete levels in the pre-equilibrium state are the most important reaction mechanism. Because of light mass, the recoil effect must be taken into account exactly to maintain the energy balance [2]. To do so in this way the file-6 could be obtained with full energy balance.

In the case of E_n < 20 MeV, all of the reaction for n+^{12}C proceeds via several sequential decay process between discrete levels. The energy, spin and parity of the levels are taken from the "Table of Isotopes"(1996)[3] .

By using LUNF code for n+^{12}C, the calculated results of double differential cross sections of outgoing neutron at E_n=14.1 MeV and 18.0 MeV agree fairly well with the measurements[2], which are shown in Figs. 1~7. The optical parameters of all kinds of particles are obtained by APMN94 code.

The (n,n3α) reaction is an important channel and there are some measurements[4,5~8], with large discrepancy. In JENDL-3 neutron data library, this channel was not included directly and the information of the outgoing neutron from (n,n3α) reaction channel was given in the inelastic scattering channel with the pseudo levels (MT=52, 54~57, 59~75 and MT=91) for continuum state calculated by using 4-body breakup process. It should stress that the data for MT=51, 52 and 58 were calculated with coupling channel code in JENDL-3.2, which are the first three excited levels of ^{12}C. So the cross section of inelastic-scattering channel is not the real one, and needs to be re-evaluated. Now, the cross section and the double-differential cross section of this reaction channel can be calculated by LUNF code with the threshold energy of 7.8865 MeV. The file-6 of (n,n3α) reaction channel can also be given with full energy balance. Meanwhile, there is no (n,np) reaction channel involved in JENDL-3 neutron data library, while our model calculation also indicates that this

channel is opened with very high threshold energy of 17.32 MeV, and the cross section is too small, so it is are neglected, therefore (n,np) reaction channel is also not included in CENDL-3 neutron data library.

1 Reaction Channels of n+^{12}C Reaction below 20 MeV

In view of n+^{12}C reaction for E_n<20 MeV the reaction channels are (n,γ), (n,n'), (n,p), (n,d), (n,α), (n,np), and (n,n3α), while the reaction channels of (n,t), (n,^{3}He), (n,2n) are not open due to the threshold energies >20MeV. The (n,α) reaction is given by the α particle reached to the ground state of ^{9}Be, while the excitation states of ^{9}Be can be decay and belong to the (n,n3α) reaction. Reaction mechanism in the n+^{12}C system leading to the decay into one neutron and three α particles reactions may proceed via a number of different reaction channels, as sequential two-body reaction or two body break-up process, the different approach strongly differs each other in their respective neutron and alpha-particle energy-angular distributions. The reaction channels to ^{12}C(n,n′)3α channel involved in the model calculation are as follows :

(a) $n + {}^{12}C \longrightarrow \alpha + {}^{9}Be^*$,
$^9Be^* \longrightarrow n + {}^{8}Be$,
$^8Be \longrightarrow \alpha + \alpha$

(b) $n + {}^{12}C \longrightarrow \alpha + {}^{9}Be^*$,
$^9Be^* \longrightarrow \alpha + {}^{5}He^*$,
$^5He^* \longrightarrow n + \alpha$

(c) $n + {}^{12}C \longrightarrow n + {}^{12}C^*$,
$^{12}C^* \longrightarrow \alpha + {}^{8}Be$,
$^8Be \longrightarrow \alpha + \alpha$

(d) $n + {}^{12}C \longrightarrow {}^{5}He + {}^{8}Be$,
$^8Be \longrightarrow \alpha + \alpha$,
$^5He \longrightarrow \alpha + n$

The inelastic scattering channel is given mainly by the contributions from the first and the second excited levels.

2 Cross Sections (MF=3)

2.1 Thermal Cross Section

The 2200m/s are as follows:

Total cross section $\sigma_t = 4.750$ barns

Elastic scattering $\sigma_{el} =$ 4.746 barns

Radiation capture $\sigma_\gamma = 0.0035$ barns

The resonance parameter is given by the scattering radius. The data were taken from JENDL-3.2[8].

2.2 Total Cross Section (MT=1)

Taken from JENDL-3.2[8]

2.3 Elastic Scattering Cross Section(MT=2)

Taken from JENDL-3.2[9] , below 10 eV σ_{el} = 4.746 barns.

2.4 Inelastic Scattering Cross Section (MT=4, 51-53)

MT=4, total inelastic scattering is the sum of MT=51-53,

MT=51 inelastic scattering to the first excited level,

MT=52 inelastic scattering to the second excited level,

MT=53 inelastic scattering to the third excited level, which is the MT=58 in JENDL-3.2.

At first the calculations are performed with LUNF code [2], then evaluated to normalize the total inelastic scattering cross section based on the cross sections and double-differential measurements[10~13]. The discrete levels, which only give too small cross sections, for instance less than 0.1 μb, are omitted.

Notation: In JENDL-3.2 library

MT=52, 54, 57, 59~75 are pseudo levels and

MT=91 for (n,n3α) is the contribution from the calculation of 4-body breakup spectra.

2.5 ^{12}C(n,n′)3α Reaction Cross Section (MT=29)

Evaluated based on the calculations with LUNF code to fit the measurements, while there is no this reaction channel in JENDL-3.2, only the neutron formation was given in the inelastic scattering channel with the pseudo levels and pseudo continuum spectrum. The values of the cross section are given by the summation over the cross sections of the corresponding pseudo levels and the pseudo continuum part indicated in the JENDL-3.2.

2.6 ^{12}C(n,γ) Radiation Capture Reaction Cross Section (MT=102)

Taken from the recommend data in the "Reference Neutron Activation Library" IAEA-TECDOC-1285 April 2002[14].

2.7 ^{12}C(n,p) Reaction Cross Section(MT=103)

Taken from JENDL-3.2, which was evaluated based on the measurement[15].

2.8 ^{12}C(n,d) Reaction Cross Section(MT=104)

Taken from JENDL-3.2, which was evaluated based on the measurements[16-25].

2.9 ^{12}C(n,α) Reaction Cross Section (MT=107)

Taken from JENDL-3.2[8]

3 Angular Distribution (MF=4)

The angular distribution of the secondary neutrons.

MT=2 is taken from JENDL-3.2.

MT=51, 52 and 53 are taken from JENDL-3.2 based on the measurements[26~30].

Notation: In JENDL-3.2 MT=52, 54-57, 59-75 are isotropic in CMS. In CENDL-3 the pseudo levels mentioned above are included in the corresponding reaction channels, which are given from the double-differential cross sections of file-6, except MT=52.

4 Double-Differential Cross Section(MF=6)

MT=29 for (n,n3α) reaction channel calculated with LUNF code[2] to fit the experimental data[31], is showed in Fig.1~Fig.7. The experimental data in the Figures were taken from Baba[4].

5 Photon-Production Multiplicity(MF=12)

MT=102 for ^{12}C(n,γ) is taken from JENDL-3.2.

6 Photon Angular Distributions(MF=14)

MT=102 is assumed to be isotropic.

7 Conclusion Remark

The neutron reaction data files of n+ ^{12}C has been established from 10^{-5} eV to 20 MeV. Besides the improvements on the cross section of (n,γ), the major changes of n+^{12}C in the CENDL-3 neutron data library are as follows:

(1) The reaction channels of (n,n3α) is included physically in terms of the model calculation by fitting the double-differential measurements.

(2) To do so in this way the pseudo levels and the pseudo continuum states used in JENDL-3.2 neutron data library are disappeared. Now, the inelastic scattering channel is the reality in both file-3 and file-4.

(3) The double-differential cross sections of neutron and alpha particle from the reaction channels of (n,n3α) is given by the model calculations. Therefore the file-6 is established with full energy balance.

The comparison of the files in JENDL-3.2 and CENDL-3 are shown in Table 1.

Table 1 The files in JENDL-3 and CENDL-3

MF	JENDL-3.2	CENDL-3
3	4,51-75,91, 102,103,104,107	4,29,51-53, 102,103,104,107
4	2,51-75,91	2,51-53,
5	91	
6		29
12	91,102	51,52,102
14	91,102	51,52,102

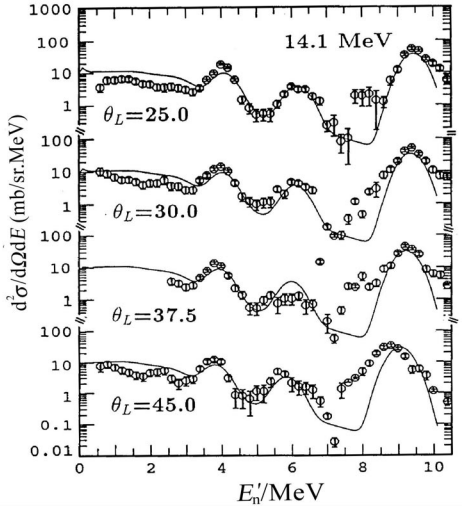

Fig.1 The energy-angular spectra of 25°, 30°, 37.5°, and 45° for n+^{12}C at E_n=14.1 MeV.

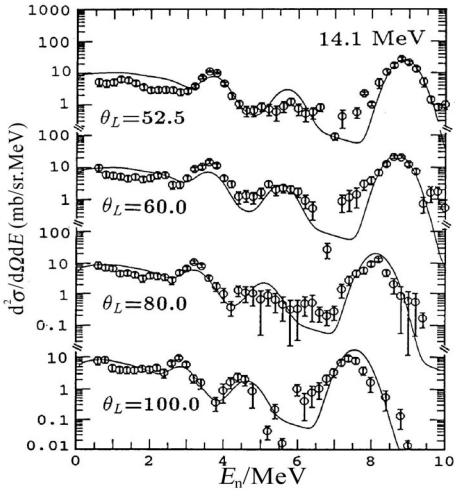

Fig.2 The energy-angular spectra of 52.5°, 60°, 80°, and 100° for n+^{12}C at E_n =14.1 MeV.

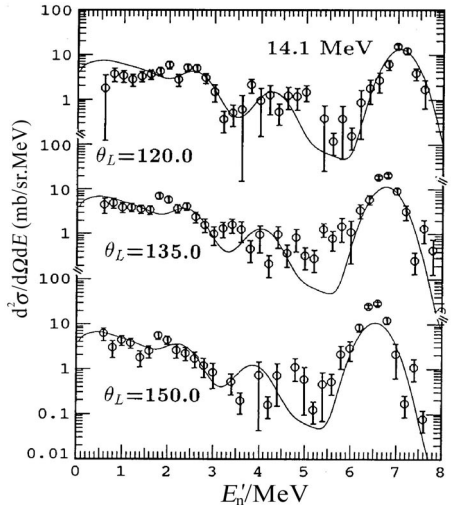

Fig.3 The energy-angular spectra of 120°, 135°, and 150° for n+^{12}C at E_n =14.1 MeV.

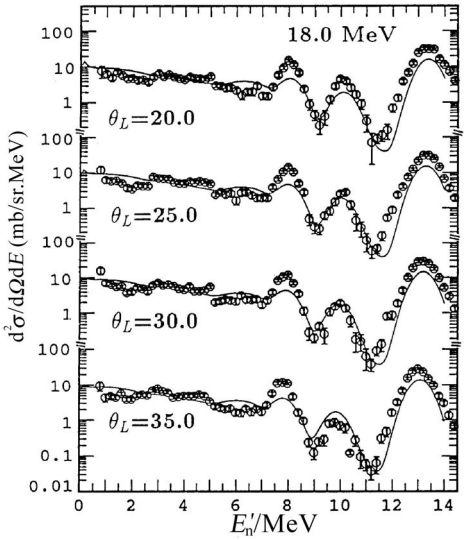

Fig.4 The energy-angular spectra of 20°, 25°, 30°, and 35° for n+^{12}C at E_n =18 MeV.

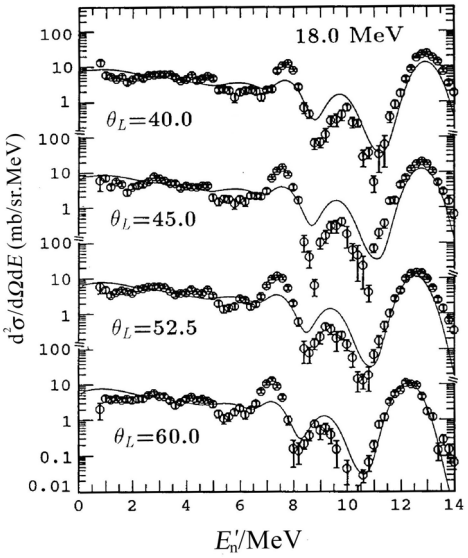

Fig.5 The energy-angular spectra of 40°, 45°, 52.5°, and 60° for n+^{12}C at E_n =18 MeV.

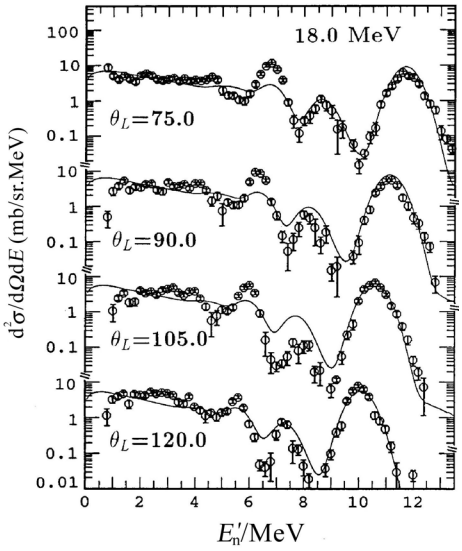

Fig.6 The energy-angular spectra of 75°, 90°, 105°, and 120° for n+^{12}C at E_n =18 MeV.

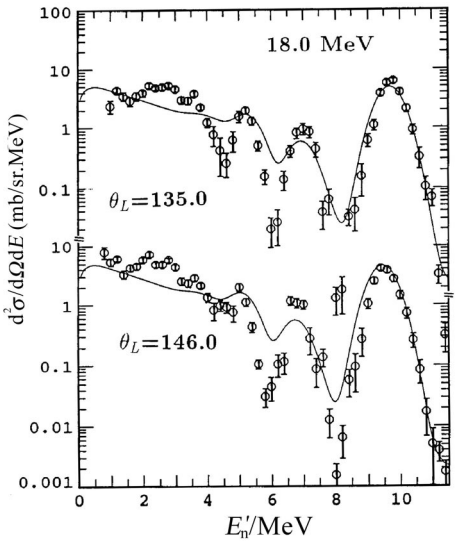

Fig.7 The energy-angular spectra of 135° and 146° for n+^{12}C at E_n =18 MeV.

References

[1] Muir D. W, et al. INDC(NDS)-423 May 2001 p12.
[2] ZHANG Jingshang, et al. Nncl. Sci. Eng. 133 (1999) 218.
[3] Firestone R.B, et al. Table of Isotopes 8$_{th}$., John Wiley & Sone (1996).
[4] Baba M. Proc. Int. Conf. Nuclear Data for Basic and Applied Scince, Santa Fe, New Mexico, (1985).223
[5] Frye G. M, et al. Phys. Rev. 99 (1955)1375.
[6] Brade H. J, et al. Nucl. Sci. Eng. 107 (1991) 22.
[7] Antolkovic B, et al. Nucl. Sci. Eng. 107 (1991) 1.
[8] Stevens A. P. INIS-MF-3596 (1976).
[9] Shibata, K.: JAERI-M 83-221 (1983).
[10] Morgan, G.L, et al. ORNL-TM-3702 (1972).
[11] Haouat, G, et al. CEA-R-4641 (1975).
[12] Glasgow D.W, et al.: Nucl. Sci. Eng. 61 (1976) 521.
[13] Rogers V.C, et al.: DNA 3495F (1974).
[14] IAEA-TECDOC-1285 "Reference neutron activation library (2002)31.
[15] Mengoni, et al. Phys. Rev. C 52 (1995) R2334 and OHSAKI, T., et al. New Measurement of the

12C(n,)13C Reaction Cross Section Astro-Phys. J. 422 (1994) 912..
[16] Rimmer, E.M, et al. Nucl. Phys. A108 (1968) 567.
[17] Chatterjee, M.L, et al. Nucl. Phys. 51 (1964) 583.
[18] Huck, A. et al,: J. De Physique C1 (1966) 88.
[19] Brendle, M, et al.: Z. NATURFORSCH. 23A (1968) 1229.
[20] Kitazawa, H, et al. Phys. Soc. JPN. 26(1969)600.
[21] Kardonsky, S, et al. Phys. Rev. C4 (1971) 840.
[22] Stevens, A.P. INIS-MF-3596 (1976).
[23] Retz-schmidt, T, et al. BULL. AM. Phys. Soc. 5 (1960) 110.
[24] Verbinski, V.V, et al. Phys. Rev. 170 (1968) 916.
[25] Obst, A.W, et al. Phys. Rev. C5 (1972) 738.
[26] Deconninck, G, et al. J.-P.Phys. Rev. C1 (1970) 1326.
[27] Galati, W, et al. Phys. Rev. C5 (1972)1508.
[28] Velkley, D.E, et al. Phys. Rev. C7 (1973) 1736.
[29] Thumm, M, et al. Nucl. Phys. A344 (1980) 446.
[30] Spilling, P, et al. Nucl. Phys. A113 (1968) 395. JAERI-M 88-065, P.279, (19883).
[31] Baba M, et al. JAERI-M 90-025, P.383 (1990).

Evaluation of Complete Neutron Data of n +^{55}Mn from 10^{-5} eV to 20 MeV

YU Baosheng WANG Shunuan MA Gonggui*
China Nuclear Data Center, CIAE, P.O.Box275(41), Beijing 102413
**Institute Of Nuclear Scince and Technolog Sichuan University, Chengdu 610064*

【**abstract**】*Manganese is an important construction material and there is only one stable isotope ^{55}Mn for it. Because its special physical property and its (n,2n), (n,γ) reactions cross sections are usually used as good activation indicators, its data are very useful for nuclear science and technology applications. A complete set neutron data including cross sections, angular distributions, double differential spectra of n + ^{55}Mn from 10^{-5} eV to 20 MeV were evaluated based on experimental data and theoretical calculation, given in ENDF/B-6 format.*

1 Resonance Parameters

The resonance parameters in MLBW formula were taken from JENDL-3.3. The resolved resonance range is from 1.0^{-5} eV to 100 keV and two negative resonances were given so as to fit experimental thermal cross sections.

The smooth cross section at boundary should be reasonably in conjunction with the cross section calculated from resonance parameters, which was checked. The conjunction is in good agreement in general. When the conjunction is not smooth enough, the data in smooth region were adjusted around boundary so as to make the smooth cross section consist with the calculated one from resonance parameters. After adjusting, the cross sections at boundary are all in good conjunction within fixed errors.

2 Evaluations and Adjusting Smooth Cross-Sections

2.1 Total and Elastic Cross Section

For ^{55}Mn, there are still obvious resonance structure above 100 keV until 4 MeV. For the earlier experimental data, there are large differences and discrepancies.

With the improvement of neutron energy resolution and ratio of effect-background, some high resolution cross sections were measured. The high resolution total cross sections were measured by S.Cierjacks[1] using time–of-flight spectrometer in energy region from 0.5 MeV to 32 MeV. The neutron flight path is more than 50 meters and the energy resolution is 0.057 ns/m. The data were corrected for background and dead time. The data were also measured by W.F.E Pineo[2] from 19.7 keV to 650 keV by a step of 5 keV. The total cross sections were measured from 0.584 keV to 200 keV by J.B.Garg[3] with 99.1% of ^{55}Mn sample using time of flight spectoumeter at Los Alamos Laboratory in 1978. The neutron flight path is 200 meters. The data were also measured from 5.29 MeV to 559 MeV by W.P.Abfalteror[4] in 1991. W.P.Abfalteror's data are consistent with S.Cierjacks[1]. These data mentioned above cover wide energy region, have high-energy resolution and accurate energy calibration, and are in good agreement with other accurate measurement at some energy points or some energy region. So, these data[1~3] were adopted. The recommended total cross section was obtained by fitting them, which are consistent with JENDL-3.3 and showed in Fig.1.

2. 2 ^{55}Mn(n,2n) ^{54}Mn Reaction

The ^{55}Mn(n,2n) ^{54}Mn is an important dosemetry and activation indicator reaction, which is very useful for nuclear science and applications. The cross section was measured using absolute and ratio measurement techniques. The measured data[5~26] from 1965 up to now were collected, analyzed, evaluated and all summarized in Table 1.

Table 1 Survey of measured cross section for ^{55}Mn(n,2n)^{54}Mn reaction

Year	Author	E_n/MeV	$\sigma\pm\Delta\sigma$/mb	Detector	Monitor	R1	R2	σ/mb
1997	A.A.Filatenkov	14.78	781±28	SCIN	^{93}Nb(n,2n)	0.9815		767
		13.56~14.78						
1994	M .Bostan	11.64~12.85		Ge(Li)	^{27}Al(n,α)			
1992	T.S.Socwarsong	17.55~38.26		SCIN	^{7}Li(n,p)			
1990	I.Kimura	14.1	775.4±28.6		^{27}Al(n,α)	1.0718	0.9870	820
1989	Lu Hanlin	14.58	812±28.9	Ge(Li)	absolute	1.0021		813.7
		12.37~18.26			Normalized.			
1988	Y. Ikeda	14.67	820±47	Ge(Li)	^{27}Al(n,α)	0.9927		814
		13.35~14.93						
1988	K.Kobayashi	14.05	775.4±28.6	Ge(Li)	^{27}Al(n,α)	1.0800	0.9870	826
1987	L.R.Greenwood	14.8	807±	Ge(Li)	^{93}Nb(n,2n)	0.9794	1.0277	808
		14.5~14.9						
1987	J.W.Meadows	14.74	765±	Ge(Li)	^{235}U(n,f)	0.9855	0.9942	749
1984	B.M.Bahal	14.7	741±22	Ge(Li)	^{27}Al(n,α)	0.9896	1.0133	743
1984	M.Berrada	14.6	730±26	Ge(Li)	^{27}Al(n,p)	1.0000	0.9847	718
1979	K. Kayashima	14.6	884±58	Ge(Li)	^{27}Al(n,α)	1.0000		884
1976	O.Schwerew	14.6	775±80	Ge(Li)	^{27}Al(n,α)	1.0000	1.0140	785
1975	F.Deak	14.7	680±300	SCIN	H(n,n)	0.9896	0.9670	650
1973	J.Arrminowiez	14.6	643±65	NaI(TL)	^{63}Cu(n,2n)	1.0000	0.9711	624
1972	G.N.Maslov	14.6	866±65	NaI(TL)	^{65}Cu(n,2n)	1.0000	0.9954	862
1972	O.A.Salnikov	14.36	540±70	NaI(TL)	absolute	1.0312		556
1969	R.C.Barrall	14.6	785±80	NaI	^{27}Al(n,α)	1.0000		785
		14.8	750±60	NaI	H(n,n)	0.9842		738
1969	M.Bormann	14.1	798±78	NaI	H(n,n)	1.0718	0.9937	849
		12.99~ 18.06						
1968	H.Vonach	14.1	786±78	NaI		1.0718		842
1967	H.O.Menlove	14.96	854±79		^{235}U(n,f)	0.9636		822
		12.7~19.39						
1965	A.Paulsan	14.71	945±57	NaI	H(n,n)	0.9886		934
		12.63~ 19.59						

BPAIR: Scintillation pair spectrometer
GEMUC : Mica end-window Geiger muller counter
IOCH : End-window counter
SCIN: Scintillation counter
R1 : Adjusted factor for neutron energy
R2 : Adjusted factor for monitor cross section
Evaluated cross section is 811.19±11.27 mb at 14.6 MeV

Except for the data around 14 MeV, the multiple-value data sets were measured by A.Paulsan[5], H.O.Menlove[6], M.Bostan[25] and Lu Hanlin [22] from 12.99 MeV to 19.39 MeV, by L.R.Greewood[19], Y.Ikeda[21], A.A.Filatenkov[26] from 13.56 MeV to 14.9 MeV. The data were also measured by M.Bostan[25] using Gi(Li) detector γ spectroscopy from 11.64 MeV to 12.83 MeV and by T.S.Socwarsong[24] using Scintillator detector from 17.55 MeV to 38.26 MeV. But all of these data are discrepant around 14 MeV by 10%~38%. The reason should be analysed.

Many measurements for ^{55}Mn(n,2n)^{54}Mn reaction were performed around 14 MeV due to the availability of intense source of monoenergies neutron from Cockrofe-Walton accelerator. Furthermore the accurate cross section around 14 MeV, is very interested in developing reaction systematics and nuclear models.

Those cross sections around 14 MeV were

adjusted at energy equivalent to 14.6 MeV, depending on the shape of the excitation curve. In order to obtain the factors of energy adjustment values, the data of Zhao Wenrong[27] were used. Meantime the data around 14 MeV were adjusted for standard cross section, used the new one was taken from ENDF/B-6. The nuclear decay schemes of ^{54}Mn is very well known and the values of half-life (312.12 d) and gamma-intensity (0.99976) for 834.834 keV have not changed to any significant extent for many years. There is no problem for abundance 100% of isotope ^{55}Mn.

After these data were renormalized at 14.6 MeV, some data were rejected due to the larger discrepancies with others, exceeding the averaged value by three-standard deviation. The evaluated data were obtained by averaging with weight the remaining data. The weight was based on the errors given by authors and quoted errors by us. The present evaluated cross section at 14.6 MeV for ^{55}Mn(n,2n)^{54}Mn reaction is 811.19±11.27 mb.

Among the experimental data, there are 9 sets of multiple-value data from 11 MeV to 20 MeV. The data of A.Paulsan[5] were rejected due to systemically higher than others. The data of M.Bostan[25] below 12.85 MeV were adjusted by using new standard cross section. The data of M.Bostan[25] are consistent with that of LU Hanlin[22] within errors around 12 MeV, which are very useful for giving the tendency from threshold energy to 12 MeV, filling the gaps of lacking energy region. As a result, the cross section could be recommended based on the available measured data[6,19,21,22,24,25], especially the data at 14.6 MeV, the evaluated data were showed in Fig.2.

2.3 Radiation Capture Cross Section

For ^{55}Mn(n,γ)^{56}Mn reaction, there are experimental data[17,28~44] at thermal energy point and in energy region from 0.19 MeV to 19.8 MeV, listed in Table 2.

Table 2 Survey of measured cross section for ^{55}Mn(n,γ) ^{56}Mn reaction

Year	Author	E_n / MeV	Detector	Moniter	Comments
1958	J.L.Perkin	14.5	GEMUC	^{27}Al(n,α)	Detector was calibrated with beta counter. Keeping neutron back- ground to main neutron < 0.5%
1958	A.I.Leipunskj	2.6999	SCIN	^{127}I(n,γ)	No correction for low energy neutron
1958	A.I.Leipunskj	4.0	SCIN	^{127}I(n,γ)	ibid
1959	A.E.Johnsud	0.147~5.5	NaI	^{235}U(n,f)	
1961	Ju.Ja.Starissky	0.23~1.66	IOCH	^{235}U(n,f)	Energy resolution is poor
1967	H.O.Menlov	0.97~19.39	NaI	^{235}U(n,f)	Energy resolution 1.8%~8 %
1967	J.Csikai	14.7	GEMUC		Minor corrections elsewhere
1967	G..Peto	3.0	GEMUC	^{31}P(n,p)	Determined thermal neutron and neutron flux
1968	J.Colditz	2.9	GEMUC	^{115}In(n,n')	
1969	A.G.Dovbenko	0.48~3.43	GEMUC	^{235}U(n,f)	background Corrected, energy resolution ~2%. A few is 8%
1976	O.Schwere	14.6	Ge(Li)	^{27}Al(n,α)	pure Mn sample
1976	J.vuletin	14.4	Ge(Li)	^{27}Al(n,α) ^{56}Fe(n,p)	Corrected for low energy neutron
1977	J.Csikai	14.1	GE(Li)	^{27}Al(n,α) ^{115}In(n,n')	Corrected to old data
1977	M.majumder	14.8	GEMUC	^{63}Cu(n,2n)	No correction for low neutron
1979	M.Budnar	14.1	BPAIR	Absolute	Integrated value 13.5~14.7 MeV
1980	G.Magnusson	14.7	Ge(Li)	^{27}Al(n,α)	Energy resolution 2%
1984	B.M.Bahal	14.7	Ge(Li)	^{27}Al(n,α) ^{27}Al(n,p)	No information for low energy neutron
1987	Yu.N.Trofimov	2.0	Ge(Li)	^{197}Au(n,γ) ^{115}In(n,n')	pure Mn sample
1997	Yu.N.Trofimov	1.0	Ge(Li)	^{197}Au(n,γ)	inid
1990	R.P.Gautan	0.46~3.43	Ge(Li)	^{127}I(n,γ)	Energy resolution are 10%~24%

BPAIR: Scintillation pair spectrometer GEMUC : Mica end-window Geiger muller counter
IOCH : End-window counter SCIN: Scintillation counter

The earlier data were measured by using activation method in general, the activity of the residual nucleus of ^{56}Mn was measured by using mica end-window counter for β or NaI detector for γ-ray. The decay data like half-life, γ or β breaching ratio, are consistent with each other and monitor standard are also reasonable. But the data are much larger than those predicted by compound nucleus theory. Through the investigation and analysis for the ^{55}Mn(n,γ)^{56}Mn reaction measurement, it was found that the key effects on the experimental accuracy are the sample purity, determination of activity of ^{56}Mn and low neutron effects. It is well known that the ^{55}Mn(n,γ)^{56}Mn cross section is very high at low neutron energies ($\sigma_{thermal}$=13.4 b), so the contribution from D-D neutron and secondary neutron with lower energy imposes effect on ^{55}Mn(n,γ)^{56}Mn cross section, adoption of the purified to 99.9% Mn sample and keeping a fresh target is very important to reduce the effect of low energy.

For ^{55}Mn(n,γ)^{56}Mn, the cross section is only a few *mb* in MeV region, the key point is to minimize the contribution of low energy neutron and determinate the correction quantities accurately. The data are in agreement within errors by using improved experimental technique.

The data measured by G. Peto[39] were corrected for the effects of low energy neutron and D-D neutron produced on target, the intensities of thermal and epithermal neutron and the neutron flux due to deuteron deposited in the target were determinate .

The data were measured by J.L. Perkin[28] using bate counter, the efficiency of which was calibrated with a 4π β counter. In order to reduce the effect of the neutron inelastic scattering from vicinity and from D-D neutron due to the accumulation of deuterium in the tritium-target with time, the time of using target was controlled.

J.Vuletin[32] and O.Schwere[31] considered the effects from contribution of low neutron produced in target holder and sample. The corrections were carried out, about 14% by O.Schwere.

The data were measured by G. Magnusson[35] using Ge(Li) detector with Van de graaff accelerator in 1980. A tritium titanium target was used as neutron source. The data measured were corrected for gamma-ray attenuation in the sample, secondary neutron summing effects, room-scattered neutrons and sample thickness. The determination of the Ge(Li) detector efficiency, monitor cross section, and decay parameters used activity build-up, correction are all reasonable. The data of J.L.perkin[28], H.O.Menlove[29], O.Schwere[31], J.Vuletin[32] and G.Magunusson[35] are in agreement within errors around 14 MeV. Meantime the data of H.O.Menlove[29] give the trend from 0.97 MeV to 19.39 MeV, which are very useful in this energy region due to locking data in general.

There are resonance structures for ^{55}Mn(n,γ) cross sections up to MeV region. Therefore, the measurements of the data require good energy resolution and high effect-background ration.

The data were measured by A.E. Johnsud [41] from 0.147 MeV to 5.5 MeV, by A.G. Dovbenko [40] from 0.418 MeV to 3.43 MeV, by Ju.Ja.Stavisskiy[42] from 0.23 MeV to 1.66 MeV and by R.P.Gautan[36] from 0.46 MeV to 3.43 MeV, respectively. In 1980s, Yu.N.Trifimov[37] measured data at 2 and 3 MeV by using Ge(Li) detector and metallic monoisotopic sample.

The data measured by Ju.Ja.Stavisskij[42] were with poor energy resolution. R.P.Gautan's data[36] were averaged ones from 2 runs in1990, for example, the datum at 0.76 MeV was the averaged value from 4.90±0.6 and 6.06±mb. In addition, most of incident energy resolution was 12%~20%. The neutron sample used by M.Budnar[34] was too close to the tritium target, as a result the neutron energy was spread. The data are spectrum average over a solid angle of 2π, neutron energy from 13.5 MeV to 14.7 MeV. Therefore, these three sets of data [34,36,42] were rejected.

At the thermal energy point, datum was evaluated by E.J.Axton[44] in 1986. Up to now there were no new experimental data, the evaluated value was 13.408 ±0.00307 b and was adopted in this work.

All of data measured[17,28,29,31,32,35,37,38~40] cover whole energy region from thermal energy to 20 MeV. The evaluated data were obtained based on experimental data, shown in Fig.3.

2.4 (n,α) and (n, p) Cross Sections

^{55}Mn(n,α)^{52}V reaction cross section measurements were performed using activation method. For the data measured early, NaI detector and β counter were used to measure the activity, the fluctuation of the count was quite large due to the poor effect-background ration.

1980s, the data were measured by E.Zupranska[45] using Gi(Li) detector and high purity sample from 13 MeV to 17.8 MeV. The data were researched jointly by A.Fessler, Y.Ikeda and J.M.Meadows[46] from GEL, JAERI and ANL laboratories, respectively. Pure Mn sample and high purity Ge(Li) detector were used and the measured data were corrected for neutron absorption and multiple scattering in sample, neutron flux fluctuation and contribution from lower energy neutron. The data of them are very accurate in the energy region from 16.0 MeV to 20.13 MeV. The data were measured by M.Bostan[25] from 6.33 MeV to 11.97 MeV at Julich CV28 variable-energy compact cyclotron. The trend of M.Bostan's data were consistent with that of

E.Zupranska[45] around 12~13 MeV. All of these measured data cover the energy region from threshold energy to 20 MeV and the curve of the cross section is reasonable in physics. Meantime, the data at 14.7 MeV measured by R.Vaenskae[47] using rotating tritium target, are very accurate and consistent with ones of E.Zupranska[45]. Therefore, the data were recommended based on the measured data[25,45~47], shown in Fig. 4.

For ^{55}Mn(n, p) ^{55}Cr reaction cross section, there are a few measured data. The data were mainly measured by M.Bostan[47] from 6.33 MeV to 11.97 MeV. The neutron flux was monitored with ^{56}Fe(n,p) reaction in the neutron energy range from 6 MeV to 8 MeV, and ^{27}Al(n,α) reaction between 8 MeV and 13 MeV. The data were corrected for background neutron and break-up neutrons. The activity of ^{55}Cr was measured using low-level beta counting and the beta count was corrected for ^{52}V interfering effects from ^{55}Mn(n,α)^{52}V reaction. The data of M.Bostan[25] are quite accurate and useful for giving the trend of the cross section from threshold energy to 13 MeV. Because the data measured are very scattering and with large errors above 13 MeV, the recommended data for ^{55}Mn(n,p) ^{55}Cr reaction cross section were based on the data measured by M. Bostan[25] and theoretical calculated data, shown Fig 5.

3 Theoretical Calculation and Parameter Adjusting

3.1 Total and Nonelastic Cross Section

There are resonance structures for total cross section of ^{55}Mn up to 4 MeV. In order to meet the requirement for searching the neutron spherical optical potential parameters, the resonance structures were treated into smooth one.

The measured nonelastic scattering cross sections are lack, the cross sections were calculated based on the measured and evaluated data concerned, including total, capture, (n,n), (n,2n), (n,3n) and (n,x) etc.. There are enough elastic scattering angular distribution data in incident neutron energy E_n=0.1~11.0 MeV. A set of neutron spherical optical potential parameters was obtained with the automatically searching codes.

Using this set of neutron optical potential parameters and adjusted level density and giant dipole resonance parameters, the reaction cross sections, angular distributions, double differential cross section and gamma production data of n + ^{55}Mn were calculated by WANG shunuan[48] with UNF code[49].

3.2 Inelastic Scattering Cross Section

The inelastic scattering cross sections were evaluated and calculated. The total inelastic scattering cross sections were sum of partial inelastic scattering cross sections (MT=51 to 64 and 91).

The direct component was calculated with coupled channel optical model code ECIS[50]. The neutron inelastic angular distribution to the ground rotational band 0.126,0.984,1.292 and 1.884 MeV levels, were calculated from threshold to 20 MeV. The compound nucleus contributions calculated with UNF[49] code were summed up with the direct components. For other levels, the data were calculated by the statistical theory with width fluctuations using UNF[49] code.

In order to calculate the inelastic scattering cross sections, these direct inelastic scattering data and the optimum set of optical potential parameters were used as the input data of UNF. The parameters of discrete levels were taken from China Nuclear Parameter Library.

Using the adjusted parameters, including optical potential, levels, and other parameters concerned, a complete set nuclear data of n+^{55}Mn was calculated.

4 Comprehensive Recommendation

4.1 Reaction Cross Sections

The total, (n,2n),(n,γ) and (n,α) cross sections were recommended based on experimental data, and the others, including (n,n'), (n,3n), (n,x) etc. were recommended based on the measured and theoretically calculated data.

4.2 Energy-Angle Distributions

The energy-angle distributions for (n,2n), (n,3n), (n,np), (n,nα) and (n,n'$_{continuum}$) reactions were calculated with code UNF. There are experimental data of double differential cross section of n+^{55}Mn at 14.1 MeV. The calculated results were compared with available experimental data[51,52], shown in Fig.6.

4.3 Photon-Production Data

The calculation for all photon-production data were carried out with code UNF.

The data of MT=51~64 and for MF=12 and 14, and MT=102 for MF=15 were given.

5 Remarking Summary

The complete set of data in the energy region from 10^{-5} eV to 20 MeV for ^{55}Mn was evaluated based on experimental and theoretically calculated data.

Based on all available ratio and absolutely experimental data, especially around 14 MeV, the energy-angle distributions for (n,2n), (n,3n), (n,np), (n,nα) and (n,n'$_{continuum}$) reactions were calculated

with code UNF and compared with available experimental data of M.Baba [51] and A.Takahashi[52] at 14.1 MeV. It was found that the calculated results are lower than the experimental ones in the energy region 1~3 MeV and 7~12 MeV. In addition, the calculated data are also a little lower in other energy region. It means that the nonelastic cross section may be lower, especially the (n,2n), (n,3n), (n,n'p) (n,nα) and (n,n') cross sections. But comparing these cross sections with experimental data and evaluated data from JENDL-3.3, no large differences were found. Any way, the difference should be studied further and need to be improved.

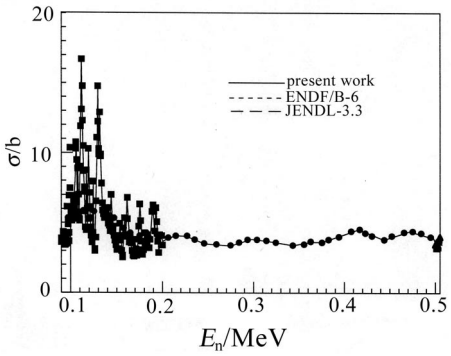

Fig.1a Evaluated and measured cross section for ^{55}Mn(n,tot) reaction

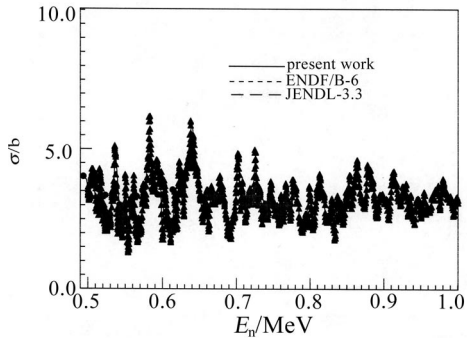

Fig.1b Evaluated and measured cross section for ^{55}Mn(n,tot) reaction

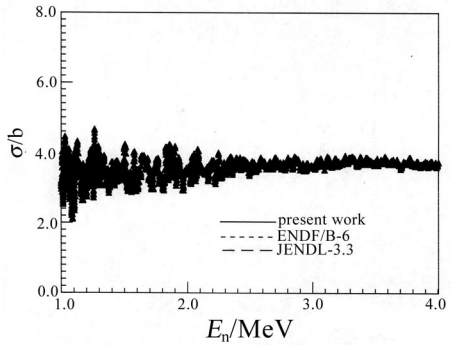

Fig.1c Evaluated and measured cross section for ^{55}Mn(n,tot) reaction

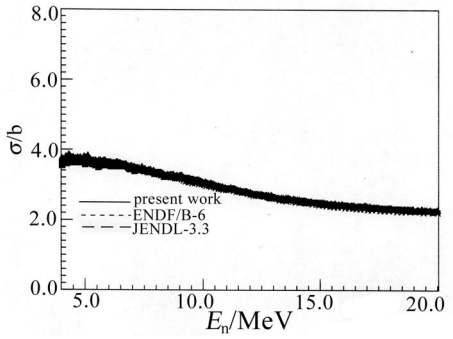

Fig.1d Evaluated and measured cross section for ^{55}Mn(n,tot) reaction

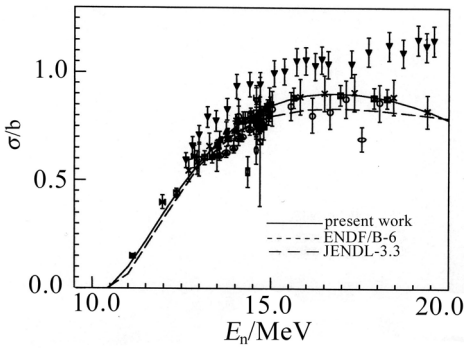

Fig.2 Evaluated and measured cross section for ^{55}Mn(n,2n) reaction

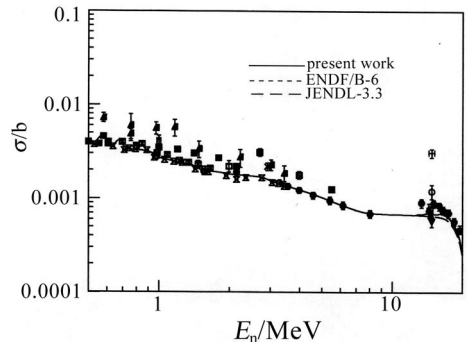

Fig.3 Evaluated and measured cross section for ^{55}Mn(n,γ) reaction

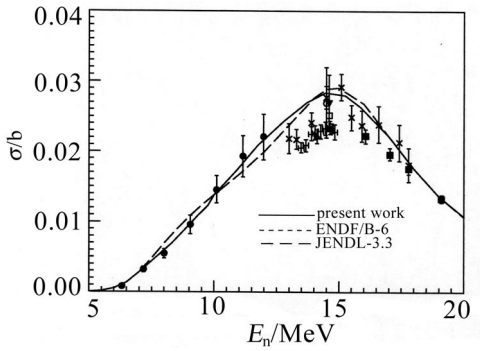

Fig.4 Evaluated and measured cross section for ^{55}Mn(n,α) reaction

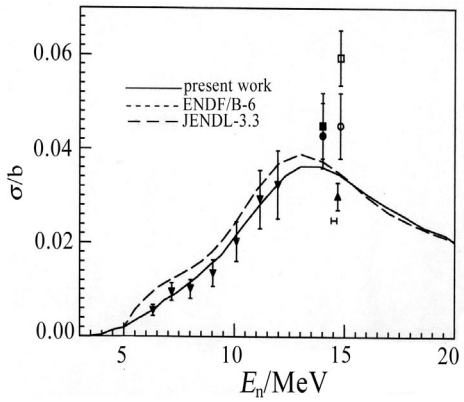

Fig.5 Evaluated and measured cross section for ^{55}Mn(n,p) reaction

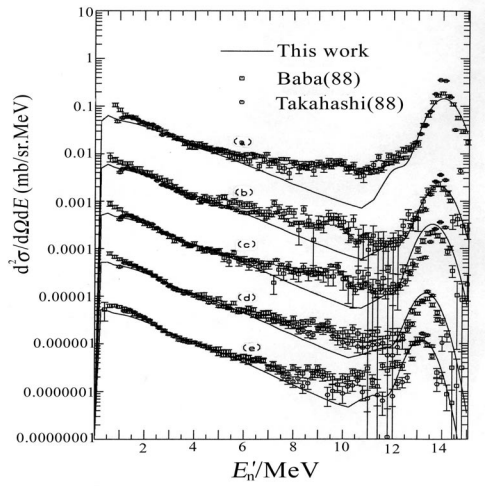

Fig.6 DDX of ^{55}Mn at 14.1 MeV

References

[1] S.Cierjacks, et al. KFK-1000,(Supp.2)(1969)

[2] W.F.E Pineo, et al. AP,84,165(1974)

[3] J.B.Garg, et al. Nucl.Scin.Eng.,65,76(1978)

[4] W.P.Abfalteror, et al. Phis.Rev/C,63, (2001)

[5] Paulsan, et al. JNE/AB,19,1970(1965)

[6] H.O.Menlove, et al. Phys.Rev.,163,1308(1967)

[7] H.Vonach, et al. EXFOR Data N0.21533002 (1968)

[8] M.Bormann, et al. Nucl.Phys./A,130,195(1969)

[9] R.C.Barrall, et al. AFWL-TR-68-134(1969) Nucl.Phys./ P,138,387(1969)

[10] Salnikov, et al. YK-7,102(1972)

[11] G.N.Maslov, et al. YK-9,50(1972)

[12] J.Arrminowiez, et al. INP-1464,14(1973)

[13] F.Deak, et al. AHP,38,209(1975)

[14] Schwerew, et al. EXFOR Data N0.20811006 (1976)

[15] K. Kayashima, et al. NEANDC (J)-61U, 94(1979)

[16] M.Berrada, et al. EXFOR Data N0.30805002 (1984)

[17] B.M.Bahal, et al. GKSS-84-E(1984)

[18] J.W.Meadows, et al. ANE,14,489(1987)

[19] L.R.Greenwood, et al. ASTM-STP-956, 743(1987)

[20] K.Kobayashi, et al. 88MITO,261(1988)

[21] Y. Ikeda, et al. JAERI-1312(1988)

[22] LU Hanlin, et al. INDC(CPR)-16(1989)

[23] Kimura, et al. Nucl.Scin.Eng.,106,332(1990)

[24] T.S.Socwarsong, et al. JAERI-M-92-027, 354 (1992)

[25] M .Bostan, et al. Phys.Rev./C,49,226(1994)

[26] A.A.Filatenkov, et al. INDC(CCP)-402(1997)

[27] ZHAO Wenrong, et al. INDC(CRP)-16(1989)

[28] J.L.Perkin, et al. J.PPS,72,505(1958)

[29] H.O.Menlov, et al. Phys.Rev.,163,1299(1967)

[30] J.Csikai, et al. Nucl.Phys/A,95,229(1967)

[31] Schwere, et al. Nucl.Phys/A,264,105(1976)

[32] J.Vuletin, et al. J.NCL,10,1(1974)

[33] M.Majumder, et al. BOS,40,81(1977) EXFOR Data N0.30296008(1979)

[34] M.Budnar, et al. INDC(YUC)-6(1979)

[35] G.Magnusson, et al. Physical Scripta,21,21(1980)

[36] R.P.Gautan, et al. Indian Journal of Pure and Applied Physics ,A,28,235(1990)

[37] Yu.N.Trofimov, et al. J.YK,4(1987)

[38] J.Colditz, et al. J.OSA,105,236(1968)

[39] G.Peto, et al. J.JNE,21,797(1967)

[40] A.G..Dovbenko, et al. AE,26,67(1967)

[41] A.E.Johnsud, et al. Phys.Rev.,116,927(1959)

[42] Ju.Ja.Stavisskij, et al. AE,10,508(1961)

[43] A.I.Leipunskij, et al. Proceeding conf. on Peaceful Uses of Atomic Energy, 15,50(1958). Geneva, 8~20, Aug. 1955.

[44] E.J.Axton, et al. Annals of Nuclear Energy, 13, 627 (1986)

[45] E.Zupranska, et al. APP/B,11,853(1980)
[46] Fessler, et al. Nucl.Scin.Eng.,134,171(2000)
[47] R.Vaenskae, et al. NIM,171,281(1980)
[48] WANG Shunuan, et al. to be published
[49] ZHANG Jingshang, et al. CNIC-01616, CNDC-0032 (2001)
[50] J.raynal, et al. Note on ECIS 94, CEN-N2772(1994)
[51] M.Baba, et al. C,88MITO,209(1988)
[52] Takahashi, et al. JAERI-M-214(1989)

n+^{55}Mn (≤20 MeV) Nuclear Data Calculation and Analysis

WANG Shunuan[1] YU Baosheng[1] MA Gonggui[2]

1 China Nuclear Data Center, CIAE, P.O.Box275(41), Beijing 102413

2 Institute of Nuclear Science and Technology, Sichuan University, Chengdu 610064

【abstract】 *n+ $^{55}_{25}$Mn (≤20MeV) whole set of nuclear data calculation in ENDF/B6 format was carried out by using spherical optical model, coupled channel optical model, pre-equilibrium exciton model and equilibrium statistical model. The calculated cross sections, angular distributions, spectrum and double differential cross sections by using codes of APOM[1], ECIS95[2] and UNF[3] are compared with all existential measured nuclear data for n+ $^{55}_{25}$Mn (≤20MeV) taking from EXFOR. The calculated results are analyzed from theoretical model and model parameters used.*

1 Spherical Optical Model Calculation and Analysis

The n+ $^{55}_{25}$Mn (≤20 MeV) experimental data of total cross section and non-elastic cross section as well as angular distributions were evaluated by Profs. YU Baosheng and MA Gonggui before doing theoretical calculation using code of APOM. According to those evaluated data with running code APOM, the whole set of optimum spherical optical model 21 parameters were obtained by automatically searching for main 14 parameters based on the formula described in Ref. [3] as the following:

AR=0.64889604	AS=0.43464568
AVV=0.32882652	ASO=0.64889604
XR=1.24915159	XS=1.39492059
XV=1.63509786	XSO=1.24915159
XC=1.250000	
	(in fm)
U0=-1.38532853	U1=0.16954480
U2=0.00068179	V0=55.38682175
V1=-0.59981227	V2=-0.00999689
V3=-24.0	V4=0.0
VSO=6.2	W0=11.12653351
W1=-0.30288908	W2=-12.0
	(in MeV)

The calculated n+ $^{55}_{25}$Mn (≤20 MeV) total cross section, elastic cross section and its angular distributions, non-elastic cross section are compared with all existential measured data taking from EXFOR and also with ENDF/B-6 and JENDL-3. The satisfied agreement is obtained as a whole. Figs.1-1,1-2,2,3 show the comparison among calculated and evaluated experimental total cross section, elastic cross section, non-elastic cross section and ENDF/B-6 , JENDL-3.

2 Coupled Channel Optical Model ECIS95 Calculation and Analysis

The direct inelastic scattering cross sections and angular distributions for discrete levels of 0.126, 0.984, 1.292, 1.884 MeV were calculated by coupled channel optical model code of ECIS95 and PRECIS using spherical optical model parameters recommended in ENDF/B-6 and JENDL-3 with β_2=0.2 and β_4=0.02. There exist some angular distribution experimental data for ^{55}Mn(n,n') discrete levels of 0.984, 1.289, 1.528, 1.884 MeV at E_n=3.4 MeV taking from EXFOR. By adding the contribution of compound nuclear reaction calculated using UNF code, the whole ^{55}Mn(n,n') angular distribution for discrete levels of 0.984, 1.289, 1.528, 1.884 MeV at E_n=3.4 MeV were obtained and compared with experimental data shown in Fig.4,5,6,7, respectively. It can be seen from Fig.4,7

that the calculated angular distributions by ECIS95 for discrete levels of 0.984, 1.884 MeV are a little forward peaked by taking into account of the direct inelastic scattering, but are not enough as shown by experimental data. It can be seen from Fig.5,6 that calculated angular distributions by UNF for discrete levels of 1.289, 1.528 MeV are 90° symmetrical in CM system as described by equilibrium statistical theory.

3 Comparison and Analysis

Fig.8,9,10,11,12 show the comparison among calculated results, experimental data, and ENDF/B-6, JENDL-3 for ^{55}Mn(n,γ), (n,n'), (n,2n), (n,p), (n,α) cross sections respectively. There no any other cross section experimental data except reaction channels mentioned above. Fig.10 shows that the shape of ^{55}Mn (n,2n) cross section as a function of energy is very reasonable, it fits the experimental data measured by LU Hanlin (1989, EXFOR 30615002 and 30615003) as well as by Menlove (1967, EXFOR 11421005) quite well, and it is better than ENDF/B-6 and JENDL-3.3. From Fig.11 we can see that the shape of ^{55}Mn(n,p) cross section as a function of energy is also very reasonable, it fits the experimental data better than ENDF/B-6 and JENDL-3.3.

For the pre-equilibrium exciton model calculations of spectrum and double differential cross sections, the free parameter *K*-value of the square of the average two-body residual interaction matrix element formulated by C.Kalbach et al.[4] was taken as 400 MeV^3. We have two reasons for doing this chosen. First of all, in our previous papers[5,6] this value was used for analyzing neutron inelastic scattering cross section and double differential cross sections at 14.6 MeV and 15 MeV for more than 34 elements compared with experimental data of Hermsdorf et al. 1974[7]. We think it works very effectively. Secondly, a non-relativistic exciton transition rate (<60 MeV) was calculated using the imaginary part of both the phenomenological and microscopic optical potential with Skyrme interaction in our previous paper [8]. The general conclusion in this work is that the empirical formula for the square of the average two-body residual interaction matrix element with the free parameter *K* formulated by C.Kalbach et al. is reasonable in the energy range below 60 MeV, while the value of the free parameter *K* should be taken as about 400 MeV^3. The calculated spectrum compared with existential experimental data is shown in Fig.13 for Mn(n,x) at 14.6 MeV .

The calculated double differential cross sections of neutron emission compared with existential experimental data are shown in Fig.14~19 at 14.1 MeV, and at 30°, 60°, 90°, 120°, 150°, respectively. From Fig.14~19 it could be discussed as the following: A, Calculated results are lower than the experimental data at low energies of emitting particles obviously. This means that the contribution of compound reaction is not taking into account enough properly. B, In the statistical model calculations, the last discrete level energy of nucleus ^{55}Mn is 2.3658 MeV. From those Figs., we can see that there is a shoulder on the side of elastic scattering peak and the width of the shoulder is just about 2.5 MeV. This indicates that the both contribution of direct reaction and statistical model for discrete inelastic scattering of ^{55}Mn(n,n′) at 14.1 MeV is described well and the calculated result is more closed to the experimental data. C, The calculated results after the shoulder are much lower than the experimental data around emitted particle energies of 10 MeV in a rather wide energy range. On the one hand, it can be improved by taking more discrete levels to extend the shoulder, but we do not think that it shall work effectively as expected for $^{55}_{25}$Mn , such an odd-odd nucleus without more enough discrete levels experimental information. On the other hand, the Gilbert-Cameron level density formula [9] used in the statistical model code UNF is not sufficient for describing the continuum levels connected with last discrete level. And besides, it is completely different from the formula presented by Gilbert-Cameron for positive and negative parity uniform distribution. In fact, all of 18 levels up to 2.398 MeV from the discrete level experimental information are all with the negative parity. Up to now the discrete level calculation can be done as many as we wish so we have enough experimental levels information. Thus the pair correction energy parameter in the formula used in UNF to describe the continuum levels is much less exact original physical meaning, and generally pair correction energy parameter taken from CENPL[10] or RIPL [11] is not so small. There are two calculated lines in Figs15~18. The solid line represents the result for *K*=400 MeV^3 which is used in the present work. The dashed line represents the result for *K*=190 MeV^3 which is the lowest value used for (n,p) reaction in the literature. It is quite reasonable that the dashed line is higher than the solid line. It can be understood well that the smaller *K* value, the longer life time of exciton state, the more contribution of pre-equilibrium emission, the more hard of the "tail" of the emission spectrum.

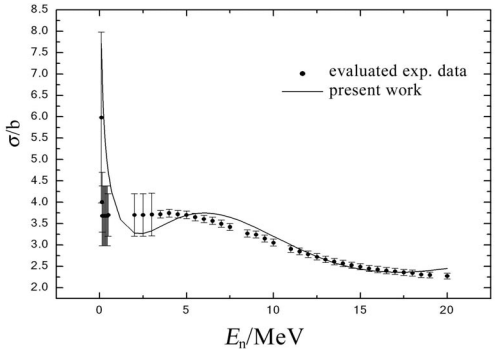

Fig.1-1 Calculated and evaluated experimental total cross section

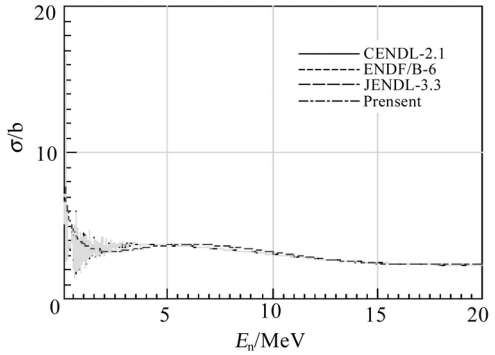

Fig.1-2 Comparison of calculated total cross section with that of ENDF/B-6, JENDL3.3, CENDL2.1

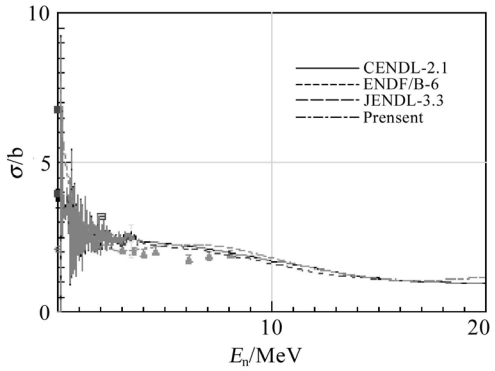

Fig.2 Calculated elastic cross section and compared with exp. data and ENDF/B-6, JENDL-3

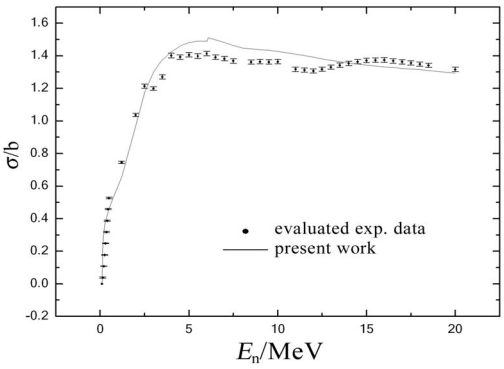

Fig.3 Comparison of calculated and evaluated experimental non-elastic cross section

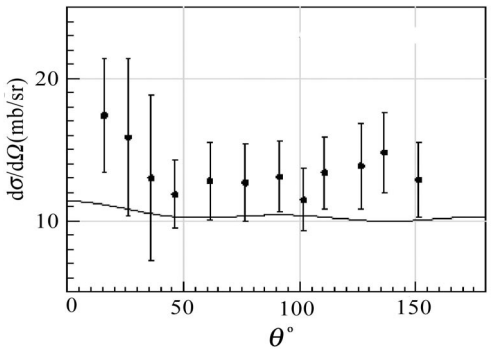

Fig.4 Calculated angular distribution of level 0.984 MeV at E_n=3.4 MeV and compared with experimental data

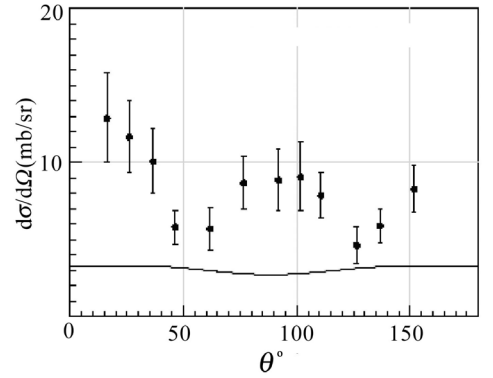

Fig.5 Calculated angular distribution of level 1.289 MeV at E_n=3.4 MeV and compared with experimental data

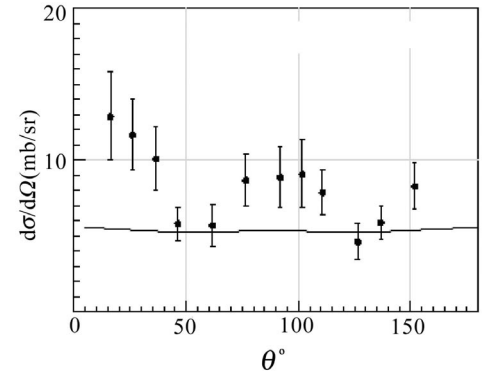

Fig.6 Calculated angular distribution of level 1.528 MeV at E_n=3.4 MeV and compared with experimental data

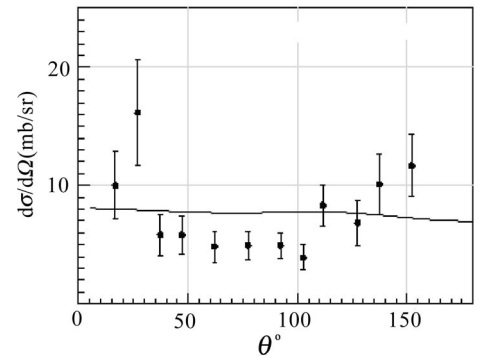

Fig.7 Calculated angular distribution of level 1.884 MeV at E_n=3.4 MeV and compared with experimental data

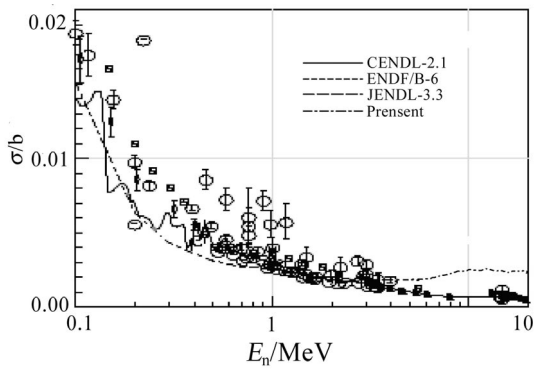

Fig.8 Comparison among calculated results, experimental data and ENDF/B-6, JENDL-3 for Mn(n,γ) cross sections

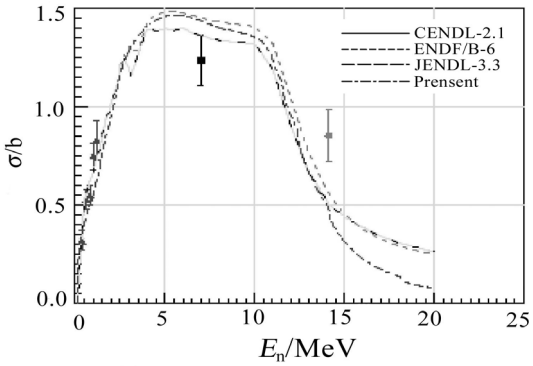

Fig.9 Comparison among calculated results, experimental data and ENDF/B-6, JENDL-3 For Mn (n,n') cross sections

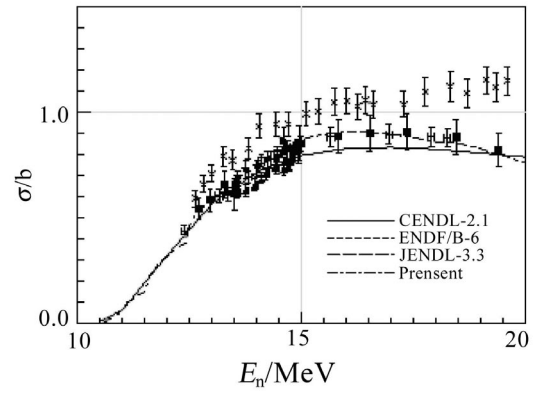

Fig.10 Comparison among calculated results, experimental data and ENDF/B-6,JENDL-3 for Mn (n,2n) cross sections

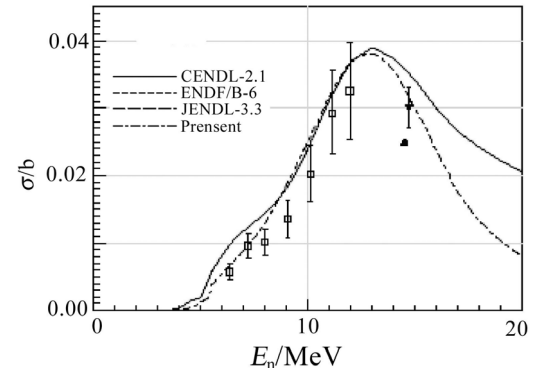

Fig.11 Comparison among calculated results, experimental data and ENDF/B-6,JENDL-3 for Mn (n,p) cross sections

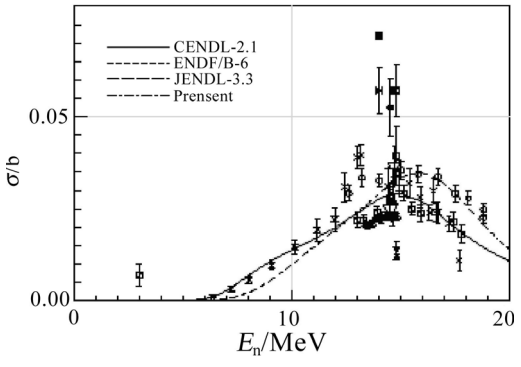

Fig.12 Comparison among calculated results, experimental data and ENDF/B-6,JENDL-3 for Mn (n,α) cross sections

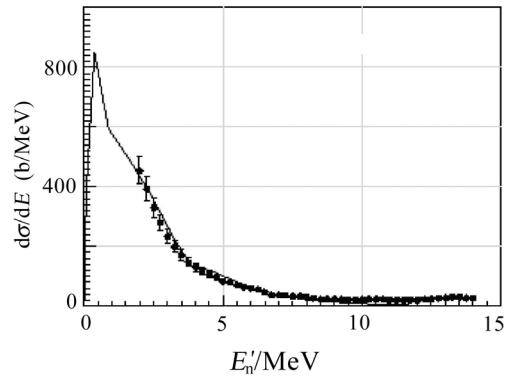

Fig.13 Calculated spectrum of neutron emission compared with experimental data at 14.6 MeV

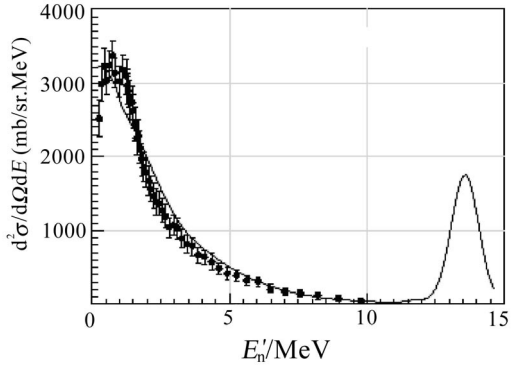

Fig.14 Calculated double differential cross sections of neutron emission compared with experimental data at 14.1 MeV,92°

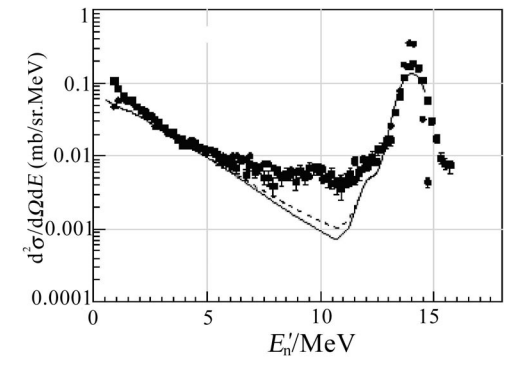

Fig.15 The calculated double differential cross sections of neutron emission compared with experimental data at 14.1 MeV, 30°

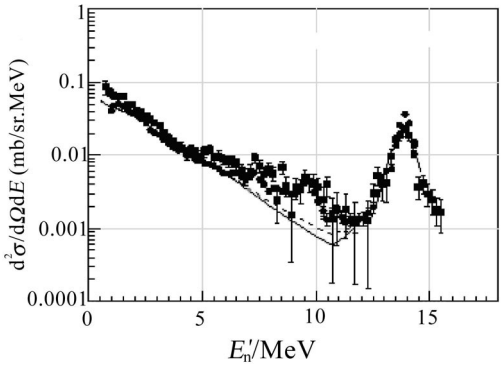

Fig.16 The calculated double differential cross sections of neutron emission compared with experimental data at 14.1 MeV, 60°

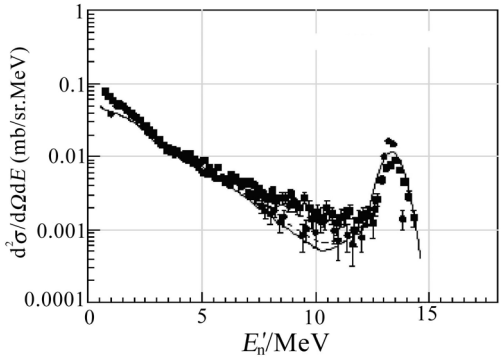

Fig.18 The calculated double differential cross sections of neutron emission compared with experimental data at 14.1 MeV, 120°

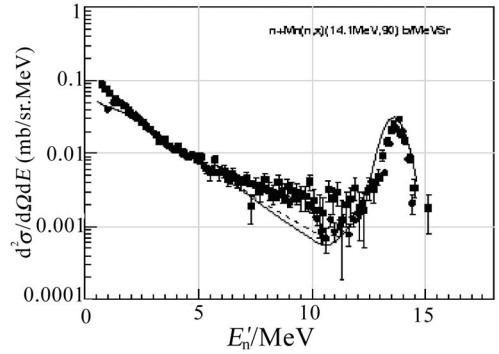

Fig.17 The calculated double differential cross sections of neutron emission compared with experimental data at 14.1 MeV, 90°

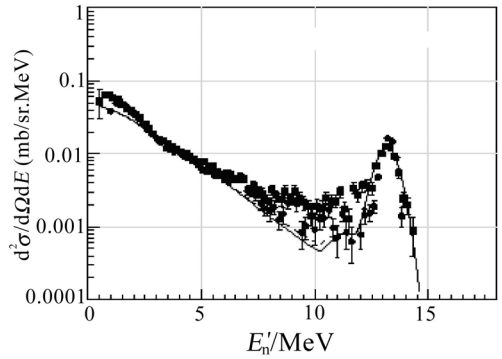

Fig.19 The calculated double differential cross sections of neutron emission compared with experimental data at 14.1 MeV, 150°

References

[1] SHEN Qingbiao. CNDP.7,43,1992.

[2] J.Raynal. Note on ECIS94, CEN-N2772,1994; B. V. Carlson, The Optical Model ECIS95, Workshop on Nuclear Reaction Data and Nuclear Reactos-Physics, Design and Safety, H4.3MR/921-3, 15 April-17 May 1996, Miramare, Trieste Italy.

[3] ZHANG Jingshang. CHIC-01616,CNDC-0032,2001.

[4] C.Kalbach. Nucl.Phys. A210,590 (1973).

[5] SUN Ziyang, et al. Z.Phys.A 305,61-68 (1982).

[6] SUN Ziyang, et al. Nuclear Data for Science and Technology, K.H. Bockhoff(ed.), 603-605(1983).

[7] D.Hermsdorf et al. Zeentralinstitut fur Kernforschung, Rossendorf bei Dresden Report No.ZFK-277(1974).

[8] SHEN Qingbiao, et al. Chinese Jour. Nucl. Phys., Vol.6, 245 (1984).

[9] A.Gilbert, et al. Can.J. Phys., 43, 1446 (1965).

[10] SU Zongdi et al. Commu. Nucl. Data Progress 7, 73 (1992).

[11] IAEA-TECDOC-1034.

Reevaluation of Neutron Nuclear Data of ^{98,100}Mo in the energy region 0.1~20 MeV

CAI Chonghai

Department of Physics, Nankai University, Tianjin 300071

【**abstract**】 *The complete sets of nuclear data below 20 MeV are calculated and evaluated for n + ^{98,100}Mo reactions. All kinds of cross sections, angular distributions, energy spectra and/or double-differential cross sections of all emitted particles, gamma production data (production cross sections and multiplicity, energy spectra) are included. In most cases, the calculated cross sections are in rather good accordance with the experimental values.*

Introduction

For the element molybdenum, there are seven stable isotopes: ^{92}Mo (14.84%), ^{94}Mo (9.25%), ^{95}Mo (15.92%), ^{96}Mo (16.68%), ^{97}Mo (9.55%), ^{98}Mo (24.13%) and ^{100}Mo (9.63%), which are important fission products, also rather important structure material nuclei. This paper only refers to ^{98}Mo and ^{100}Mo, the existed evaluation files include ENDF/B-6, JEF-2, JENDL-3.2 and CENDL-3. However, the evaluation files in ENDF/B-6(1980) only include (n,γ) data(MT=102 in file 3,8,9). The present results were only compared with JEF-2, JENDL-3.2 and CENDL-3 and experimental data in Figs. 1~9. All the experimental data in these figures were taken from EXFOR, the references indicated in EXFOR for every set of data were not given in this paper. In some cases perhaps the first author and the published year were indicated.

The complete sets of neutron nuclear data of ^{98,100}Mo in JEF-2 were really evaluated before 1990, and in JENDL-3.2 before 1993. The experimental data after 1989 for JEF-2 and after 1992 for JENDL-3.2 were not used. The calculations of ^{98,100}Mo for CENDL-3 were made by us in 1997; but we did not carefully analyse the experimental data coming from different authors and different years, simply dealing with them in equal weight. So CENDL-3 had a little improvement. Furthermore, for ^{98,100}Mo, there are no double differential cross sections and gamma production data in JEF-2, JENDL-3.2 and CENDL-3. The new version 2001 of program UNF[1] improved much in comparison with version 1997, especially it can calculate the reaction cross section leaving the residual nucleus in a isomeric state. Thus it is necessary for us to recalculate and reevaluate the complete sets of neutron nuclear data of ^{98,100}Mo, considering some newer reliable experimental data and those of isomeric state, and including double-differential cross sections and gamma production data in ENDF/B-6 format output.

1 Parameters Used in UNF and Direct Inelastic Contribution

There are three sets of experimental total cross sections for ^{98}Mo (Smith75, Lambropoulos73 and Divadeenam68) and ^{100}Mo (Pasechnik80, Smith75 and Lambropoulos73) below 5.5 MeV, respectively. For elastic scattering angular distributions, there are five sets of experimental data (Rapaport79, Daniel77, Ferrer77, Smith75 and Lambropoulos73) for ^{98}Mo and ^{100}Mo, respectively. Based on these experimental data and one set of experimental total cross sections of natural molybdenum (Larson80) above 2 MeV, we used the program APMN[2] to automatically search for the optimal optical potential parameters of ^{98}Mo and ^{100}Mo in neutron channel. For five charged particle channels, we usually used the universal optical potential parameters[3], in order to make the calculated (n,p), (n,α) and (n,d) reaction cross sections agree with experimental data, we also adjusted some optical potential parameters in charged particle channels by hand. The meaning of all the parameters is explained in Eqs. (1), (2), (6) and (7) of Ref. [2]. The optical potential parameters used in our final calculations are given in Table 1(a) and (b) for ^{98}Mo and ^{100}Mo, respectively, and were also used in calculations of the direct inelastic cross sections as well as angular distributions with DWUCK4[4]. Levels and their deformation parameters β_2 used in direct inelastic calculation are given in Table 2.

The optical potential parameters in Table 1 and the direct inelastic cross sections as well as angular distributions obtained with DWUCK4 were used as a part of input data for the main code UNF.

In UNF, Gilbert-Cammeron formula is employed for calculation of the level density. The level density parameter a, the pair energy correction Δ and the two peak giant resonance parameters for gamma emission were obtained from the Parameters Library in CNDC. The data of levels and their spin, parity and the branch ratio of gamma emission were taken from the Parameters Library in CNDC and/or the Web Site of NNDC at BNL, USA. In calculation, in order to make the calculated cross sections accord with experimental data better, some of the level density parameters *a* and the pair energy corrections Δ were adjusted. The *a* and Δ′s values used in our final calculations are given in Table 3.

The adjustable Kulbach parameter in exciton model was determined mainly based on the total neutron spectra, its value obtained is *CK*=490.0 for both ^{98}Mo and ^{100}Mo.

Besides above mentioned parameters, there are the adjustable factor in (n,γ) cross section calculation *CE1*=7.5 for ^{98}Mo and 8.3 for ^{100}Mo, the adjustable parameter in direct (n,γ) calculation *DGM*=0.80 for ^{98}Mo and for ^{100}Mo.

Table 1(a) Optical potential parameters of ^{98}Mo used in this work

channel	n	p	alpha	^{3}He	d	t
a_r	0. 6395463	0.75	0.52	0.72	0.71	0.72
a_s	0. 7221944	0.51	0.52	0.88	0.78	0.84
a_v	0. 5753700	0.51	0.52	0.88	0.78	0.84
a_{so}	0.6395463	0.75	0.52	0.72	0.71	0.72
r_r	1.2194120	1.17	1.302	1.20	1.17	1.20
r_s	1.1006970	1.32	1.242	1.40	1.30	1.40
r_v	1.2627100	1.32	1.242	1.40	1.30	1.40
r_{so}	1.2194120	1.01	1.302	1.20	0.64	1.20
r_c	1.2500000	1.25	1.25	1.30	1.30	1.30
W_{v0}	−6.000000	−2.70	22.4	0.0	0.0	0.0
W_{v1}	0.1762000	0.22	0.0	0.0	0.0	0.0
W_{v2}	−0.0049100	0.0	0.0	0.0	0.0	0.0
V_0	53.1990700	54.0	164.7	151.9	90.6	165.0
V_1	−0.6815308	−0.32	0.0	−0.17	0.0	−0.17
V_2	0.01244627	0.0	0.0	0.0	0.0	0.0
V_3	−24.00000	24.0	0.0	50.0	0.0	−6.4
V_4	0.2461383	0.4	0.0	0.0	0.0	0.0
V_{so}	6.200000	6.2	0.0	2.5	7.13	2.5
W_{s0}	7.897237	11.8	0.0	41.7	12.0	46.0
W_{s1}	0.1317190	−0.25	0.0	−0.33	0.0	−0.33
W_{s2}	−12.00000	12.0	0.0	44.0	0.0	−110.0

And a_{s1}=0.7, a_{v1}=0.7 for p channel.

Table 1(b) Optical potential parameters of ^{100}Mo used in this work

channel	n	p	alpha	^{3}He	d	t
a_r	0. 6318183	0.75	0.52	0.72	0.71	0.72
a_s	0. 7543195	0.51	0.52	0.88	0.78	0.84
a_v	0. 5753700	0.51	0.52	0.88	0.78	0.84
a_{so}	0. 6318183	0.75	0.52	0.72	0.71	0.72
r_r	1.2166270	1.17	1.442	1.20	1.17	1.20

Cont Table 1(b)

channel	n	p	alpha	^{3}He	d	t
r_s	1.1567090	1.32	1.442	1.40	1.30	1.40
r_v	1.2627100	1.32	1.442	1.40	1.30	1.40
r_{so}	1.2166270	1.01	1.442	1.20	0.64	1.20
r_c	1.2500000	1.25	1.25	1.30	1.30	1.30
W_{v0}	–6.000000	–2.70	22.4	0.0	0.0	0.0
W_{v1}	0.1762000	0.22	0.0	0.0	0.0	0.0
W_{v2}	–0.0049100	0.0	0.0	0.0	0.0	0.0
V_0	53.3747400	54.0	164.7	151.9	90.6	165.0
V_1	–0.7000000	–0.32	0.0	–0.17	0.0	–0.17
V_2	0. 01250275	0.0	0.0	0.0	0.0	0.0
V_3	–24.00000	24.0	0.0	50.0	0.0	–6.4
V_4	0.26240200	0.4	0.0	0.0	0.0	0.0
V_{so}	6.2000000	6.2	0.0	2.5	7.13	2.5
W_{s0}	8.2557200	11.8	0.0	41.7	12.0	46.0
W_{s1}	0.09751599	–0.25	0.0	–0.33	0.0	–0.33
W_{s2}	–12.00000	12.0	0.0	44.0	0.0	–110.0

And a_{s1}=0.7, a_{v1}=0.7 for p channel.

Table 2 levels and deformation parameters β_2 used in direct inelastic calculation

^{98}Mo				^{100}Mo			
Level / MeV	J	π	β_2	Level / MeV	J	π	β_2
0.787384	2.0	+1	0.14	0.53557	2.0	+1	0.15
				1.06379	2.0	+1	0.13
				1. 13611	4.0	+1	0.12
				1. 46391	2.0	+1	0.10
				1. 60737	3.0	+1	0.10
				1. 76652	2.0	+1	0.08
				1. 77115	4.0	+1	0.08
				1. 97734	2.0	+1	0.06

Table 3 The a and Δ's values used in calculations

reaction channel		n,γ	n,n'	n,p	n,α	n,^{3}He	n,d	n,t	n,2n	n,nα	n,2p	n,3n
^{98}Mo	a	14.560	14.537	14.386	11.071	13.970	14.508	14.046	11.108	10.726	13.987	11.123
	Δ	+0.27	+0.00	–0.35	–2.44	+2.50	–0.50	+0.00	+0.17	+0.17	+1.35	+0.89
^{100}Mo	a	16.988	14.854	15.528	13.887	14.761	16.988	15.296	13.560	12.970	16.672	12.037
	Δ	+0.52	+0.25	-0.25	+0.18	+2.15	–2.60	+0.00	–0.20	+1.80	+1.00	+0.98

2 Some Calculated Results, Evaluation and Discussion

With above mentioned parameters and the direct inelastic data calculated by DWUCK4 as the input data, we calculated the complete sets of neutron nuclear data of ^{98}Mo and ^{100}Mo with the code UNF.

Because the resonance parameters were taken from JENDL-3.2, we only calculated and evaluated the data in 0.1~20 MeV energy region, and we had to make our evaluated $\sigma_{tot,}$ σ_{el} and $\sigma_{n,\gamma}$ smoothly connecting with the corresponding values in JENDL-3.2 at 0.1 MeV. In the figures, "this calculation" means present calculated values with the code UNF, "this evaluation" means present evaluated values. For both ^{98}Mo and ^{100}Mo, our calculated and evaluated σ_{tot} and σ_{el}, those in JENDL-3.2 and CENDL-3 are all in good agreement with experimental data.

In our evaluation, the Legendre coefficients of elastic scattering angular distribution in file 4 were calculated with the new version of the code APMN which was supplemented by us. In Fig.1 and Fig.2, "this work" means that our differential cross sections of elastic scattering were obtained from above mentioned Legendre coefficients and the evaluated σ_{el} value in file 3. From Fig.1a and Fig.2a we can see that below 3 MeV for both ^{98}Mo and ^{100}Mo, "this work" are in a little better accordance with experimental data, and the values of low energy at large angles in CENDL-3 are not good in accordance with experimental data. From Fig.1b and Fig.1c we can see that for ^{98}Mo above 4 MeV, "this work" are in a little better accordance with experimental data than CENDL-3. From Fig.2b and Fig.2c we can see that for ^{100}Mo above 4 MeV, "this work" and CENDL-3 are almost in the same good accordance with experimental data.

The total neutron spectra of ^{98}Mo and ^{100}Mo at E_L=14.5 MeV are given Fig.3a and Fig.3b, in which "this work" means that the normalized neutron spectra of (n,n'), (n,2n) and (n,nx) reaction were calculated with the code UNF, and the corresponding reaction cross sections were taken as our recommended values in file 3. From Fig.3a we can see that for ^{98}Mo, all the differential cross sections of "this work", CENDL-3 and JENDL-3.2 are almost in same good accordance with experimental data, only with some small differences. From Fig.3b we can see that for ^{100}Mo, "this work", CENDL-3 and JENDL-3.2 are all in rather good accordance with experimental data, there are only with a little different shape.

There are no experimental data for the inelastic scattering cross sections of ^{98}Mo and ^{100}Mo, and all calculated and evaluated values are reasonable in physics except JEF2, its values above 10 MeV are very small as showed in Fig.4. The (n,2n) reaction cross sections of ^{98}Mo and ^{100}Mo are given in Fig.5a and Fig.5b, respectively, the $\sigma_{n,2n}$ in CENDL-3 with good shape are in good agreement with newer experimental data (Filatenkov99, Kong91) for ^{100}Mo, so we take the $\sigma_{n,2n}$ in CENDL3 as our evaluated values. From Fig.5b we can also see that JENDL3.2 took some lower values mainly based on some old data (Marcinkowski86, Rahman85), JEF-2 took very large values (higher than all experimental data) and with unreasonable shape. There are no experimental $\sigma_{n,2n}$ for ^{98}Mo, we gave 2 newer sets of data of ^{100}Mo in Fig.5a from which we can see that for ^{98}Mo, our calculated and evaluated $\sigma_{n,2n}$ and those in CENDL-3 and JENDL-3.2 are little lower than the experimental data of ^{100}Mo, which is reasonable in physics, JEF-2 took very large values (much higher than the experimental data of ^{100}Mo) and with unreasonable shape. Since our evaluated values of $\sigma_{n,2n}$ are different from our calculated ones, to keep consistency in data file and to make total neutron spectra at 14.5 MeV accord with experimental values better, the corresponding changes were made in our evaluated $\sigma_{n,n'}$.

The $\sigma_{n,\gamma}$ of ^{98}Mo and ^{100}Mo are given in Fig.6a and Fig.6b, respectively. From Fig.6a we can see that for ^{98}Mo, calculated $\sigma_{n,\gamma}$ are not very good in accordance with the newer data (Wang91, Trofimov87 and Trofimov84), and our evaluated $\sigma_{n,\gamma}$ and those in CENDL-3 are very good in accordance with those newer data, JENDL-3.2 and JEF-2 are in good accordance with the old data (Musgrove76 and Stupegia68) and higher than the newer data. From Fig.6b we can see that for ^{100}Mo, our calculated $\sigma_{n,\gamma}$ are in rather good accordance with experimental data below 2.2 MeV, our evaluated $\sigma_{n,\gamma}$ and those in CENDL-3 and JEF-2 are very good in accordance with experimental data, JENDL-3.2 are with some higher values than experimental data above 0.2 MeV. In Fig.6a "C82F68P67" means its data come from three different groups of authors, and in Fig.6b

"W80C82T87L59C77" means its data come from five different groups of authors.

There is a specific circumstance in ^{98}Mo(n,p)^{98}Nb reaction. The isomeric state of the residual nucleus ^{98}Nb is at $J^{\pi}=5^{+}$, $T_{1/2}$=51.3 min, the ground state of ^{98}Nb has its $J^{\pi}=1^{+}$, $T_{1/2}$=2.86 sec. Because the $T_{1/2}$ of ^{98g}Nb is much shorter than that of ^{98m}Nb, the cross sections measured by activation method are those of the isomeric state, that is ^{98}Mo(n,p)^{98m}Nb reaction. There are 22 sets of experimental data, they show consistency except Guirathi 66, Srinivasa 79, Bramlitt 63 and Artenev 80. ^{98}Mo(n,p)^{98}Nb cross section from Fig.7a we can see that for $\sigma_{n,p}$ of ^{98}Mo, JENDL-3.2 gave their evaluated values based on the set of data Rahman85 in 8~10 MeV and the weight average of data Garlea92 and Artem'ev80 at 14.8 MeV, CENDL-3 evaluation is also based on experimental data mentioned above. However, they gave the cross sections of ^{98}Mo(n,p)^{98m}Nb reaction, not ^{98}Mo(n,p)$^{98g+m}$Nb. We calculated the $\sigma_{n,p}$ corresponding to M-state based on the three newer consistent sets of data, at the same time we automatically obtained the $\sigma_{n,p}$ of ^{98}Mo(n,p)$^{98g+m}$Nb which are higher than those in CENDL-3 and JENDL-3.2. In Fig.7a, "this work" means that our evaluated $\sigma_{n,p}$ are the same as our calculated values. From Fig.7b we can see that for ^{100}Mo, there is only one set of experimental $\sigma_{n,p}$ (Cuzzocrea65), "this work", CENDL-3 and JENDL-3.2 took almost equal $\sigma_{n,p}$ values passing through the lower experimental data, but JEF-2 took much smaller values.

From Fig.8a we can see that for $\sigma_{n,\alpha}$ of ^{98}Mo, "this work" (our evaluation=calculation values) and CENDL-3 are in very good agreement with experimental data, JENDL-3.2 took little lower values and still in good accordance with experimental data, but JEF-2 are with much smaller values. In Fig.8b "G93A84A80Q74" means the data come from four different groups of authors. From Fig.8b we can see that for $\sigma_{n,\alpha}$ of ^{100}Mo, "this work" and JENDL-3.2 are in good accordance with experimental data, CENDL-3 took some smaller values not passing through the data set Liskien89 above 15 MeV, JEF-2 are still with much smaller values.

For ^{98}Mo, there are no experimental data for $\sigma_{n,d}$, there is only one datum(Qaim82) for $\sigma_{n,d+np}$ (i.e. the cross section of reaction ^{98}Mo(n,x)^{97}Nb) and one set of data(Yamauchi93) corresponding to the residual nucleus ^{97}Nb in its isomeric state. From Fig.9a we can see that "this work" (our evaluation, i.e. calculated $\sigma_{n,d+np}$) passes through the datum of (Qaim) and is higher than the data set of Yamauchi93-M. CENDL-3 took some higher values and JENDL-3.2 took some lower values. There are no $\sigma_{n,np}$ given in JEF-2, so in Fig.9a we give the line of $\sigma_{n,d}$ for JEF-2, which is higher than the datum of Qaim, that is unreasonable. From Fig.9b we can see that for $\sigma_{n,d}$ of ^{100}Mo, "this work" (our evaluation, i.e. calculated values) passes through the only one datum of Yamauchi, CENDL-3 and JENDL-3.2 took some lower values, JEF-2 took some higher values.

3 Conclusion Remark

The elastic scattering angular distributions, $\sigma_{n,p}$, $\sigma_{n,\alpha}$ and $\sigma_{n,d}$, were improved in "this work", because they are obviously in good agreement with experimental values. To benefit users, two kinds of B6 format output results (one includes File 1, 2, 3, 6, 12, 14, 15, and another includes File 1, 2, 3, 4, 5) are given for ^{98,100}Mo in this work.

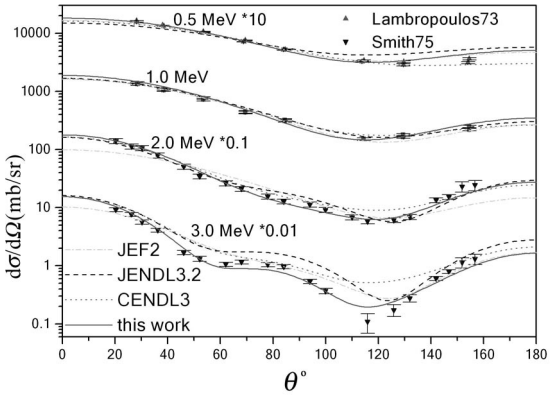

Fig.1a Angular distributions of elastic scattering of ^{98}Mo (1)

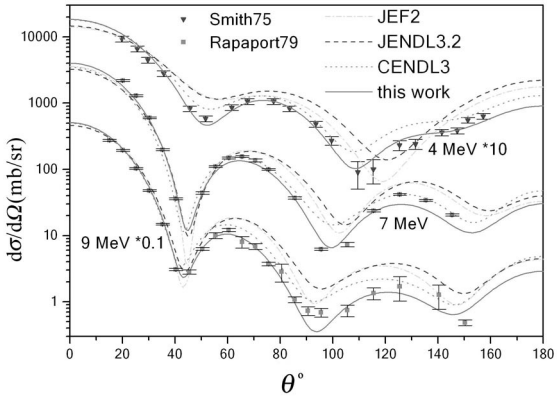

Fig.1b Angular distributions of elastic scattering of ^{98}Mo (2)

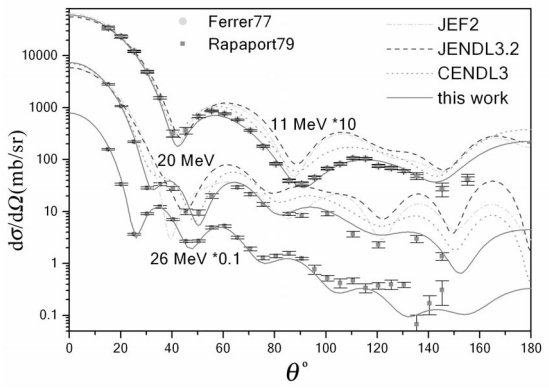

Fig.1c Angular distributions of elastic scattering of ^{98}Mo (3)

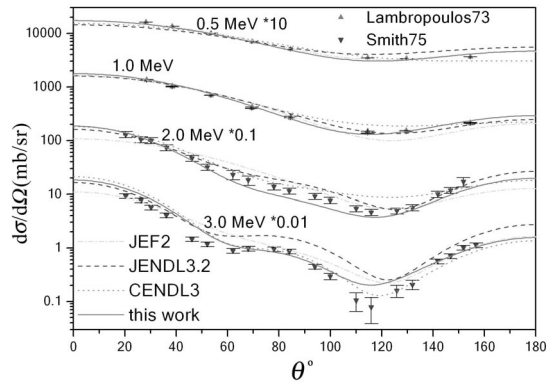

Fig.2a Angular distributions of elastic scattering of ^{100}Mo (1)

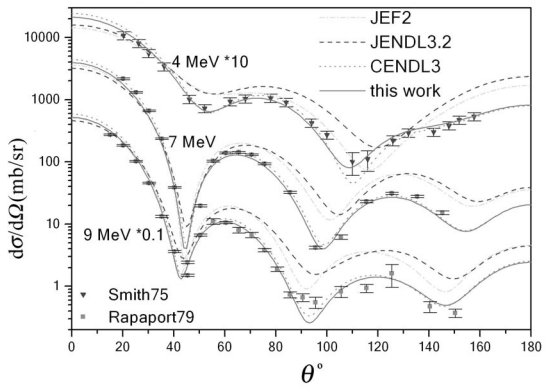

Fig.2b Angular distributions of elastic scattering of ^{100}Mo (2)

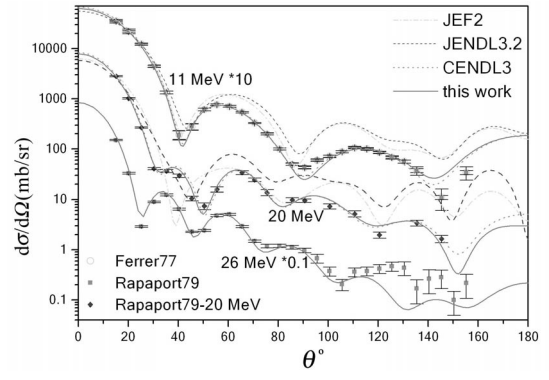

Fig.2c Angular distributions of elastic scattering of ^{100}Mo (3)

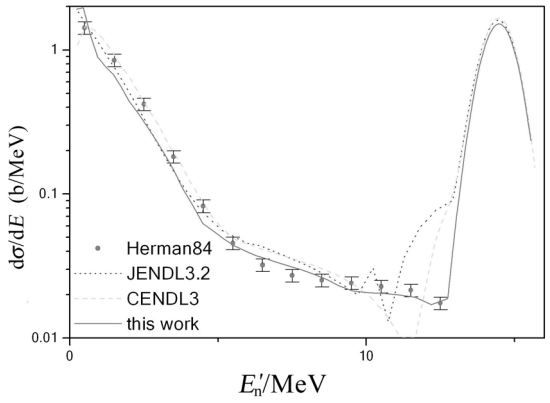

Fig.3a Total neutron spectra of ^{98}Mo at E_L=14.5 MeV

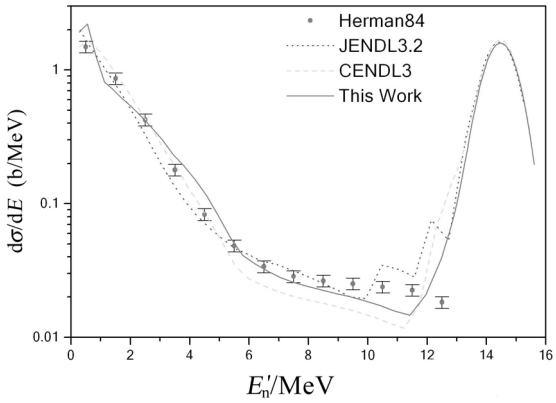

Fig.3b Total neutron spectra of ^{100}Mo at E_L=14.5 MeV

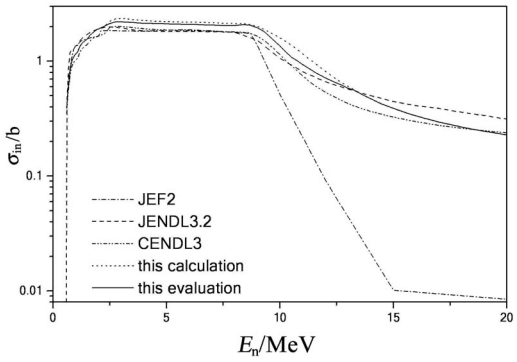

Fig.4 Inelastic scattering cross sections of ^{100}Mo

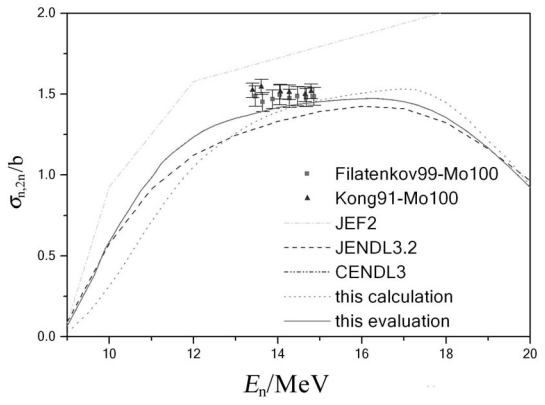

Fig.5a (n,2n) reaction cross sections of ^{98}Mo

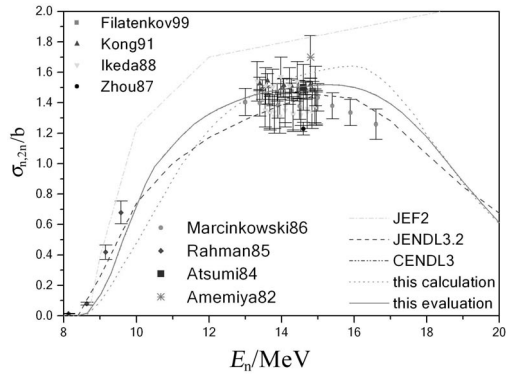

Fig.5b (n,2n) reaction cross sections of ^{100}Mo

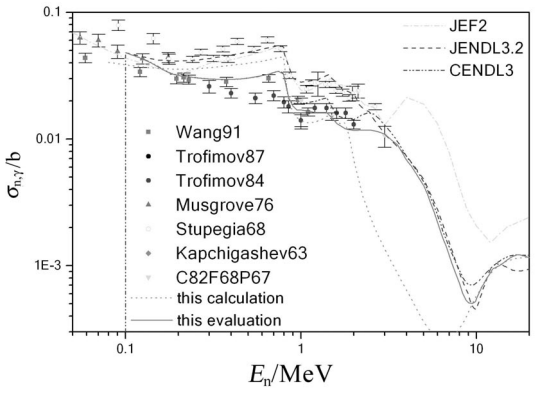

Fig.6a Capture cross sections of ^{98}Mo

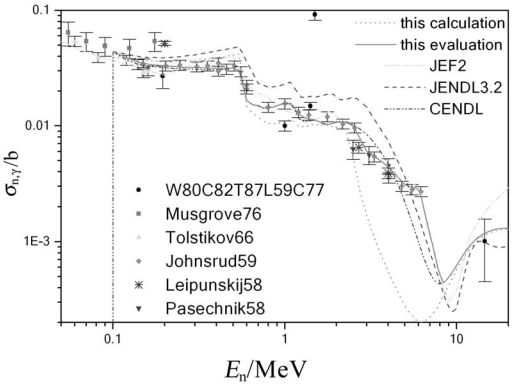

Fig.6b Capture cross sections of ^{100}Mo

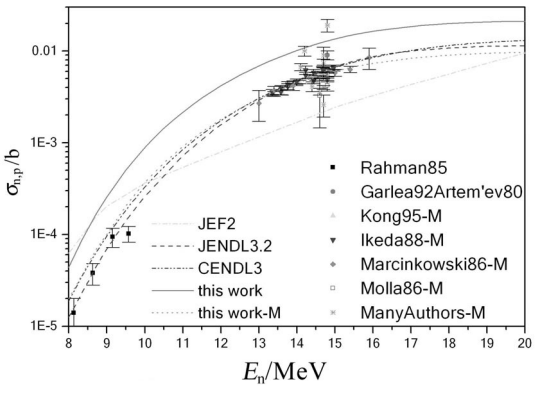

Fig.7a (n,p) reaction cross sections of ^{98}Mo

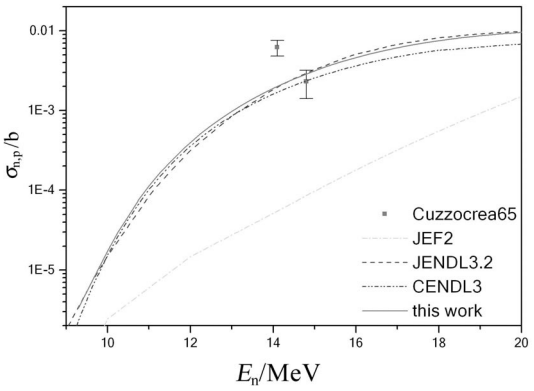

Fig.7b (n,p) reaction cross sections of ^{100}Mo

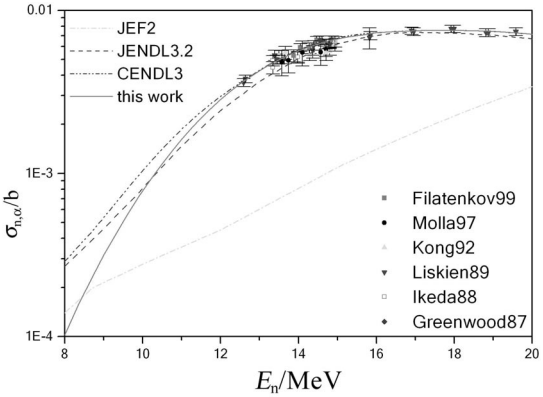

Fig.8a (n,α) reaction cross sections of ^{98}Mo

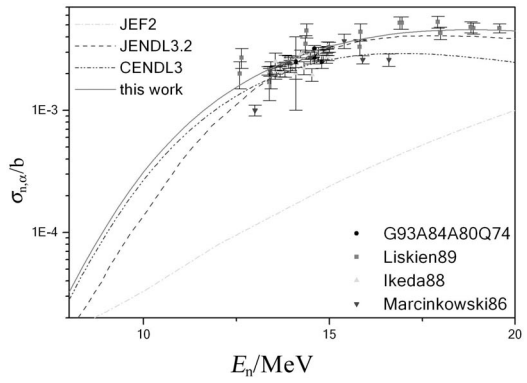

Fig.8b (n,α) reaction cross sections of ^{100}Mo

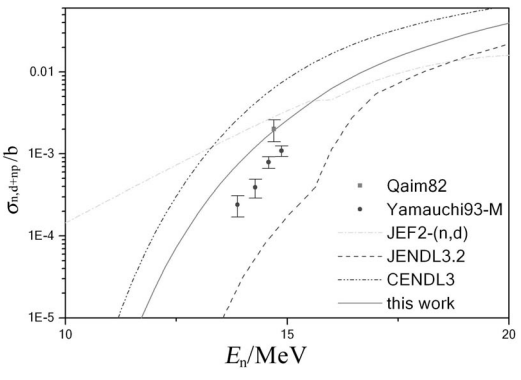

Fig.9a (n,d)+(n,np) reaction cross sections of ^{98}Mo

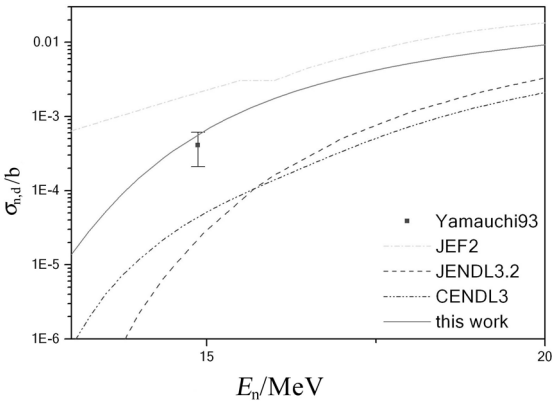

Fig.9b (n,d) reaction cross sections of ^{100}Mo

References

[1] ZHANG Jingshang. UNF Code for Fast Neutron Reaction Data Calculations. Nucl. Sci. Eng., 142,207(2002)

[2] SHEN Qingbiao. A Code APMN for Automatically Searching Optimal Optical Potential Parameters below 300 MeV, Commu. Nucl. Data Progress (INDC(CRP)-053/L) No.25, p19, June 2001; Nucl Sci. Eng., 141,78(2002)

[3] C.M.Perey, et al. Compilation of Phenomenological Optical-Model Parameters, Atomic Data & Nucl. Data Tables, 17, p1-101, 1976;

[4] P.D.Kunz. A DWBA Code DWUCK4, University of Colorado, USA (unpublished);

Benchmark Testing Calculations for ^{232}Th

LIU Ping

China Nuclear Data Center, CIAE, P.O.Box275(41), Beijing 102413

【**abstract**】 *The cross sections of ^{232}Th from CNDC and JENDL-3.3 were processed with NJOY97.45 code in the ACE format for the continuous-energy Monte Carlo Code MCNP4C. The K_{eff} values and central reaction rates based on CENDL-3.0, JENDL-3.3 and ENDF/B-6.2 were calculated using MCNP4C code for benchmark assembly, and the comparisons with experimental results are given..*

Introduction

Because of the shortage of energy resource and the lack in reserve of traditional nuclear fuel, the research for the generation and waste transmutation by using intermediate energy proton accelerator driven radioactive clean nuclear system (ADS) has attracted internationally considerable attention. New concepts of nuclear technology for power production are being investigated to satisfy these needs. Thorium-based nuclear fuel cycle offers many advantages: a) Neutron capture in ^{232}Th yields ^{233}U, which is a highly efficient nuclear fuel. A thermal breeder (or near-breeder) reactor concept based on thorium fuel is feasible. b) World reserves of thorium are much more than reserves of uranium. c) Thorium fuel is more proliferation-resistant due to highly radioactive constituents, which can not be separated out by chemical means.

Based on the above advantages there is a rising interest in innovative fuel cycle concepts based on thorium fuel. Therefore the quality of nuclear data for ^{232}Th is very important. The data of ^{232}Th were evaluated in China Nuclear Data Center using the newest experimental data and UNF [1] code, which calculates nuclear reaction cross sections with advanced theoritical method. In order to test the reliability of these data, it's necessary to do benchmark tests. Monte Carlo code MCNP4C[2] was used to do the calculation of $k_{\rm eff}$ values and central reaction rates, and the comparisons were given with experimental results and the results of JENDL-3.3, ENDF/B-6.2.

1 Data Processing

The ENDF60 library[3], which is generated in LANL(Los Alamos Laboratory) with ENDF/B-6.2 was used in the calculations. The data of ^{232}Th from CNDC and JENDL-3.3 were processed with the NJOY97.45 code[4] in ACE-format for the MCNP4C code. The thinning tolerances reconstructing and Doppler broadening of cross section data were 0.2%, and the tolerance for thinning distributions was 0.

2 Benchmark Calculations

The benchmark calculations were performed using the Monte Carlo code MCNP4C. The $k_{\rm eff}$ values and central reaction rate ratios were calculated. Table 1 gives out the description for the benchmark assembly[5]. In this calculation, the calculated results of ENDF/B6 were based on ENDF60 library, and the ACE format files for ^{239}Pu, ^{240}Pu, ^{241}Pu and Gallium were also from ENDF60 library.

Table 1 The description of the benchmark assembly used

Isotope/Element	Atom Density (atoms/barn-cm)
Plutonium Core	
^{239}Pu	3.6049*10
^{240}Pu	1.9562*10
^{241}Pu	1.1459*10
Gallium	1.3338*10
Thorium reflector	
^{232}Th	$3.0054*10^{-2}$

3 Results and Discussions

The $k_{\rm eff}$ values and central reaction rate ratios were calculated, and the comparisons with the experimental results were given for different evaluated data libraries. Table 2 and Table 3 give out the $k_{\rm eff}$ values and central reaction rates, respectively.

Table 2 The calculated results for k_{eff} values

Assembly	Experiment	Present	ENDF/B6[*]	JENDL-3.3
One-dimension	1.000(～0.001)	1.00661	1.00581	1.00969
Two-dimension	1.000(～0.001)	1.00495	1.00433	1.00682

*: The data library is from ENDF60 library.

Table 3 The results for central reaction rate ratios

Reaction	Experiment	Present	ENDF/B6[*]	JENDL-3.3
$\sigma_f(^{238}U)/\sigma_f(^{235}U)$	0.195±0.003	0.1735	0.1723	0.1727
$\sigma_f(^{237}Np)/\sigma_f(^{235}U)$	0.92±0.02	0.8352	0.8277	0.834
$\sigma_f(^{232}Th)/\sigma_f(^{238}U)$	0.26±0.01	0.2565	0.2472	0.25
$\sigma_{n,\gamma}(^{238}U)/\sigma_f(^{235}U)$	0.083±0.003	0.074	0.0735	0.074
$\sigma_{n,2n}(^{238}U)/\sigma_f(^{238}U)$	0.053±0.003	0.055	0.055	0.0546
$\sigma_{n,\gamma}(^{232}Th)/\sigma_{n,\gamma}(^{238}U)$	1.20±0.06	1.22	1.29	1.2
$\sigma_{n,2n}(^{232}Th)/\sigma_{n,2n}(^{238}U)$	1.04±0.03	1.13	1.09	1.001

*: The data library is from ENDF60 library.

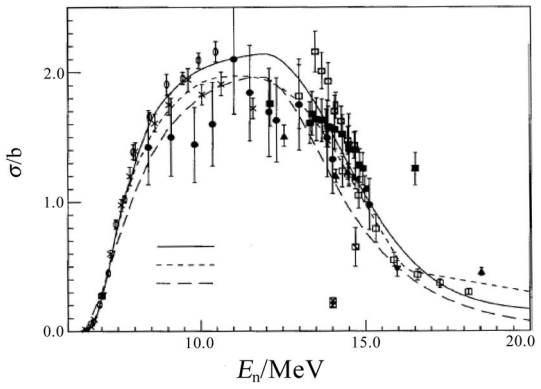

Fig.1 The comparisons of (n,2n) cross-section for ^{232}Th

Table 2, the calculated k_{eff} values based on present data, ENDF/B-6.2 and JENDL-3.3 are overestimated and compared with the experimental results, and it can be seen that the results based on present data are close to ENDF/B-6.2.

Table 3 show that the fission reaction rate ratios of ^{232}Th **(**$\sigma_f(^{232}Th)/\sigma_f(^{238}U)$**)** and the capture reaction rate ratio of ^{232}Th **(**$\sigma_{n,\gamma}(^{232}Th)/\sigma_{n,\gamma}(^{238}U)$**)** based on present data are in better agreements with the experimental results, but the $\sigma_{n,2n}(^{232}Th)/\sigma_{n,2n}(^{238}U)$ value are higher than the experimental one and the results from ENDF/B-6.2 and JENDL-3.3. According to the testing results, the (n,2n) reaction cross sections of present ^{232}Th data should be decreased. In Fig.1 is given the comparisons of the (n,2n) cross sections. It can be seen that the present (n,2n) reaction cross section is actually larger than those of ENDF/b6 and JENDL-3.

Reference

[1] ZHANG Jingshang, et.al. Nucl. Sci. & Eng. 133, 218-234 (1999).

[2] Judith F. Briesmeister, Editor. The Manual: "MCNP – A General Monte Carlo N-Particle Transport Code", LA-13709 – M, Issued: March. 2000.

[3] Los Alamos National Laboratory, "ENDF60 Library, Neutron Cross section Library", XTM: SCF-96-363, Date: Sept. 23, 1996.

[4] R.E. MacFarlane and D. W. Muir. " The NJOY Data Processing System Version 97," LA-12740-M (1997).

[5] "International Handbook of Evaluated Criticality Safety Benchmark Experiments", NEA/NSC/DOC (95), September 2000.

Energy Level Calculation of Mg-like Ion Br XXIV

CHEN Huazhong

China Nuclear Data Center, CIAE, P.O.Box275(41), Beijing 102413

【**abstract**】*Energy levels of Mg-like ions were calculated by means of GRASP code. The calculations were performed based on multi-configuration Dirac-Fock technique. Corrections to the energy levels due to the retarded Coulomb interaction (Breit interaction) and the polarization of the vacuum by the nuclear distribution and electron self-energy are included in a perturbation approximation. Comparisons with the experimental data (observed in HI-13 Tandem Accelerator in CIAE) are presented.*

Introduction

Atomic spectra are fundamental characteristics of atoms and ions, the main source of information on their structure and properties. Now the new important application fields are: diagnostics of thermonuclear plasmas, solid physics, biomedicine, beam-foil spectroscopy and so on. Laser in the "water window" wave band (2.33-4.37nm) can be used in biological specimen photography.

The system (Mg-like ions) consists of the $1s^2 2s^2 2p^6$ core and two valence electrons. The energy levels were obtained by diagonalization of the energy matrix calculated between all the $3l_1 3l_2$ states of the same parity and of the same total angular momentum J. The lowest order of the perturbation theory was treated exactly, whereas higher orders were included through an effective interaction.

The parameters of atomic structure were obtained by means of GRASP[1](General-purpose Relativistic Atomic Structure Program), which extends the previously published program[2] for solving the atomic multiconfigurational Dirac-Fock(MCDF) equations and supplying atomic orbital wavefunctions and energy levels. The transverse Breit interaction, self-energy and vacuum polarization corrections to the energy levels were considered in the extension. The transverse Breit interaction is a leading correction to the Coulomb repulsion between electrons in quantum electrodynamics. The self-energy corrections are an approximate estimate based on interpolation among the hydrogenic results for various atomic numbers supplied by Mohr[3] .

Identification of the spectra of the systems (Mg-like ions) above mentioned is impossible in practice without corresponding theoretical analysis. So, the accurately theoretical energy levels and wavelengths prediction can be of great value.

1 Theory

Relativistic atomic structure theory is ultimately based on quantum electro-dynamics. The GRASP approximation for the calculation of atomic stationary states and transitions among them was described in the literatures [4-6].

From the theoretical point of view, the atom is considered a many-body system. Instead of considering the wave function of the whole atom, it is considered that each electron moves in a central nuclear charge field and in the screening field of the remaining electrons. The wave function of this electron is represented as a product of radial and spin-angular parts. As described more fully in Ref.[7], we construct atomic state functions (ASF) from a linear combination of configuration state functions (CSF), which are eigenfunctions of J^2, J_z and parity. These are built from single-electron Dirac equation in turn.

Nature of physical problem in GRASP is the theoretical calculation of atomic energy levels, orbital, and radiative transition data within the relativistic formalism. Making use of GRASP, one can be in a position to perform calculations of the energy spectra, transition probabilities of all atoms in the Periodical Table and ions of any ionization degree. Such calculations could be done prior to the corresponding experimental observations or after them to help with explaining the interesting phenomena found in experimental analyzing.

All the dominant interactions in the highly stripped ions are included in the Dirac-Coulomb Hamiltonian

$$\mathrm{H}^{\mathrm{DC}} = \sum_{i=1}^{N} \mathrm{H}_i + \sum_{i=1}^{N-1} \sum_{j=i+1}^{N} \left| r_i - r_j \right|^{-1} \qquad (1)$$

in the first term (in atomic units)

$$H = c\sum_{i=1}^{3}\alpha_i p_i + (\beta - 1)c^2 + V_{nuc}(r) \qquad (2)$$

is the one-body contribution for an electron due to its kinetic energy and interaction with the nucleus, the rest energy, c^2, has been subtracted out, r is the position vector of the electron , c is the velocity of light, $p \equiv -i\nabla$ is the momentum operator, $V_{nuc}(r)$, is the nuclear potential energy.

In the calculation we chose the GRASP code's extended optimized (EAL) level option[1]. There are large fluctuations for the radiative corrections due to admixtures of wavefunctions. In order to minimize the fluctuations, the corrections should be calculated by using EAL option of the code[8].

2 Results and Discussion

From the paper[9] we know that GRASP is an available program for researching the atomic structure. Wavelengths and energy levels of highly ionized atoms Mg-like Br XXIV were calculated by means of GRASP code. In Table 1 there is the comparison of transition wavelengths calculated with the experimental data measured at Department of Nuclear Physics of the China Institute of Atomic Energy (CIAE)[10-11]. The energies of $3l_13l_2$ [J](even parity) states and $3l_13l_2$ [J](odd parity) states are listed respectively in Table 2 and Table 3.

Table 1 shows Mg-like Br XXIV transitions spectra within the n=3 complex, i.e. between the $3s^2$, 3s3p, $3p^2$, 3s3d and 3p3d configuration. Based on these transition lines, 19 observed energy levels (Table 2 and Table 3) were experimentally determined, among them 14 energy levels are new experimental values. From these comparisons we can see that there are differences (special in intensities) between theory and experiment for ionized atom Mg-like Br XXIV. The main differences come from correlation effects not completely being considered in this work，such as electric quadrupole effects. We will improve the GRASP code by including correlation effects completely in the future.

Table 1 Wavelength comparison between calculated & measured data for Bromine XXIV (Br^{23+})

Configuration	Terms	Intensity		*J-J*	Wavelength(nm)	
		Exp.(CIAE)	This wok		Exp.(CIAE)	This work
$3S^2$-3s3p	^1S—^1P	1370	1145	0-1	16.677	15.908
$3S^2$-3s3p	^1S—^3P	62	87	0-1	25.373	25.218
3s3p-$3p^2$	^3P—^3P	120	135	0-1	17.263*	17.128
3s3p-$3p^2$	^3P—^3P	125	117	1-1	17.908*	17.784
3s3p-$3p^2$	^1P—^1S	95	98	1-0	18.433*	18.387
3s3p-$3p^2$	^3P—^3P	100	116	1-0	20.079*	19.800
3s3p-$3p^2$	^3P—^3P	90	88	2-1	20.371*	20.177
3s3p-3s3d	^3P—^3D	20	35	0-1	13.351*	13.322
3s3p-3s3d	^3P—^3D	115	98	1-1	13.723*	13.716
3s3p-3s3d	^3P—^3D	610	389	2-3	14.769	14.744
3s3p-3s3d	^3P—^3D	60	78	2-2	14.991*	14.974
3s3p-3s3d	^3P—^3D	70	82	2v1	15.135*	15.097
$3p^2$-3p3d	^3P—^3P	88	78	1-0	13.720*	13.779
$3p^2$-3p3d	^3P—^3D	98	116	0-1	13.842*	13.903
$3p^2$-3p3d	^3P—^3D	116	179	1-2	14.411*	14.475
$3p^2$-3p3d	^3P—^3D	72	66	1-1	15.114*	15.182
$3p^2$-3p3d	^3P—^3D	82	46	1-2	15.758*	15.880
3s3d-3p3d	^3D—^3P	117	168	2-2	17.903*	17.864
3s3d-3p3d	^3D—^3P	66	70	2-1	18.069*	18.020
3s3d-3p3d	^3D—^3D	19	33	2-3	18.285*	18.106
3s3d-3p3d	^3D—^3P	31	45	3-3	18.572*	18.455
3p3d-$3d^2$	^3F—^3D	23	43	3-2	15.114*	15.017
3p3d-$3d^2$	^3F—^3F	43	64	4-4	14.987*	14.920
3p3d-$3d^2$	^3D—^3F	117	230	1-2	15.207*	15.191

* Measured data are published first time.

Table 2 Energies of $3l_13l_2$ [J](even parity)

Conf.	Term	*J*	Energies(exp.) cm^{-1}	Energies(This work) cm^{-1}
$3s^2$	^1S	0	0	0
$3p^2$	^3P	0	892175±77	897819
$3p^2$	^3P	2	947481±65	959946
$3p^2$	^3P	1	952793±102	987516
$3p^2$	^1D	2	1032036±30	107555
$3p^2$	^1S	0	1141979±152	115439
3s3d	^3D	1	1122646±144	112839
3s3d	^3D	2	1129043±90	113433
3s3d	^3D	3	1138923±33	114563
3s3d	^1D	2	1257260±33	121110

Table 3 Energies of $3l_13l_2$ [J](odd parity)

Conf.	Term	*J*	Energies(exp.) cm^{-1}	Energies(This work) cm^{-1}
3s3p	^3P	0	373572±147	374609
3s3p	^3P	1	394142±18	396618
3s3p	^3P	2	461920±25	464784
3s3p	^1P	1	599474±24	629681
3p3d	^3F	2	1524220±165	152913
3p3d	^3F	3	1567514±78	157384
3p3d	^1D	2		159248
3p3d	^3D	1		162026
3p3d	^3F	4	1626942±124	163432
3p3d	^3D	2		165419
3p3d	^3D	3	1677864±200	168855
3p3d	^3P	0		168850
3p3d	^3P	1		169032
3p3d	^3P	2	1687171±215	169587
3p3d	^1F	3	1778691±150	179711
3p3d	^1P	1		179886

References

[1] Dvall K. G, et al. Comput. Phys. Commun. 55 (1989) 425

[2] Grant I. P, et al. Comput. Phys. Commun. 21 (1980) 207;

[3] P.J.Mohr. Am. Phys. 88 (1974) 52

[4] I.P.Grant. Advan. Phys. 19 (1970) 747

[5] I.P.Grant. J.Phys. B7 (1974) 1458

[6] I.P.Grant. Methods in Computational Chemistry, Vol, 2, Relativistic Effects in Atoms and Molecules, ed. S. Wilson (Plenum, New York, 1988) p.1.

[7] I.P.Grant and B.J.Mchenzie. J. Phys. B13 (1980) 1671

[8] G.X.Chen, Q.Y.Fang, W.Cai. Chinese Journal of Atomic & Molecular Physics 12 (1995) 91 .

[9] CHEN Huazhong. Commu. of Nucl. Data Progress, 138, 145 (1999).

[10] C.Jupen, et al. Physica Scripta, Vol. 61, 443 (2000)

[11] X.T.Zeng, et al. Physica Scripta, Vol. 61, 464 (2000)

ENSDF Codes and their Application to Atomic Radiations Arising from Nuclear Decay

ZHOU Chunmei HUANG Xiaolong WU Zhendong

China Nuclear Data Center, CIAE, P.O.Box275(41), Beijing 102413

Calculation Codes and Functions

The data calculation codes[1] for atomic radiations arising from internal conversion electron emission and electron capture decay and their functions are listed in Table 1. We got them from ENSDF (Evaluated Nuclear Structure Data File) physics analysis codes[2], which are maintained and updated by the National Nuclear Data Center (NNDC) at Brookhaven National laboratory, USA, for the International Network of Nuclear Structure and Decay Data Evaluation.

Application

Example 1: atomic radiations arising from internal conversion electron emission

^{129}I β^- decay scheme [2] is relatively simple. It is taken as an example and the calculation results are given. In Table 2, the γ-ray data of ^{129}I β^- decay are listed, where the internal conversion coefficients α_K, α_L, α_M, and α are calculated by HSICC code，and normalization factor N=1 is given to calculate γ-ray absolute intensities. In Table 3, the calculation parameters of x–ray and Auger electron data for K- and L-shell are given. In Table 4, the radiation data of ^{129}I β^- decay are given. In Fig.1, the scheme of ^{129}I β^- decay is shown.

Example 2: atomic radiations arising from electron capture decay

^{55}Fe ε decay scheme [4] is very simple. It is taken as an example and the calculation results are given. In Table 5, the electron capture data of ^{55}Fe ε decay are listed, where the electron capture probabilities $P_{\varepsilon K}$, $P_{\varepsilon L}$ and $P_{\varepsilon M}$ are calculated by LOGFT code，and normalization factor $N(\varepsilon+\beta^+)$=1 is given to calculate electron capture absolute intensities. In Table 6, the calculation parameters of x-ray and Auger electron data for K- and L-shell are given. In Table 7, the radiation data of ^{55}Fe ε decay are given. In Fig.2, the scheme of ^{55}Fe ε decay is shown.

Example 3: atomic radiations arising from internal conversion emission and electron capture decay

The scheme for ^{207}Bi ε decay scheme [5] is a simpler. It is taken as an example and the calculation results are given. In Table 8, the γ-ray data of ^{207}Bi ε decay are listed, where the internal conversion coefficients α_K, α_L, α_M and α are calculated by HSICC code. The γ-ray intensity normalization factor N=1 is given to calculate γ-ray absolute intensities. In Table 9, the electron capture data of ^{207}Bi ε decay are listed, where the electron capture probabilities $P_{\varepsilon K}$, $P_{\varepsilon L}$ and $P_{\varepsilon M}$ are calculated by LOGFT code. The normalization factor $N(\varepsilon+\beta^+)$=1 is given to calculate electron capture absolute intensities. In Table 10, the calculation parameters of x-ray and Auger electron data for K- and L-shell are given. In Table 11, the radiation data of ^{207}Bi ε decay are given. In Fig.3, the scheme of ^{207}Bi ε decay is shown.

Table 1 Codes and Functions of Data Calculation for Atomic Radiation arising from Nuclear Decay

Code name	Main function
FMTCHK	ENSDF formatted data check
HSICC	Internal conversion coefficient calculation of α_n （n=K, L, M, N atomic shell）and α
LOGFT	Electron capture probability calculation of $P_{\varepsilon n}$（n=K, L, M, N atomic shell）
RADLST	Energy and intensity calculation for atomic radiations
ENSDAT	Calculation data output shown in Tables and drawings

Table 2 γ-ray intensity and internal conversion coefficients for ^{129}I β⁻ Decay

E_γ /keV	I_γ	α_K	α_L	α_M	α
39.578	7.51 # 23	10.4943 10	1.428 11	0.2882 23	12.31 1

#, uncertainties ("Errors") : The uncertainty in any number is given one space after the number itself.
For an example, 7.51 23 means 7.51± 0.23.

Table 3 Calculation Parameters[3] of Atomic Radiation Data for ^{129}I β⁻ Decay

Element	ω_K	ω_L	n_{KL}	$R_{\beta\alpha}$	$R_{\alpha 2\alpha 1}$
$_{54}$Xe	0.888 5	0.097 5	0.902 4	0.2327 24	0.5398 25

Table 4 Radiation Data of ^{129}I β⁻ Decay

Radiation type	Energy/keV	Absolute intensity/%	Radiation type	Energy/keV	Absolute intensity/%
β^-_1 max	154 3		$XK_{\alpha 1}$	29.779 1	36.9 17
avg	40.9 12	100.	XK_β	33.6	13.2 6
e_{AuL}	3.430	74 5	γ_1	39.578 4	7.51 23
e_{AuK}	24.60	8.8 4	e_{Ce1K}	5.017 4	79. 4
XL	4.11	7.9 25	e_{Ce1L}^+	34.125 4	10.7 5
$XK_{\alpha 2}$	29.458 1	19.9 9	e_{Ce1M}	38.436 5	2.16 10

+ e_{Ce1L} means internal conversion electron of γ_1 ray from L-shell

Table 5 Electron capture probability for ^{55}Fe ε Decay calculated by LOGFT code

Nuclide	E_L/keV	$I_{\varepsilon+\beta+}$	$P_{\varepsilon K}$	$P_{\varepsilon L}$	$P_{\varepsilon M}$
^{55}Mn	0.0	100	0.8854	0.0975	0.01709

Table 6 Calculation Parameters[3] of Atomic Radiation Data for ^{55}Fe ε Decay

element	ω_K	ω_L	n_{KL}	$R_{\beta\alpha}$	$R_{\alpha 2\alpha 1}$
$_{25}$Mn	0.321 5	0.0047 7	1.478 4	0.1359 14	0.5099 25

Table 7 Radiation Data of ^{55}Fe ε Decay

Radiation type	Energy/keV	Radiation intensity/%	Radiation type	Energy/keV	Radiation intensity/%
EC_1		100.	$XK_{\alpha 2}$	5.888 1	8.24 11
e_{AuL}	0.610	140 4	$XK_{\alpha 1}$	5.899 1	16.29 12
e_{AuK}	5.19	60.1 3	XK_β	6.49	3.29 7
XL	0.640	0.42 1			

Table 8 γ-ray intensity and internal conversion coefficients for ^{207}Bi ε Decay

E_γ /keV	I_γ	α_K	α_L	α_M	α
328.12 12	0.00067 8	0.285	0.0486	0.01139	0.348
569.702 2	97.74 3	0.01590	0.00445		0.0218
897.8 1	0.121 8	0.0201	0.00334		0.0245
1063.662 4	74.5 2	0.097	0.024	0.008	0.130
1442.2 2	0.130 3	0.00273	0.00047		0.0032
1770.237 10	6.87 4				

Table 9 Electron capture probability for ^{207}Bi ε Decay calculated by LOGFT code

Nuclide	E_L/keV	$I_{\varepsilon+\beta+}$	$P_{\varepsilon K}$	$P_{\varepsilon L}$	$P_{\varepsilon M}$
^{207}Pb	569.703	8.79 24	0.7965	0.1501	0.0492
	1633.368	84.18 23	0.7325	0.19853	0.06896
	2339.948	7.03 4		0.652 6	0.348 6

Table 10 Calculation Parameters[3] of Atomic Radiation Data for ^{207}Bi ε Decay

element	ω_K	ω_L	n_{KL}	$R_{\beta\alpha}$	$R_{\alpha2\alpha1}$
$_{82}$Pb	0.963 4	0.379 15	0.811 5	0.279 4	0.5950 25

Table 11 Radiation Data of ^{207}Bi ε Decay

Radiation type	Energy/keV	Absolute intensity/%	Radiation type	Energy/keV	Absolute intensity/%
EC_1		7.03 4	e_{Ce2L}	553.8412 21	0.43 10
EC_2		84.18 23	e_{Ce2M}	565.8513 21	0.43 1
EC_3		8.75 24	e_{Ce2N}	568.8084 22	0.43 1
β^+_1 max	806.5 21		γ_3	897.80 10	0.121 8
Avg	383.3 10	0.0374 11	e_{Ce3K}	809.80 10	0.0024 12
e_{AuL}	7.970	52. 4	e_{Ce3L}	881.94 10	0.00040 12
e_{AuK}	56.70	2.47 5	e_{Ce3M}	893.95 10	0.00040 12
XL	10.60	36. 4	e_{Ce3N}	896.91 10	0.00040 12
$XK_{\alpha2}$	72.8042 9	21.8 5	γ_4	1063.662 4	74.5 2
$XK_{\alpha1}$	74.9694 9	36.8 7	e_{Ce4K}	975.658 4	7.2 7
XK_β	84.90	16.4 4	e_{Ce4L}	1047.801 4	1.8 7
γ_1	328.12 10	0.00067 8	e_{Ce4M}	1059.811 4	1.8 7
e_{Ce1K}	240.12 10	0.00019 7	e_{Ce4N}	1062.769 4	0.6 7
γ_2	569.7020 20	97.74 3	γ_5	1442.20 20	0.130 3
e_{Ce2K}	481.6975 22	1.6 10	e_{Ce5K}	1354.20 20	0.000355 5

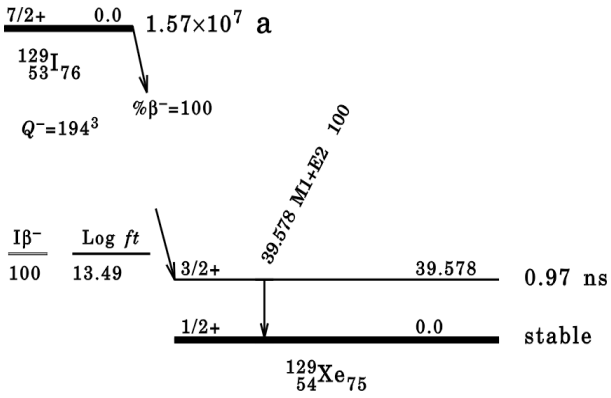

Fig.1 ^{129}I β^- Decay Scheme

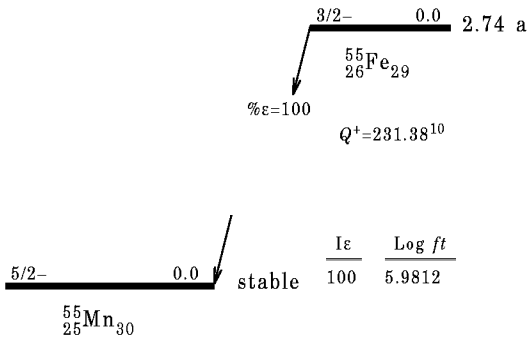

Fig.2 ^{55}Fe ε Decay Scheme

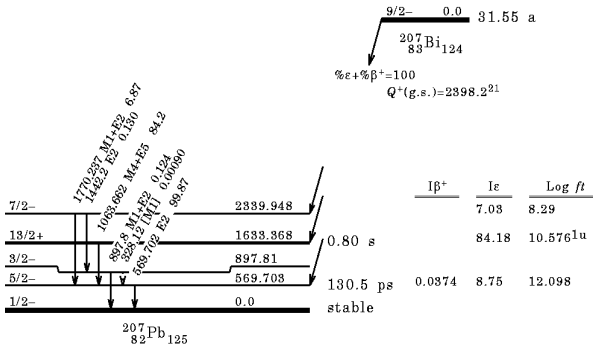

Fig.3 ^{207}Bi ε Decay Scheme

References

[1] Burrows T W. Private Communication. ENSDF Physics Analysis Codes (1998)

[2] Tendow Y. Nucl. Data Sheets, 1996, 77: 637

[3] Schonfeld E, Janben H. Nucl. Instr., Methods, Phys. Research, 1996, A369: 52

[4] HUO Junde. Nucl. Data Sheets, 1991, 64: 723

[5] Martin MJ. Nucl. Data Sheets, 1993, 70: 315

Study of Nuclear Data Online Services

FAN Tieshuan[1], GUO Zhiyu[1], LIU Wenlong[1], YE Weiguo[1], FENG Yuqing[1], SONG Xiangxiang[1], HUANG Gang[1], HONG Yingjue[1], LIU Chi[1], LIU Tingjin[1,2], HUANG Xiaolong[2], CHEN Jinxiang[1], TANG Guoyou[1], SHI Zhaoming[1], and CHEN Jia'er[1]

1 Institute of Heavy Ion Physics and MOE Key Lab of Heavy Ion Physics, Peking University, Beijing 100871,China

2 China Nuclear Data Center, CIAE, P.O.Box275(41), Beijing 102413

【**abstract**】 *A web-based nuclear data service software system, NDOS (Nuclear Data Online Services), has been developed and released in Sep. 2001. Through the Internet, this system distributes charge of free 8 international nuclear databases: 5 evaluated neutron databases (BROND, CENDL, ENDF, JEF and, JENDL), Evaluated Nuclear Structure and Decay File ENSDF, Experimental Nuclear Data Library EXFOR database and IAEA Photonuclear Data Library. A software package, NDVS (Nuclear Data Viewing System), facilitates the visualization and manipulation of nuclear data. The computer programs providing support for database management and data retrievals are based on the Linux implementation of PHP and the MySQL software.*

Introduction

Nuclear data cover both the properties of nuclei and the fundamental law governing nuclear interactions. The major nuclear databases are developed by the network of co-operating Nuclear Reaction Data Center and held by the IAEA. The most comprehensive collection of nuclear data, more than 100 nuclear databases, are available free of charge to scientists in IAEA member states on computer media or online through the Internet (Worldwide Web, Telnet, FTP), like most of the other nuclear data centers[1]. The data bank of the OECD Nuclear Energy Agency maintains large databases containing bibliographic, experimental and evaluated nuclear data and makes these databases available to scientists in Member countries. Those databases are maintained in close co-operation with other nuclear data centers and allowed interactive retrieval of the data using web-based technology[2]. Through the Internet, NNDC (National Nuclear Data Center , U.S.A.) offers extensive bibliographic, experimental data, and evaluated data files[3]. The Nuclear Data Center at Japan Atomic Energy Research Institute mainly develops Japanese Evaluated Nuclear Data Library (JENDL) and offers the online data services[4]. Many very useful nuclear data instruments and software packages，such as the Nuclear Data Viewer[5] of Los Alamos, the JANIS[6] of the NEA Data Bank, the NDX[7] of the RFNC-VNIIEF (in Russia), the ZVView[8] of the IAEA and the Nuclear Reactions Video[9] of the JINR (in Russia)，were developed and offered by the different labs and nuclear data centers.

Since 1990's, the Internet services in China in nuclear field have grown step by step. Many of Chinese nuclear institutes, companies and departments of universities have constructed their own networks to offer different nuclear information services. But before 2000's for the numerical nuclear data, the users only can be served by different data dissemination services from the China Nuclear Data Center (CNDC), using different media such as ordinary mail for hardcopies of documents, PC diskettes, magnetic tapes, CD-ROMs, e-mails with attached retrieval data or electronic documents. But most of Chinese users and the public have limited access to the nuclear data information service of the international community over the Internet due to two barriers: one comes from the excessive international network traffic during working hours, the other is that most of Chinese users have to pay high international traffic cost of the Internet. In order to change this situation, a new project was sponsored and funded in the beginning of 2001 by the Minister of Education of China[10]. Its primary goal is to distribute international major nuclear data libraries via the Internet networks and to facilitate the visualization and manipulation of nuclear data by developing a web-based nuclear data services software system named as Nuclear Data Online Services (NDOS).

The following two sections will introduce main features of database support system and data services on the NDOS web site. The section IV will provide information on a plotting software, Nuclear Data Viewing System (NDVS). The last section gives the concluding words.

1 Design and Features of the NDOS

The NDOS software package has been developed since 2001 and can be divided into three parts: relational nuclear databases, database administration tools, and data service software. The relational databases of the NDOS software integrated and stored large amounts of diverse source data from the evaluated data and experimental data libraries. In the original databases, these source data are saved as the ASCII textual files in different standardized formats. For example, the evaluated nuclear reaction data are stored in ENDF (Evaluated Nuclear Data File) format which provides a comprehensive way to restore and retrieve these data. These format systems are generally too complex for a non-specialized user. The NDOS software makes a more general approach to the system design and development. Its software platform is based on the advanced relational database management system (RDBMS). Common design of tables and relations of new relational databases just keeps logical structure of those original data. The nuclear data not in original standardized formats from source libraries were loaded into the designed relational databases which are convenient for the data retrieval programming as well as visualization and manipulation of data. The user of this relational system can easily get access to numerical and graphical representations without prior knowledge of the storage structure. The NDOS also can easily reconstruct nuclear data in original standardized formats from the relational databases.

The web site (http://ndos.nst.pku.edu.cn/) of the NDOS offers access to 8 main international nuclear databases: 5 ENDF data bases for evaluated data, ENSDF for nuclear structure and decay data, EXFOR for experimental data and the international photonuclear data files. The ENDF, ENSDF and photonuclear data files also include on-line plotting capabilities. They offer some flexibility for the comparison of different nuclear data sets and on-line processing of the nuclear data and information. All of these services are available 24 hours a day, 7 days a week. Users may obtain an overview of the online services without receiving any authorization. The web page of the NDOS is shown in Fig. 1. The version 1.0 of this software was tested and released in Sep. 2001, which included the ENDF format evaluated library JENDL3.2 and on-line plotting display of the cross-section data. In May 2002, the version 2.0 was released and included all of five ENDF format evaluated neutron data libraries, the ENSDF library, the EXFOR library and the international photonuclear data library.

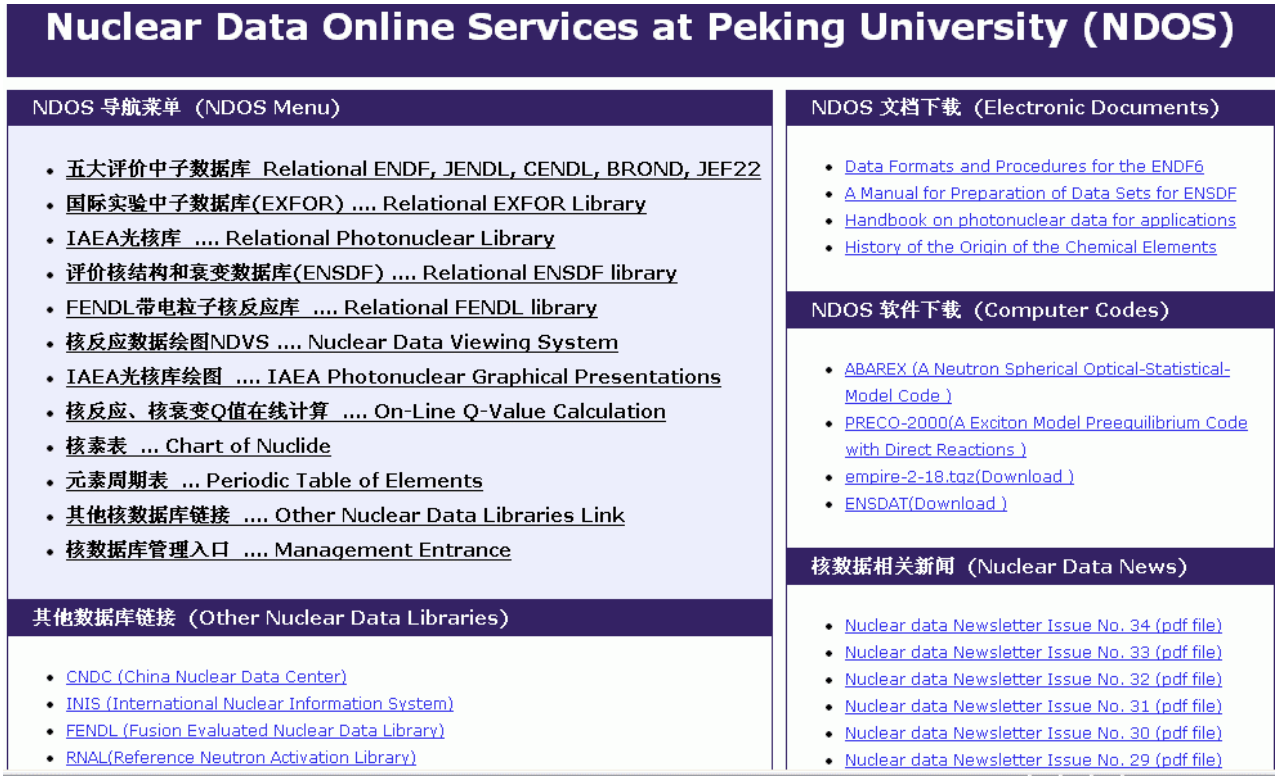

Fig. 1 Web page of the Nuclear Data Online Services (NDOS)

The computer programs providing support for database management and data retrievals are based on the Linux implementation of PHP and the MySQL software, the SQL-compliant RDBMS. PHP language is used for common software development, including programs for data loading and updating, as well as programs for access to the data through Web. The platform for nuclear data and services in this system are platform independent in the wide sense (independent of type of computer, operating system and RDBMS). Some management functions of this system such as database adding, data loading and updating can be remotely implemented. The main server of this web site is maintained and hosted by the IHIP (Institute of Heavy Ion Physics) of Peking University. A small group of the IHIP, a trio of undergraduates, graduates and professors, has developed the software system and is also responsible for providing the site hardware and networking supporting.

2 Online Nuclear Data Libraries on the NDOS web site

The web-based services of main nuclear data libraries on the NDOS web site are as follows.

2.1 Evaluated Nuclear Reaction Data Libraries (ENDF libraries)

Evaluated data sets are produced through evaluating the available experimental data, normally complemented by nuclear model calculations. For evaluated neutron data on the NDOS web site, there are five major evaluated libraries originating in different countries: BROND-2.2 (Russia), CENDL-2.1 (China), ENDF/B-VI (USA), JEF-2.2 (Europe), and JENDL-3.3 (Japan). These libraries cover the neutron energy range from 10^{-5} eV to 20 MeV with high degree of completeness[1].

The retrieval page of evaluated data files on the NDOS web site is shown in Fig. 2. It is easy to request all of numerical data from these libraries according to nuclide (material), reaction and library. The numerical data can be given in the ENDF format or listed into pointwise files. Users can construct some of plots containing evaluated data such as cross section and angular distribution.

2.2 Evaluated Nuclear Decay Data Library (ENSDF library)

Nuclear structure and decay data refer to the properties of single nuclide, such as mass, excitation energy, spin and parity, half-life, mean decay energies, decay modes, nuclear level properties, energies and intensities of Gamma-rays and emitted particles, etc. The major library is ENSDF (Evaluated Nuclear Structure Data File) which includes more than 2500 evaluated experimental data. After entering a mass number or a nuclide, users can quickly retrieve the all data from the ENSDF library on the NDOS web site. The output data files can be chosen as ENSDF format data files, decay data tables, evaluated nuclear structure drawing and tables made by the program ENSDAT. The decay data table of one retrieved dataset lists decay energy and absolute intensity for every β radiation and γ radiation. Fig. 3 shows the data table including some decay data for the EC decay from ^{26}Mg to ^{26}Al.

The program ENSDAT (Evaluated Nuclear Structure Drawings And Tables), released by the Brookhaven Science Associates, Inc., can be used to produce the PostScript file of tables and drawings in a form similar to the Nuclear Data Sheets. For each dataset of the ENSDF evaluated experimental data, all possible tables, band drawings, and gamma drawings are produced and stored into a PF file and a PDF file using the program ENSDAT. Users can easily retrieve these tables and drawings from the retrieval page of the ENSDF online service. One example of plotting of the decay scheme using the retrieved data from ENSDF library is shown in Fig.4.

2.3 Experimental Nuclear Reaction Data Library (EXFOR library)

The EXFOR (Exchange FORmat) database contains experimental nuclear reaction data mainly for incident neutrons. This library also contains experimental data's bibliographic information, like experimental facility, method, detector, source of uncertainties etc. Users may specify a reaction (or a desired residual nucleus and projectile) and the program NDOS will generate a list of data sets which satisfy the retrieval criteria. The user may select to see and/or save all or some of those data sets in original EXFOR format. The users can see those data sets in a computational format which is more suitable if the data are to be processed by the user's own programs. One example of EXFOR retrieval page from our database for all reaction channels of element Al is shown in Fig.5. But so far the experimental data (EXFOR) online graph has not been offered.

2.4 The International Photonuclear Data Library

Photonuclear data describe interactions between photons and nuclei. These data are very useful in different fields such as radiation shielding, radiotherapy and inspection technologies. The IAEA initiated a project on Compilation and Evaluation of Photonuclear Data in 1990's. The project included all active groups in compilation and evaluation of photonuclear data and produced the IAEA Photonuclear Data Library[11]. This Library includes evaluated cross sections and emission spectra data for

164 isotopes for incident photons with energies mostly up to 140MeV. The IAEA website supplies these recommended files in ENDF format, graphical presentations in PDF and other files from 6 national/laboratory libraries[12].

All data of the IAEA Photonuclear Data Library has been rebuilt into the NDOS built-in relational database. Users are allowed to online-retrieve all of these data in ENDF formats and pointwise files. The cross sections are plotted using the online retrieved data. Fig. 6 shows an example of the retrieval pages of the International Photonuclear Data Library.

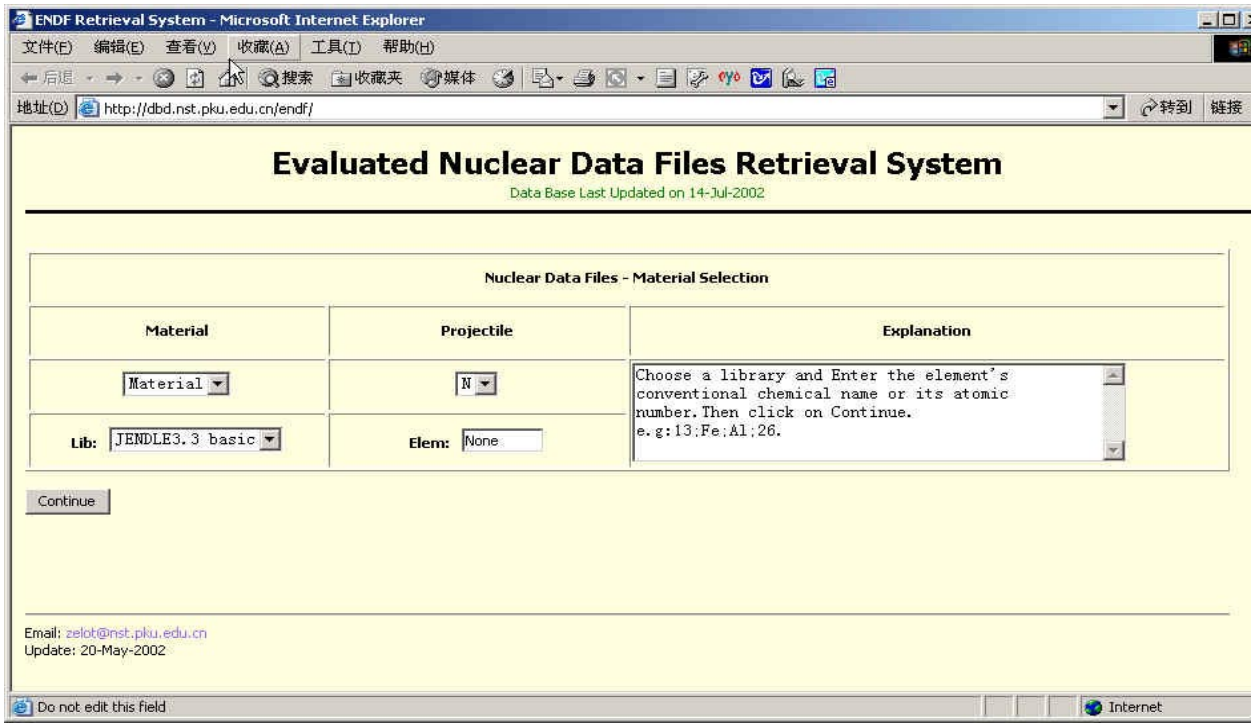

Fig. 2 ENDF retrieval page

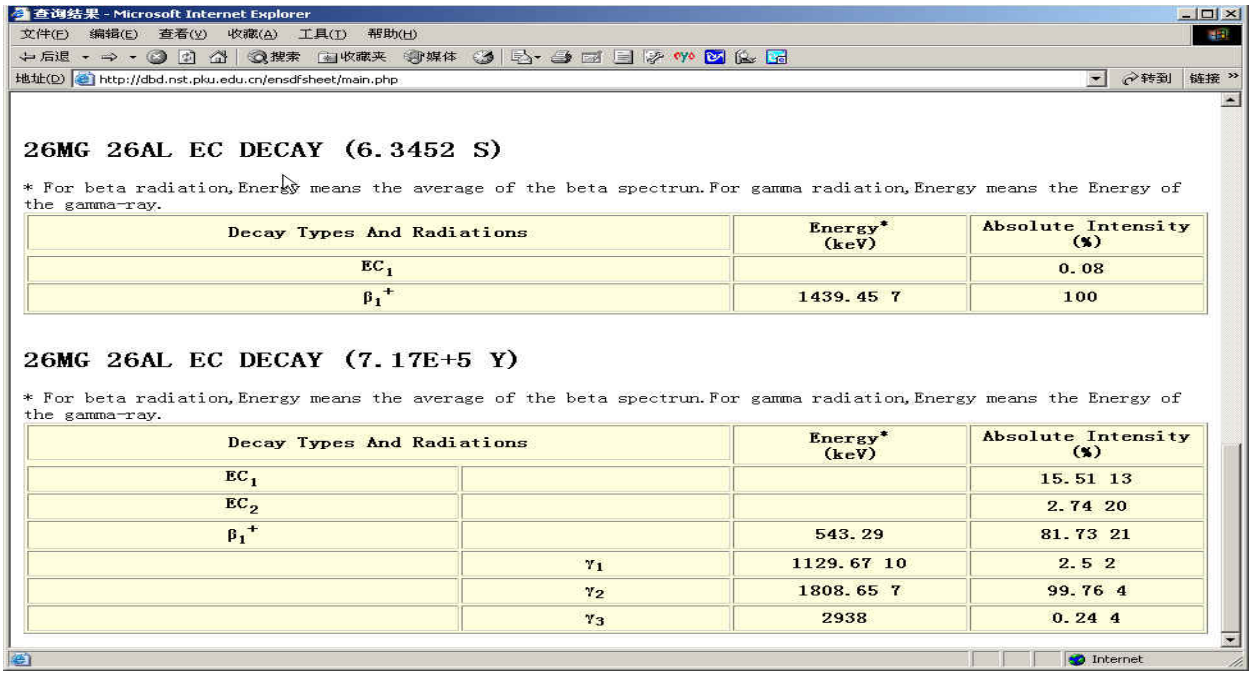

Fig. 3 Example of a database retrieved form on NDOS web page: ENSDF

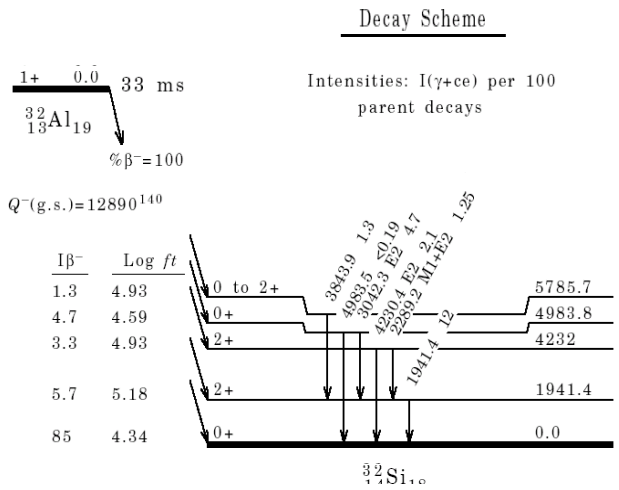

Fig. 4 Plotting of decay scheme using retrieved data from ENSDF library

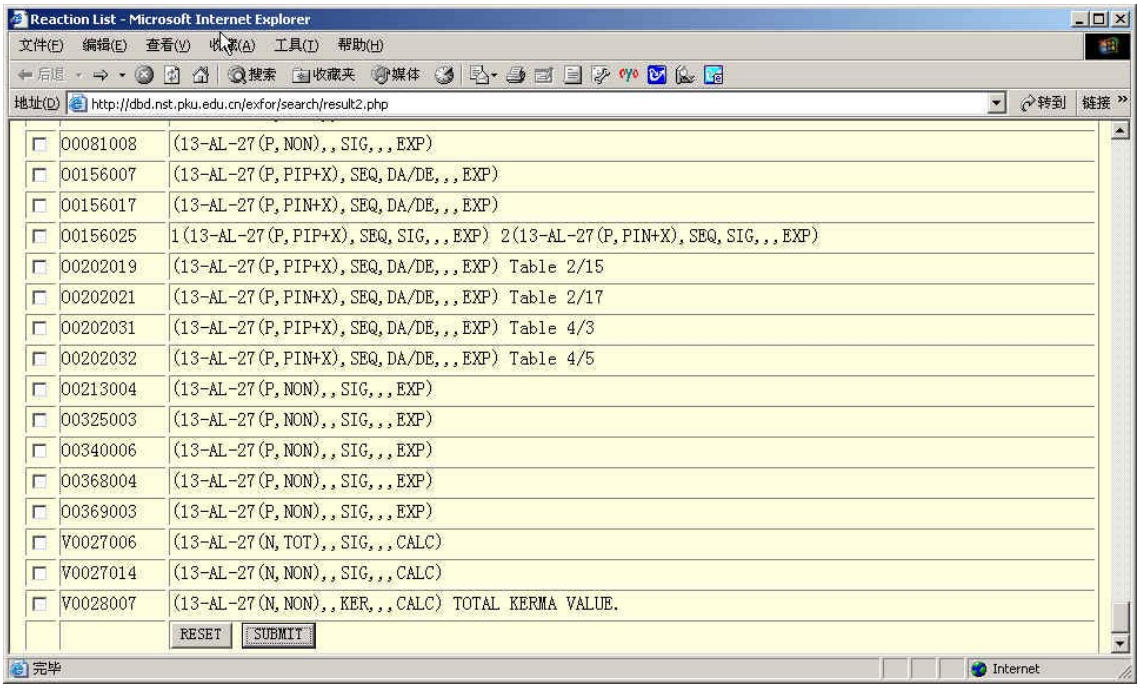

Fig. 5 Example of a database retrieved form on the NDOS web page: EXFOR

3 Nuclear Data Viewing System

One useful software package, Nuclear Data Viewing System (NDVS), has been developed and helps users access to all of the international evaluated databases on the NDOS system. Users are allowed to make online plots and over-plots for the evaluated cross section data retrieved from our different built-in nuclear databases, including BROND, CENDL, ENDF, JEF，JENDL and IAEA Photonuclear Data Library. The over plots mean that a selected cross section may be plotted on the same plot from one or more libraries. Users can use a scrolling list to select one or more library sets to be plotted. The ranges, titles and scales of X- and Y-axes are easily chosen and changed. The axes (X,Y) can be set as either linearity or logarithmic and the default is linear. Logarithmic graphs do better job for the cross sections. Whose values is in large range. These plots and overplots can be saved as high-quality Postscript graphs or GIF images and then shipped to user's computer. Users can easily see these graphs and print them on their own printer. Fig.7 shows the cross section curves for ^{56}Fe(n, total) reaction for the neutron data online-retrieved from five evaluated libraries, using different color curves to draw the different data sets.

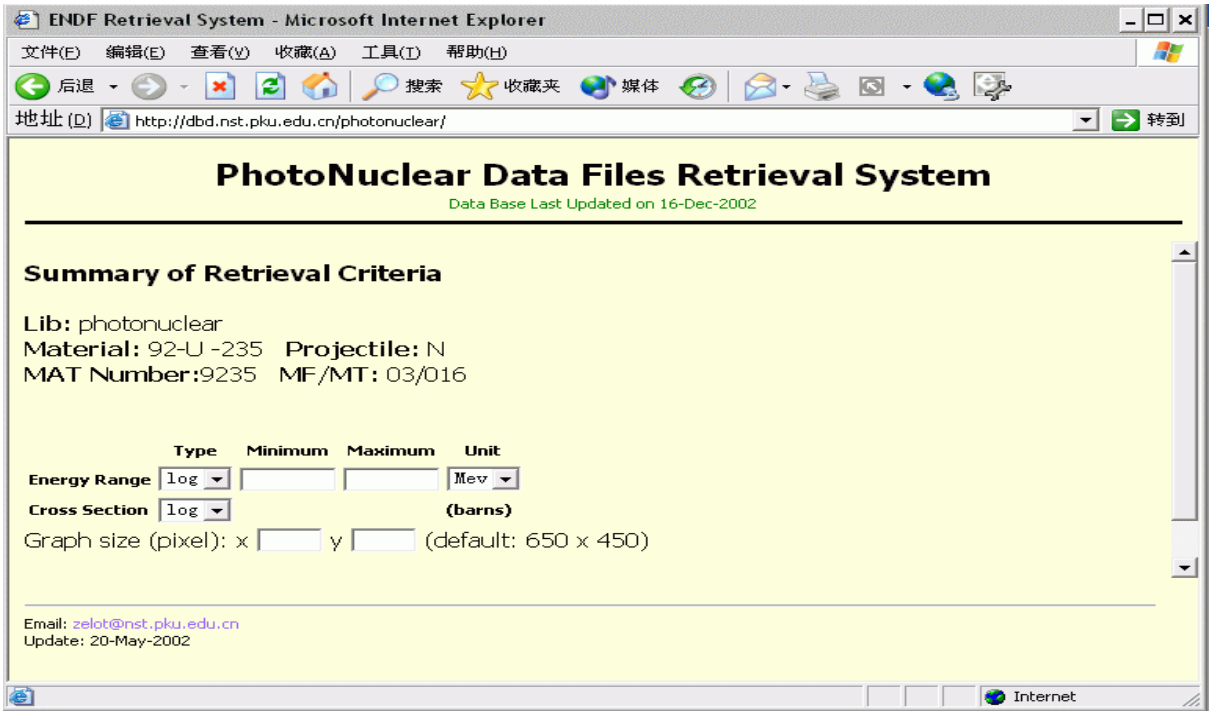

Fig. 6 Example of the retrieval pages of the International Photonuclear Data Library.

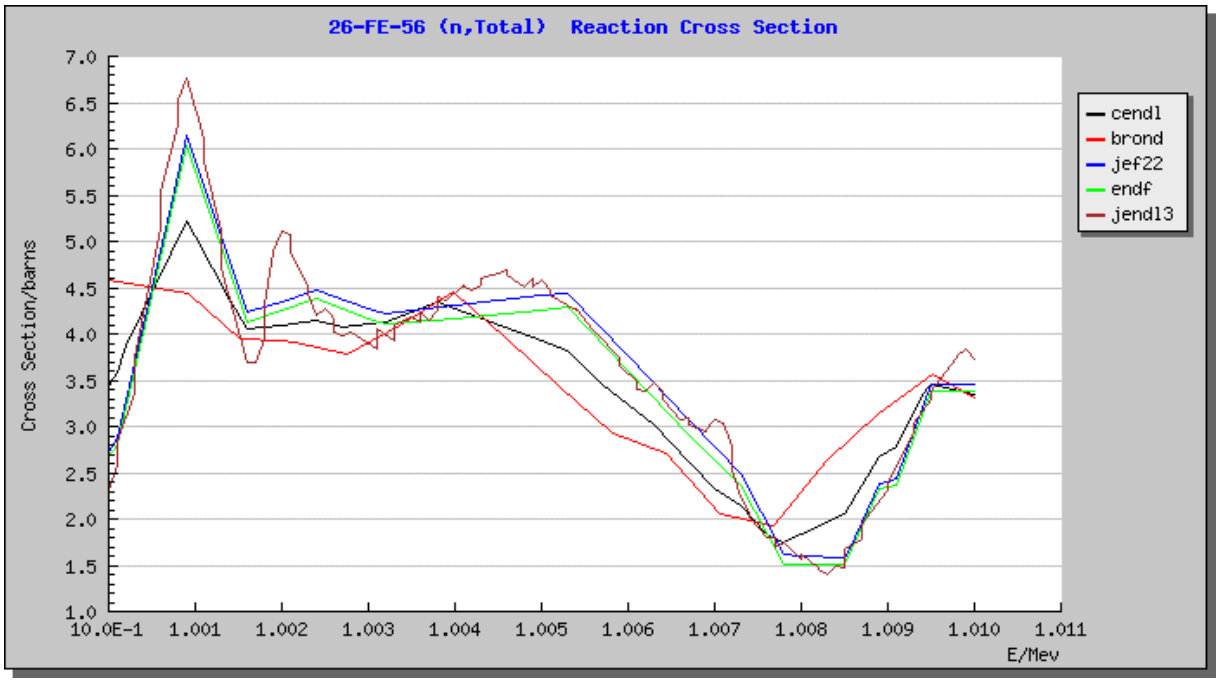

Fig. 7 Example of plotting for retrieved neutron cross-section data from five ENDF libraries: BROND, CENDL, JEF2.2, ENDF, JENDL3.3.

Angular distributions of secondary neutrons are given for the particles resulting from (n,n), (n,n'), (n,2n), and other neutron emitting reactions in the evaluated libraries. These data are widely used and presented in File 4 in ENDF format libraries. 2-D plots of angle distributions for secondary particles, using the data retrieved from our nuclear databases, can be obtained using the program NDVS and viewed on the screen of user's local computer by using an auxiliary application without any preimposed resolution limits. The absolute differential cross section and normalized probability

can be separately plotted for every element and isotope. Fig. 8 shows an example of online plotting of the angular distribution data for ^{27}Al(n, n$'$) retrieved from the JENDL3.3 database and Fig.9 the angular distribution for the same reaction at E=5.0 MeV. 3-D perspective plots, such as angular distributions vs. incident energy or secondary energy distributions vs. incident energy, will be developed and released later.

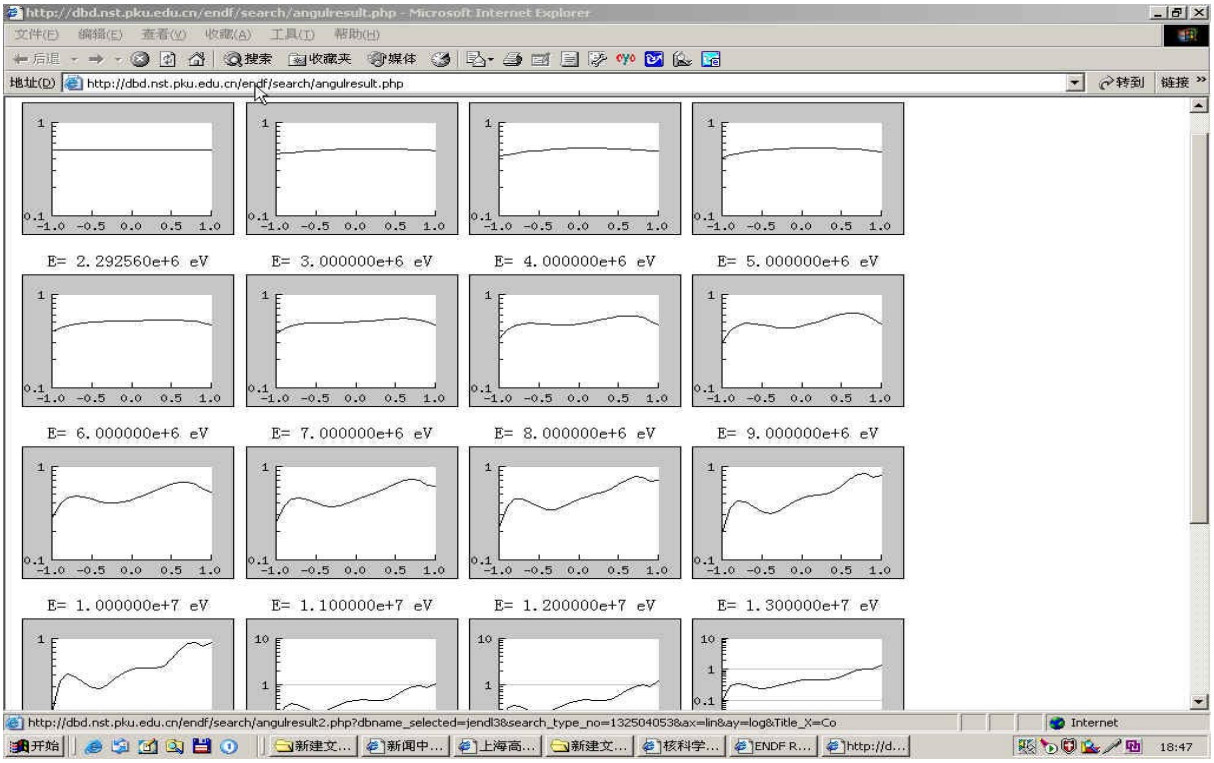

Fig. 8 Plotting of the angular distribution data for ^{27}Al(n, n$'$) from the JENDL3.3 database

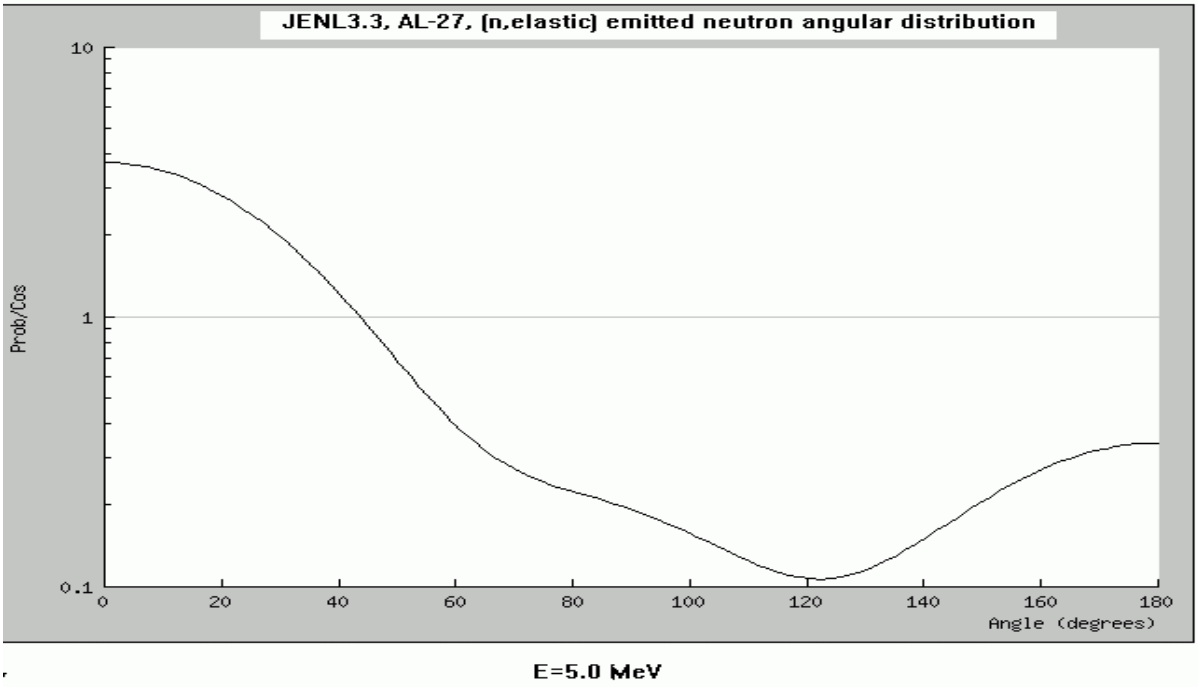

Fig.9 Angular distribution of emitted neutrons for Al^{27}(n, elastic) reaction at E=5.0 MeV.

4 Conclusions

The current version of the system NDOS described above has offered the online services of 8 international nuclear data libraries. The future developments are ongoing for adding more new databases into the relational databases and then offer better online services. The future online service system will include the CINDA (Computer Index of Neutron Data), FENDL (Fusion Evaluated Nuclear Data Library) and the charged-particle cross section data files etc. The basic functions of the software package NDVS would be expanded in the near future. For example, this online-plotting software will allow users to plot 3-D figures to enter their own numerical values, such as experimental data or theoretical points, to be plotted together with curves or data from the evaluated databases.

Acknowledgment

The authors are indebted to the China Nuclear Data Center (CNDC) for its support and kindly offering the nuclear databases CD-ROMs. Gratefully appreciation is expressed to Profs. ZHUANG Youxiang, YU Baosheng, GE Zhigang, ZHANG Jingshang, XIA Haihong , and Dr. JIN Yongli of the CNDC for many valuable discussions and helpful advice for this work.

References

[1] P.Oblozinsky, O.Schwerer. INDC(NDS)-378, September, 1998

[2] NEA Annual Report 2001, http://www.nea.fr/html/pub/annual-report.html,.

[3] Web page of the National Nuclear Data Center (NNDC) of BNL, http://www.nndc.bnl.gov/.

[4] Web page of the Nuclear Data Center at Japan Atomic Energy Research Institute , http://wwwndc.tokai.jaeri.go.jp/index.html.

[5] Web page of the Nuclear Data Viewer of Los Alamos, http://t2.lanl.gov/data/ndviewer.html.

[6] A.Nouri, P.Nagel, N. Soppera, A.Ahite, et al. J. Nul. Sce. & Tech., supp.2, 1480(August 2002)

[7] A.N.Grebennikov, N.A.Krutko, G.G.Farafontov. J. Nul. Sce. & Tech., Supp.2, 1464(August 2002)

[8] V.Zerkin. Web page of the IAEA Nuclear Data Service, http://www-nds.iaea.org/ndspub/zvview/

[9] V. I. Zagrebaev, A.Yu. Kozhin etc.. Web page of the Nuclear Data Video, http://nrv.jinr.ru/nrv/.

[10] Tieshuan Fan, Zhiyu Guo, Changxin Liu, Jiaer Chen, et al. Proc. 13th Pacific Basin Nuclear Conf., October 21~25, 2002, Shenzhen, China

[11] P. Oblozinsky. J. Nucl. Sci. & Tech., Supp. 2, 31 (August 2002)

[12] Web page of the IAEA Nuclear Data Service, http://www-nds.iaea.org/photonuclear/.

Activities and Cooperation on Nuclear Data in China During 2003

GE Zhigang

China Nuclear Data Center, CIAE, P.O.Box275(41), Beijing 102413

1 The Meeting and Symposium Held in China

1) The Symposium on Nuclear Data Library, 13-17 Jan., Nanjing.
2) The Symposium on Nuclear Data Future Need, 13-15 Oct., Yichang.
3) The Meeting of Benchmark Testing Working Group, 15-18 Oct., Yichang.

2 The International Meeting and Workshop in Nuclear Data Field Attended by Staff of CNDC

1) ZHUANG Youxiang. Technical Meeting on Coordination of the Network of Nuclear Reaction Data Centers, 16-21 Jun., Vienna, Austria.
2) YU Hongwei. The 6th workshop on Nuclear Data Production and Evaluation, 28-29 Aug., Pohang Accelerator Laboratory, Republic of Korea.
3) RONG Jian. International Workshop on Nuclear Response under Extreme Conditions, 20-25 Oct., Trento, Italy.
4) HUANG Xiaolong. The 15th Meeting of the Nuclear Structure and Decay Data (NSDD) Network, 10-14 Nov., Vienna, Austria.
5) QIAN Jing. Workshop on Nuclear Structure and Decay Data; Theory and Evaluation, 17-28 Nov. ICTP, Triest, Italy.
6) YU Hongwei. Relational Databases for Nuclear Data Development, Dissemination and Processing: EXFOR/CINDA Implementation, Maintenance and Compilation, 1-5 Dec., Vienna, Austria.

3 The Foreign Scientists in Nuclear Data Field Visited CNDC/CIAE

1) Dr. S.Yavshits. 4-10 Nov., V. G. Khlopin Radium Institute, Russian.
2) Dr. Demidov A. P., Dr. Golashvili. 2-12 Dec., ATOMINFORM, Russian.
3) Dr. Chechev V. P.. 2-12 Dec., V. G. Khlopin Radium Institute, Russian.

4 Staff of CNDC Working or Visiting Foreign Country

1) WU Zhendong. 9 Sept. 2002-6 Sept. 2003, NDC/JAERI, Japan.
2) GE Zhigang, Fan Sheng, Huang Xiaolong. 1-7 Oct., ATOMINFORM, Russian.
3) GE Zhigang, Fan Sheng, Huang Xiaolong. 7-10 Oct., V. G. Khlopin Radium Institute, Russian.
4) RONG Jian. 26 Oct.-22 Dec., University Paris-Sud, France.
5) CHEN Guochang. 1-31 Nov., Pohang Accelerator Laboratory, Republic of Korea.

CINDA INDEX

Nuclide	Quantity	Energy/ eV		Lab	Type	Documentation				Author, Comments
		Min	Max			Ref	Vol	Page	Date	
^{12}C	Calculation	1.0-5	2.0+7	APE	Theo	Jour CNDP	29	24	Dec 2003	ZHANG Jingshang, DA/DE
^{55}Mn	Evaluation	1.0-5	2.0+7	APE	Eval	Jour CNDP	29	29	Dec 2003	YU Baosheng +, SIG, DA, DA/DE
^{55}Mn	Calculation	1.0+3	2.0+7	APE	Theo	Jour CNDP	29	37	Dec 2003	WANG Shunuan +, SIG, DA, DA/DE
^{63}Cu	Covariance	1.0+5	2.0+7	ZHN	Eval	Jour CNDP	29	1	Dec 2003	JIA Min +, (n,tot), (n,g), (n,2n), (n,p),COV
^{65}Cu	Covariance	1.0+5	2.0+7	ZHN	Eval	Jour CNDP	29	1	Dec 2003	JIA Min +, (n,tot), (n,g), (n,2n), (n,p),COV
^{Nat}Cu	Covariance	1.0+5	2.0+7	ZHN	Eval	Jour CNDP	29	1	Dec 2003	JIA Min +, (n,tot), (n,g), (n,2n), (n,p),COV
^{98}Mo	Evaluation	1.0+5	2.0+7	NKU	Eval	Jour CNDP	29	42	Dec 2003	CAI Chonghai , SIG, DA, DA/DE
^{100}Mo	Evaluation	1.0+5	2.0+7	NKU	Eval	Jour CNDP	29	42	Dec 2003	CAI Chonghai , SIG, DA, DA/DE
^{233}U	Nu	1.0-5	2.0+7	APE	Eval	Jour CNDP	29	13	Dec 2003	YU Baosheng +, Neutron Yields
^{233}U	Delayed Neuts	1.0-5	2.0+7	APE	Eval	Jour CNDP	29	13	Dec 2003	YU Baosheng +, Neutron Yields
^{252}Cf	Fission Yields	Spont		APE	Eval	Jour CNDP	29	6	Dec 2003	LIU Tingjin, Fission Yields , Mass Distribution